Approved for public release. Distribution is unlimited.

ORNL/TM-2016/628

Oak Ridge National Laboratory Evaluation of Zinc-Coated Ductile Iron Pipe

Sergei A Shipilov
Kinga Unocic
Bruce A Pint

September 30, 2016

OAK RIDGE NATIONAL LABORATORY
MANAGED BY UT-BATTELLE FOR THE US DEPARTMENT OF ENERGY

DOCUMENT AVAILABILITY

Reports produced after January 1, 1996, are generally available free via US Department of Energy (DOE) SciTech Connect.

Website http://www.osti.gov/scitech/

Reports produced before January 1, 1996, may be purchased by members of the public from the following source:

National Technical Information Service
5285 Port Royal Road
Springfield, VA 22161
Telephone 703-605-6000 (1-800-553-6847)
TDD 703-487-4639
Fax 703-605-6900
E-mail info@ntis.gov
Website http://www.ntis.gov/help/ordermethods.aspx

Reports are available to DOE employees, DOE contractors, Energy Technology Data Exchange representatives, and International Nuclear Information System representatives from the following source:

Office of Scientific and Technical Information
PO Box 62
Oak Ridge, TN 37831
Telephone 865-576-8401
Fax 865-576-5728
E-mail reports@osti.gov
Website http://www.osti.gov/contact.html

This report was prepared as an account of work sponsored by an agency of the United States Government. Neither the United States Government nor any agency thereof, nor any of their employees, makes any warranty, express or implied, or assumes any legal liability or responsibility for the accuracy, completeness, or usefulness of any information, apparatus, product, or process disclosed, or represents that its use would not infringe privately owned rights. Reference herein to any specific commercial product, process, or service by trade name, trademark, manufacturer, or otherwise, does not necessarily constitute or imply its endorsement, recommendation, or favoring by the United States Government or any agency thereof. The views and opinions of authors expressed herein do not necessarily state or reflect those of the United States Government or any agency thereof.

ORNL/TM-2016/628

Materials Science and Technology Division

EVALUATION OF ZINC-COATED DUCTILE IRON PIPE

Sergei A. Shipilov
Kinga Unocic
Bruce A. Pint

Date Published: September 30, 2016

Prepared by
OAK RIDGE NATIONAL LABORATORY
Oak Ridge, TN 37831-6283
managed by
UT-BATTELLE, LLC
for the
US DEPARTMENT OF ENERGY
under contract DE-AC05-00OR22725

CONTENTS

	Abstract	4
1	Introduction	4
1.1	Fact Sheet	4
1.5	Project Outline	5
2	Characterization of Commercial Coating Systems for Ductile Iron Pipe (Task 1)	6
2.1	Cast Iron	6
	Ductile (of Nodular) Iron	6
2.2	Ductile Iron Pipe Manufacturing	8
2.2.1	Industrial Specifications for Zinc Coating on DIP	8
2.2.1.1	Manufactured by AMERICAN Ductile Iron Pipe Co.	9
	Visual Examination of AMERICAN Pipes	9
	Microstructure of Ductile iron in AMERICAN Pipe	15
	Mechanocal Properties of DIP	15
2.3	Characterization of DIP	17
	Oxidation and Time Determination	24
	Summary	26
3	Consolidate available Corrosion Data (Task 2)	27
3.1	Corrosion in Soils	27
3.1.1	Soil Corrosivity Classification	27
4	Explore Accelerated Laboratory Testing (Task 4)	27
4.1	Electrochemical Tests	27
4.2	Evaluation of NSB Corrosion Data	28

ABSTRACT

Oak Ridge National Laboratory (ORNL) received $1m in funding from the U.S. Bureau of Reclamation in order to evaluate the performance of zinc-coated ductile iron pipe (DIP) in highly- and severely-corrosive soils. The project started in May 2016 and a final report will be issued March 31, 2017. The project is being led by the Corrosion Science and Technology Group in the Materials Science and Technology Division at ORNL. This interim report is based on the work performed by an ORNL multidisciplinary team in the last two months.

The project has been broken down into four tasks. The first task is to characterize commercially available DIP. Specimens from the three major U.S. DIP manufacturers were purchased for this study via third party vendors and are being characterized. The second task is to evaluate available data on DIP corrosion in soils. The largest data set was collected by the National Bureau of Standards (now NIST) from 1910-1952 and included 95 different kinds of soil at 128 sites across the country. Because of the large amount of data and limited agreement on what defines "corrosive" soil, staff from the Computational Sciences and Engineering Division have been consulted and are currently analyzing the data using existing algorithms to look for trends between the corrosion rates and the various soil characteristics such as resistivity and pH. The third task is to develop a long-term test plan to evaluate DIP and the fourth task is to develop an accelerated test procedure to reduce the time required to evaluate soil corrosion by 1-2 orders of magnitude. By developing a better understanding of what makes a soil corrosive, including the chemical and physical properties, it may be possible to model the long-term behavior of DIP.

A full report on the work will be submitted by the March 2017 deadline. It appears that a sustained, multi-year effort in this area would be of great benefit to the Bureau of Reclamation, to the DIP industry and to the country, which is facing challenges with its infrastructure.

1. INTRODUCTION

1.1 FACT SHEET

- There are 876,000 miles of municipal water mains in the U.S.—more than 5 times longer than the national highway system. Moreover, community water systems include over 1.8 million miles of network pipes (2002).
- The average age of drinking water infrastructure in the U.S. is over 40 years of a 50-year design life. Some pipes date back to the 1880s.
- The conditions of many of these pipes are unknown, as they are buried underground out of sight, and are owned and operated by various local entities.
- Up to 20,000 miles of pipe will need to be replaced annually, beginning 2035.
- The nationwide system of wastewater infrastructure includes 600,000 miles of sanitary sewers and 200,000 miles of storm sewers. Aging sewer systems spill about 1.26 trillion gallons of untreated sewage every single year.
- Since 2000, the U.S. suffered over 5.1 million broken water mains (240,000 breaks per year), most of them caused by corrosion.
- Failures in drinking water infrastructure result in water disruption, impediments to emergency response, health issues, and damage to other types of infrastructure, such as roadways.
- In 2013, the American Society of Civil Engineers (ASCE), in its Report Card for America's Infrastructure, gave an overall grade "D" for the state of critical water/wastewater infrastructure.

- According to ASCE, “Every day, six billion gallons of drinking water disappears, mostly due to old, leaky pipes and water mains. That is enough water to serve the population of a state the size of California” (2005).
- The U.S. Conference of Mayors in their “Open Letter to the Next President of the United States” of September 2008 expressed alarm that “35% of cities in a Conference of Mayors survey do not know where their water supply will come from by 2025.”
- Leaking pipes are a concern for most cities, which can lose anywhere from 5 to 40% of their water.
- On December 14, 2015, a state of emergency due to “out-of-control corrosion” was declared in Flint, MI, after state and local government officials ignored, for more than 18 months, irrefutable evidence that the water pumped from the Flint River exposed residents to extreme toxicity. “There are potential Flints all over the Northeast and Midwest,” Rep. Duncan (R-TN) said in August 2016.

The three major reasons why in 2016 we still deal with the problem that goes back to at least the beginning of the 20th century are:

1. Although thousands of research projects have been conducted, we still do not know what happens to a specific material buried in a natural soil. Why and how the process(es) of corrosion initiates in one location, but not in the other(s) remains unknown.
2. As a result, materials (grey cast iron, DIP, steel, PVC, concrete) used as components of water mains are chosen without any justification other than based solely either on the availability of pipes of a specific diameter on the market or on their prices.
   Chemical performance (resistivity to corrosion) of the materials in a specific soil or a type of soils is not among factors that are considered. The same material can be chosen to be used in a highly corrosive soil and in a low corrosive soil.
3. We also don’t know enough about what makes a soil very corrosive and why other soils are not corrosive at all.

The problem was never addressed as a complex one. In addition, current advances in computational science were not available just a decade ago.

1.2 PROJECT OUTLINE

The team consists of researchers and technicians of three Divisions and five research groups of Oak Ridge National Laboratory including the Corrosion Science and Technology Group, the Electron Microscopy Group, and the Mechanical Properties and Mechanics Group of the Materials Science and Technology Division, the Geographic Information Science and Technology Group of the Computational Sciences and Engineering Division, and the Nanomaterials Chemistry Group of the Chemical Sciences Division.

The main goal of research is to “evaluate and develop performance data for zinc-coated ductile iron pipe (DIP) applications in highly- or severely-corrosive soils.” This performance data along with any other relevant data or information the laboratory may obtain shall be used to evaluate and recommend whether the material meets the corrosion protection requirements in the Bureau of Reclamation’s Technical memorandum 8140-CC-2004-1, “Corrosion Considerations for Buried Metallic Water Pipe.”

Research was focused on characterizing available commercial coating systems for DIP, evaluating available corrosion data for DIP and developing an accelerated test protocol for pipelines in corrosive soils. The four tasks included (but were not limited to):

- Characterization of commercial coating systems for DIP.
- Consolidate Available Corrosion Data.
- Develop Long-Term Test Plan.
- Explore Accelerated Laboratory Testing.

2. CHARACTERIZATION OF COMMERCIAL COATING SYSTEMS FOR DUCTILE IRON PIPE (Task 1)

The task is intended to characterize the thickness, composition and microstructure of coating systems deposited by commercial vendors on DIP manufactured by centrifugal casting processes, which have different surface roughness. Characterization will be performed before and after corrosion exposures.

2.1 CAST IRONS

Ductile iron (DI), also known as nodular iron and spheroidal graphite (SG) iron, is a type of cast iron (CI). CI is a material with a history stretching over two and a half millennia. DI was developed in 1943. It is not a single material but is part of a group of materials which can be produced to have a wide range of properties through control of the microstructure.

Generically, cast irons are a class of ferrous alloys with carbon contents above 2.14 wt.%; in practice, however, most cast irons contain between 3.0 and 4.5 wt.% C and, in addition, other alloying elements. This tendency to form graphite is regulated by the composition and rate of cooling. Graphite formation is promoted by the presence of silicon in concentrations greater than about 1 wt.%. Also, slower cooling rates during solidification favor graphitization (the formation of graphite). For most cast irons, the carbon exists as graphite, and both microstructure and mechanical behavior depend on composition and heat treatment. The most common cast iron types are gray, ductile (or nodular), white, malleable and compacted graphite.

Ductile (or Nodular) Iron

The common defining characteristic of DI is the shape of the graphite. In DI, the graphite is in the form of nodules rather than flakes as it is in grey iron (Figure 1). The rounded shape of the nodules inhibits the creation of cracks and provides the enhanced ductility that gives the alloy its name. The formation of nodules is achieved by the addition of nodulizing elements, most commonly magnesium. In accordance with Standard Specification for Ferritic Ductile Iron Castings Suitable for Low Temperature Service, the iron shall conform to the requirements for chemical composition shown in Table 1.

Adding a small amount of Mg to the GI before casting produces a distinctly different microstructure and set of mechanical properties (Table 2). Graphite still forms, but as nodules or sphere like particles instead of flakes (Figure 1). The resulting alloy is called ductile or nodular iron, and a typical microstructure is shown in Figure 1b. The matrix phase surrounding these particles is either pearlite or ferrite, depending on heat treatment; it is normally pearlite for an as-cast piece. However, a heat treatment for several hours at about 700 °C (1300 F) will yield a ferrite matrix as in this photomicrograph. Castings are stronger and much more ductile than gray iron, as a comparison of their mechanical properties in Table 1 shows. In fact, ductile iron has mechanical characteristics approaching those of steel. For example, ferritic ductile irons have tensile strengths ranging between 380 and 480 MPa (55 and 70 ksi), and ductilities (as percent elongation) from 10 to 20%. Typical applications for this material include valves, pump bodies, crankshafts, gears, and other automotive and machine components. Ductile iron is used also for manufacturing ductile iron pipe (DIP).

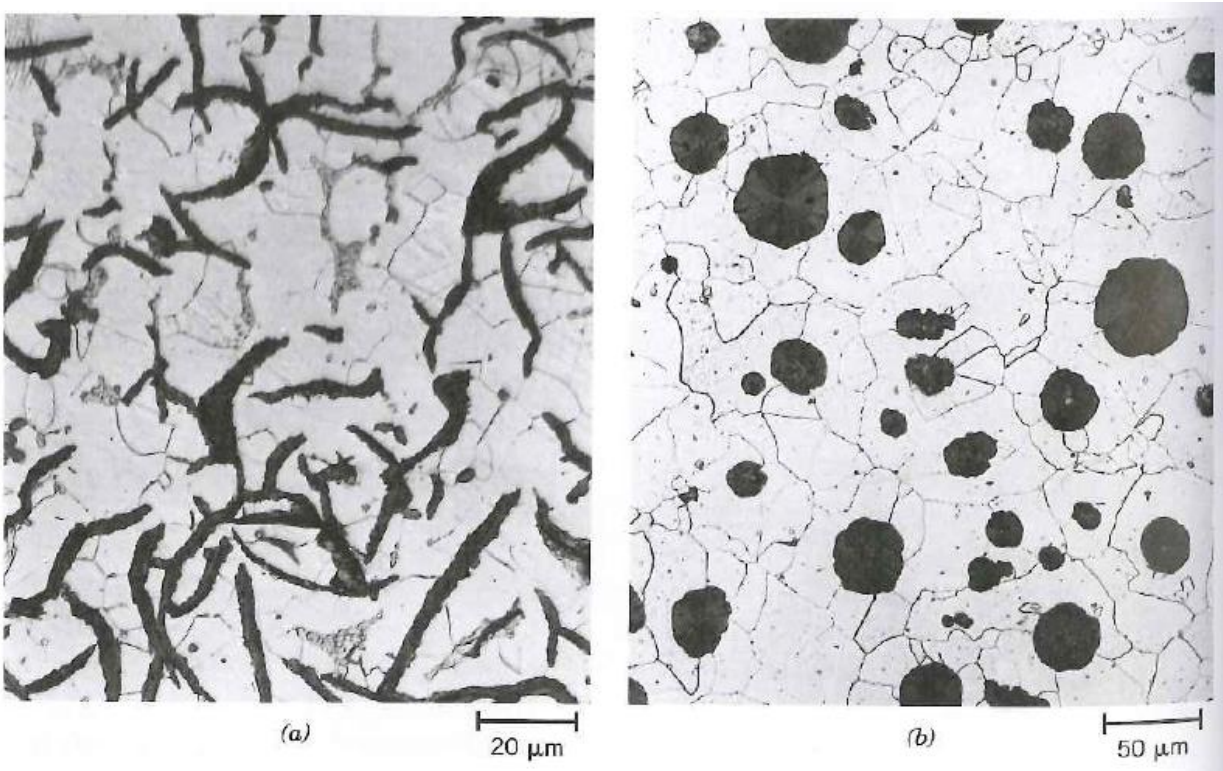

Figure 1. Optical photographs of: (a) cray iron: the dark graphite flakes are embedded in an α-ferrite matrix, 500×; and (b) ductile iron: the dark graphite nodules are surrounded by an α-ferrite matrix, 200×.

Table 1. Chemical Composition of DI. ASTM A874/A874M-98 (Reapproved 2014)

Element	Minimum, %	Maximum, %
Total carbon	3.0	3.7
Carbon equivalent (carbon + ⅓ silicon)	. . .	4.5
Silicon	1.2	2.3
Phosphorous	. . .	0.03
Magnesium	. . .	0.07
Manganese	. . .	0.25
Copper	. . .	0.1
Nickel	. . .	1.0
Chromium	. . .	0.07

Table 2. Designations, Minimum Mechanical Properties, and Approximate Compositions for DI

Grade	Composition (wt.%)	Matrix Structure	Tensile Strength [MPa (ksi)]	Yield Strength [MPa (ksi)]	Ductility [%EL]
ASTM A536 60-40-18	3.5-3.8 C 2.0-2.8 Si 0.05 Mg <0.20 Ni <0.10 Mo	Ferrite	414 (60)	276 (40)	18
ASTM A536 100-70-03		Pearlite	689 (100)	483 (70)	3
ASTM A536 120-90-02		Tempered martensite	827 (120)	621 0)	2

2.2 DUCTILE IRON PIPE MANUFACTURING

Ductile iron pipes are manufactured by a centrifugal method in accordance to ISO 2531 or BS EN 545 standards, with an internal cement mortar lining to increase flow coefficients. An external metallic zinc and bitumen coating is applied to further increase the lifespan of the pipes (Figure 2).

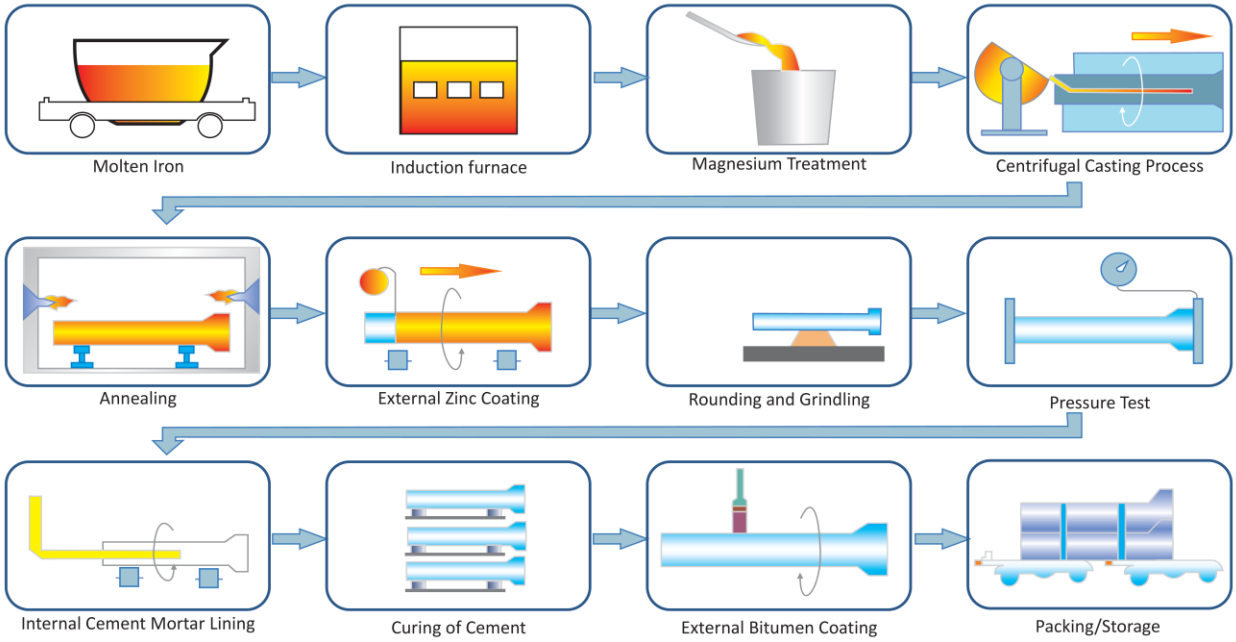

Figure 2. Manufacturing a Zn-coated DIP with cement lining.

2.2.1 INDUSTRIAL SPECIFICATIONS FOR ZINC COATING ON DIP

Three vendors exist in the U.S. and they operate under the umbrella of the Ductile Iron Pipe Research Association (DIPRA). The vendors are:

- AMERICAN Ductile Iron Pipe, Birmingham, Alabama
- McWane Ductile, Birmingham, Alabama
- U.S. Pipe and Foundry Company, Birmingham, Alabama

To obtain samples from each manufacturer, several pipes were purchased via 3rd party vendors for this study (Table 3).

Table 3 Samples of DIP Provided by Third Party Vendors.

Mark	Third Party Vendor	DIP Manufacturer	Pipe Size (D × L in)	Description	Received
A04-1	ORNL Utilities Division	American Pipe Co.	4 × 3 ft	Cl 350 DI tar coated cement lined	8/10/2016
M04-1	Consolidated Pipe & Supply Co.	McWane Ductile	4 × 18 ft	Cl 350 DI tar coated cement lined slip joint pipe	8/11/2016
U04-1	Valley Pipe and Fittings	U.S. Pipe Co.	4 × ½ ft	Class 53 DI Pipe (4.80 in. OD); tar coated cement lined	9/8/2016
A12-1	Blalock & Sons Inc.	American Pipe Co.	12 × 2 ft	DI pipe; standard cement lining with bituminous seal coat and bituminous exterior	9/23/2016
U06-1	Valley Pipe and Fittings	U.S. Pipe Co.	6 × 20 ft	DI Cl 350 Tyton Joint Pipe	Stock in Knoxville
U06-2	Valley Pipe and Fittings	U.S. Pipe Co.	6 × 20 ft	DI Cl 51 Tyton Joint Pipe	Stock in Knoxville
M36-1	Valley Pipe and Fittings	McWane Ductile	36 × 22	DI pipe; bituminous exterior	9/9/2016

2.2.1.1 Manufactured by AMERICAN Ductile Iron Pipe Co.

AMERICAN Ductile Iron Pipe Company (formerly known as AMERICAN Cast Iron Pipe Company), founded in 1905, is one of three manufacturers of DIP in the U.S.[1] The first shipment of AMERICAN ductile iron pipe was made in 1955.[2]

Visual Examination of AMERICAN Pipes

We received two samples of new DIP manufactured by AMERICAN Pipe. The pipe samples were provided by the ORNL's Utilities Division and by Blalock & Sons Inc. (Table 2.1) and marked as A04-1 and A12-1, respectively. The first letter "A" means the pipe was manufactured by AMERICAN Pipe, the digits "04" and "12" show the diameter of the pipes (4 in and 12 in, resectively), and the last digit "1" means it was the first shipment from the vendor/manufacturer.

Figure 3 shows a new A04-1 pipe in as-received condition. The pipe never was in use but the large part of the pipe was severely covered by rust while the rest of the pipe had a good tar coating on its surface. The tar coated pipe had standard cement lining. The thicknes of the pipe wall was approximately 8.5 mm and the thickness of the cement lining was approximately 5.5 mm.

Several specimens of the size of approximately 1½ in. by 1½ in. (as shown in Figure 2.4) were cut from the pipe for further investigation.

[1] "Zinc-Coated Ductile Iron Pipe." AMERICAN Ductile Iron Pipe.
[2] American Ductile Iron Pipe: Centrifugally Cast in Metal Molds or Sand-Lined Molds For Water of Other Liquids.

(a)

(b)

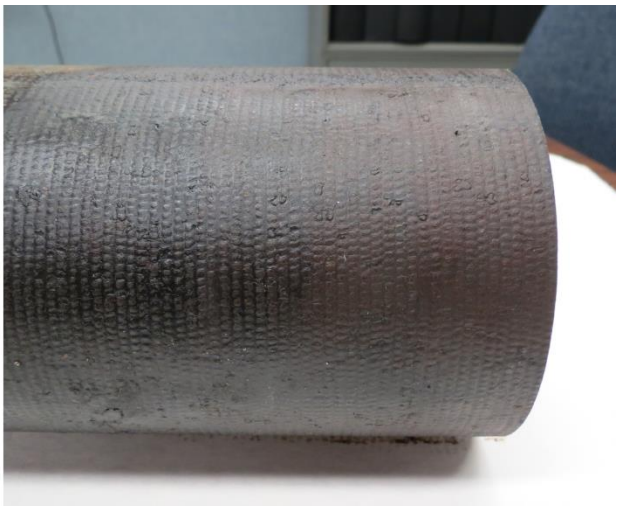

(c)

(d)

(e)

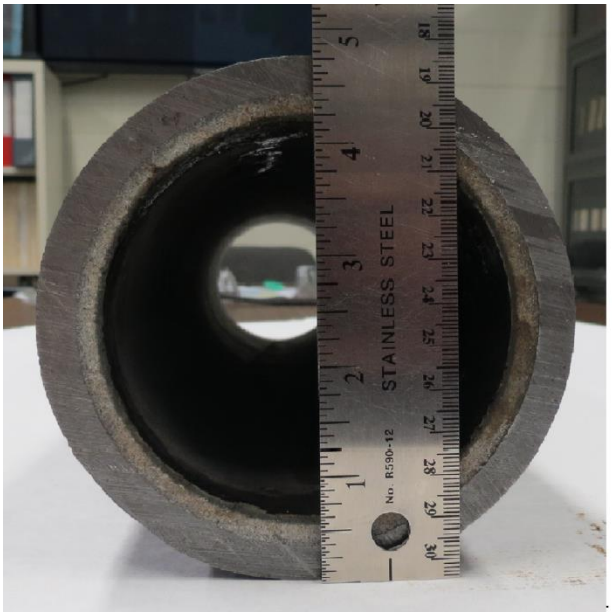

(f)

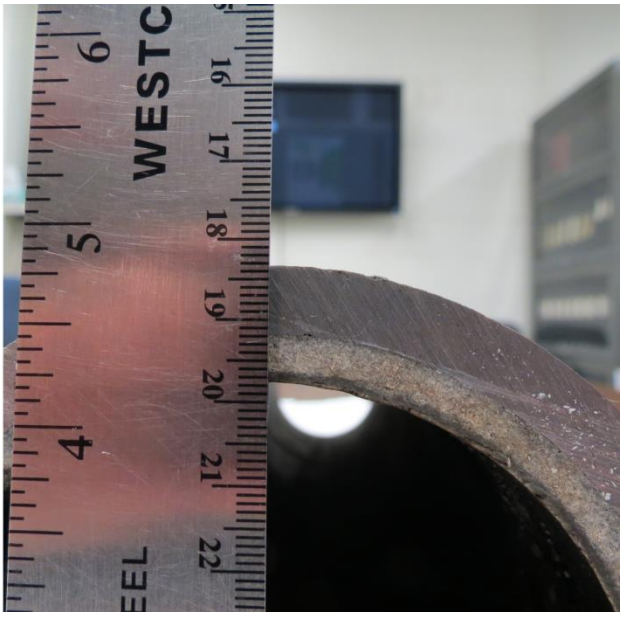

(g)

Figure 3. (a) A new DIP A04-1 manufactured by AMERICAN Pipe. (b) The part of the pipe severely covered by rust and (c) the parts of the pipe without rust. (d) A rusted area with higher magnification and (e) numerous defects in the tar coating. (f,g) The dimensions of the 4-in pipe: the outer diameter is approximately 4¾ in, the thickness of the pipe wall is approximately 8.5 mm, and the thickens of cement lining is approximately 5.5 mm.

AMERICAN ductile iron pipes prepared for their installation by Blalock & Sons Inc. in a residential area in West Knoxville are shown in Figure 4. A fragment of the 12-in. pipe is used in the investigation shown in Figure 5.

AMERICAN

(a)

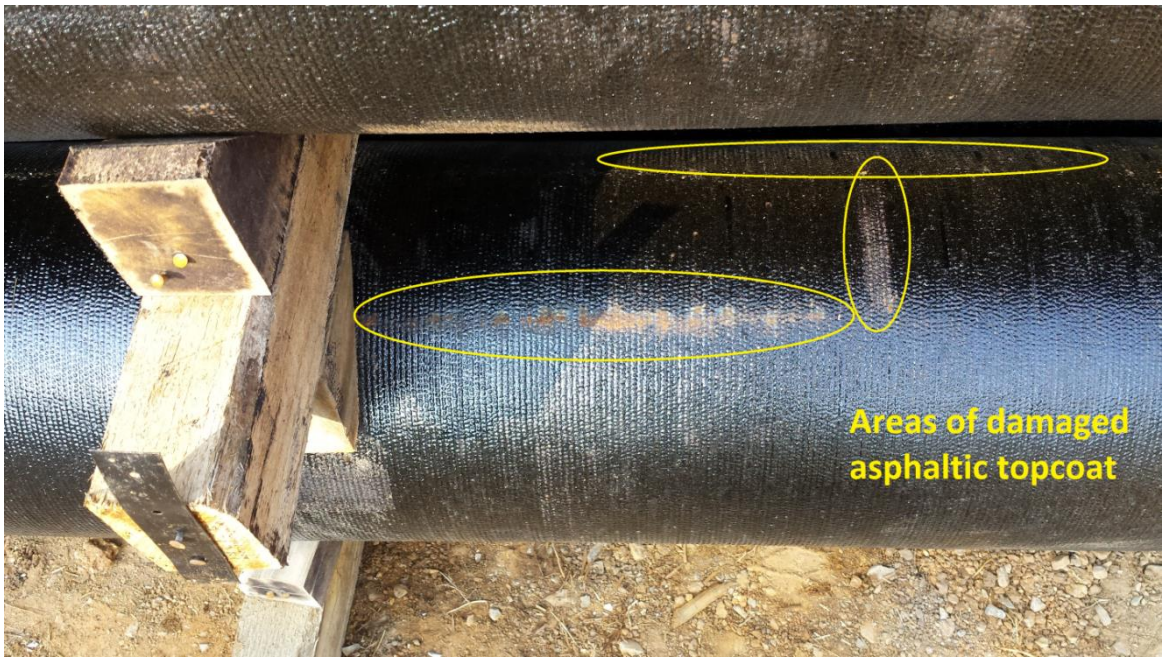
Areas of damaged
asphaltic topcoat

(b)

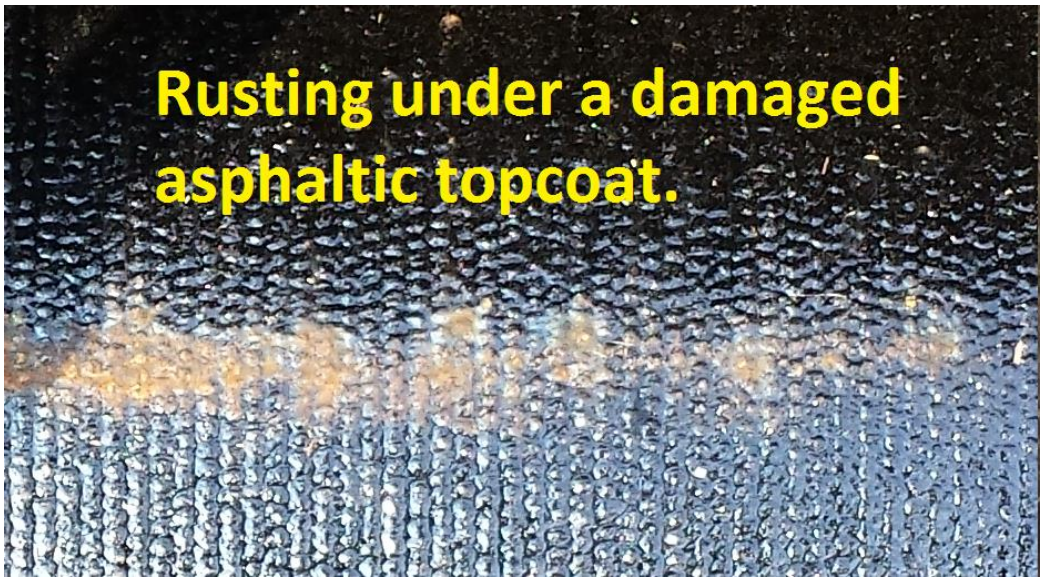
Rusting under a damaged
asphaltic topcoat.

(c)

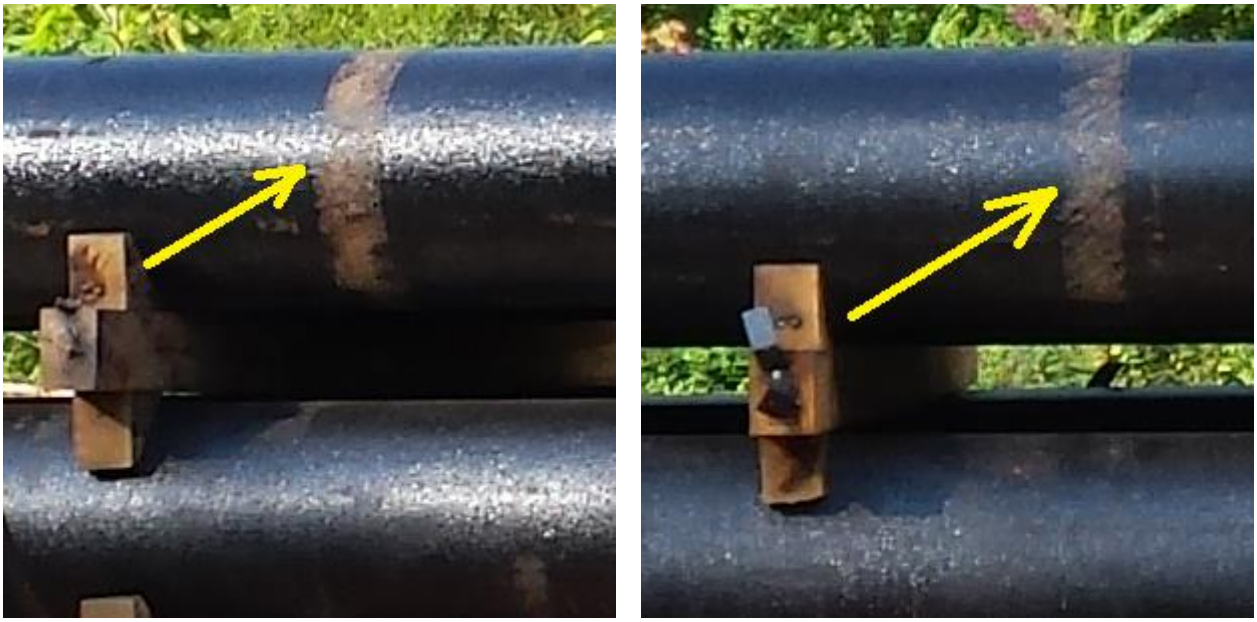

(d)

Figure 4. (a) 6-in. AMERICAN ductile iron pipes prepared for installation. (b) Damaged asphalt topcoat on one of similar quality pipes. (c) A soft asphaltic topcoat damged while heavy DIPs were either lifted by a crane, or slid on wood brackets, or both—under these circumstancers a zinc basecoat would not be damaged but seen if present. Pictures taken in Knoxville, TN, August 26, 2016.

(a)

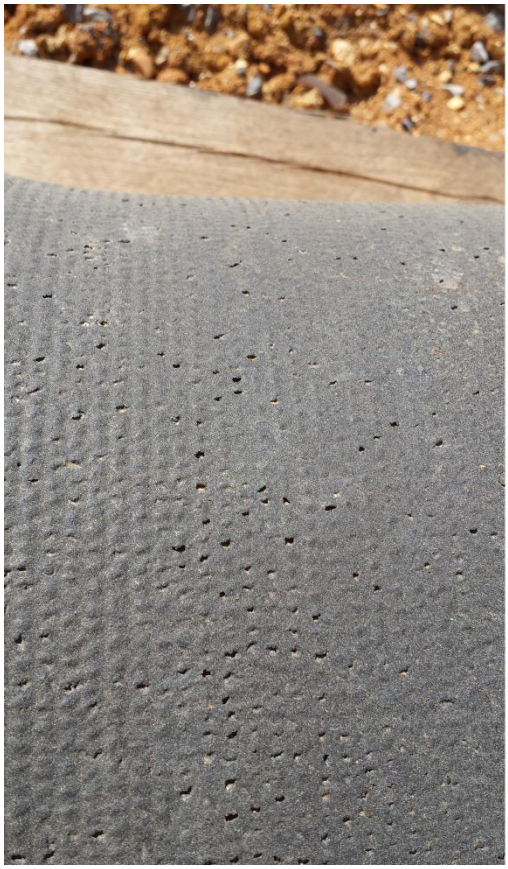

(b)

(c)

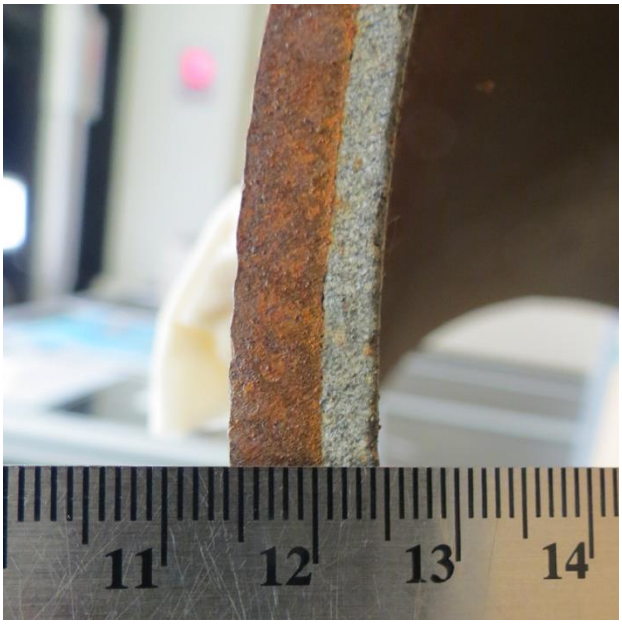

(d) WT = 6 mm.

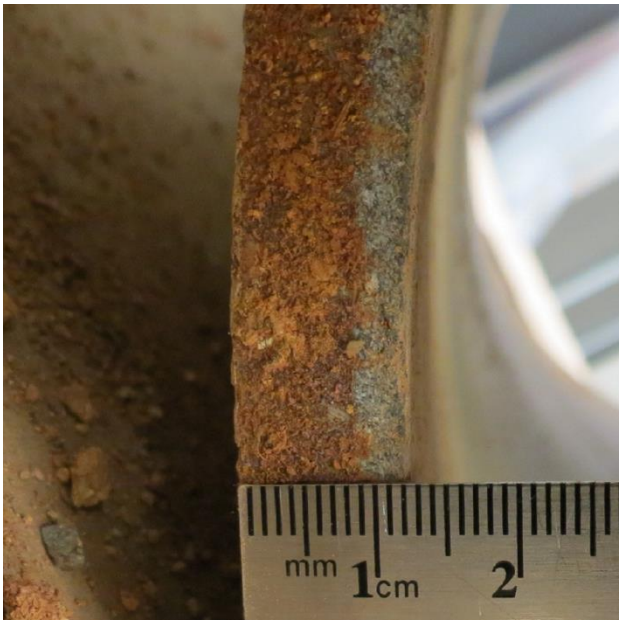

(e) WT = 9 mm.

Figure 5. (a) A fragment of the A12-1 DIP. (b) Technological defects/holes in a tar coat. (c) A mechanically-damaged tar coating. (d,e) The wall thickness (WT) of the DIP varied from approximately 6 to 9 mm. The total thichkness of the pipe (together with cement lining) varied from 10.8 to 12.2 mm.

Microstructure of ductile iron in AMERICAN pipe

The AMERICAN pipe had a ferrite-perlite microstructure (Figure 6). DIP with such a microstructure has a higher strength and a lower ductility that DIP with the microstructure of ferrite (Figure 1b).

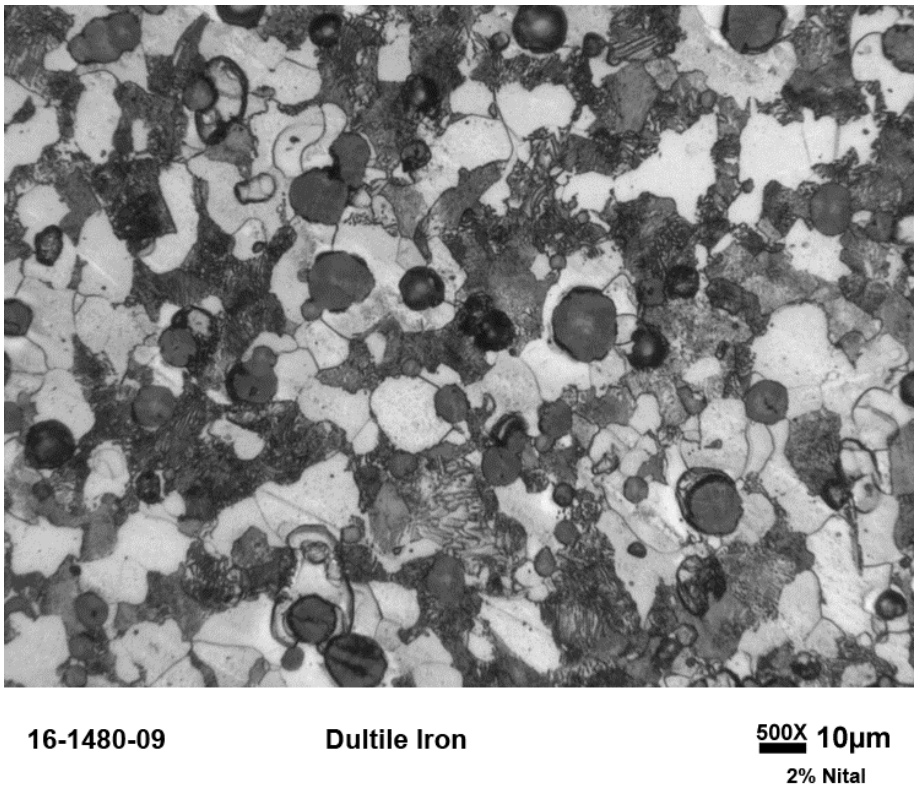

Figure 6. Optical photographs of DIP in the the AMERICAN pipe.

Mechanical Properties of DIP

According to the specification, the ductile iron in AMERICAN pipe is grade 60-42-10, an annealed grade with the following specified properties: ultimate tensile strength, 60 ksi (415 MPa), yield strength, 42 ksi (290 MPa), and percent elongation at failure, 10% (Table 4).

Results of the mechanical tests of the AMERICAN pipe (Table 4 and Figure 7a) show that the ductile iron tested in this study was significantly stronger and less ductile than specified.

Table 4. Mechanical properties of the DIPs tested

DIP	Tensile strength		Yield strength		Elongation (%)
	(ksi)	(MPa)	(ksi)	(MPa)	
Standard specification	60	413.7	42	289.6	10
A04-1	90.3	622.6	54.7	377.1	6.3
M04-1	90.0	620.5	60.1	414.4	3.1
U04-1	69.2	477.1	47.1	324.7	7.2

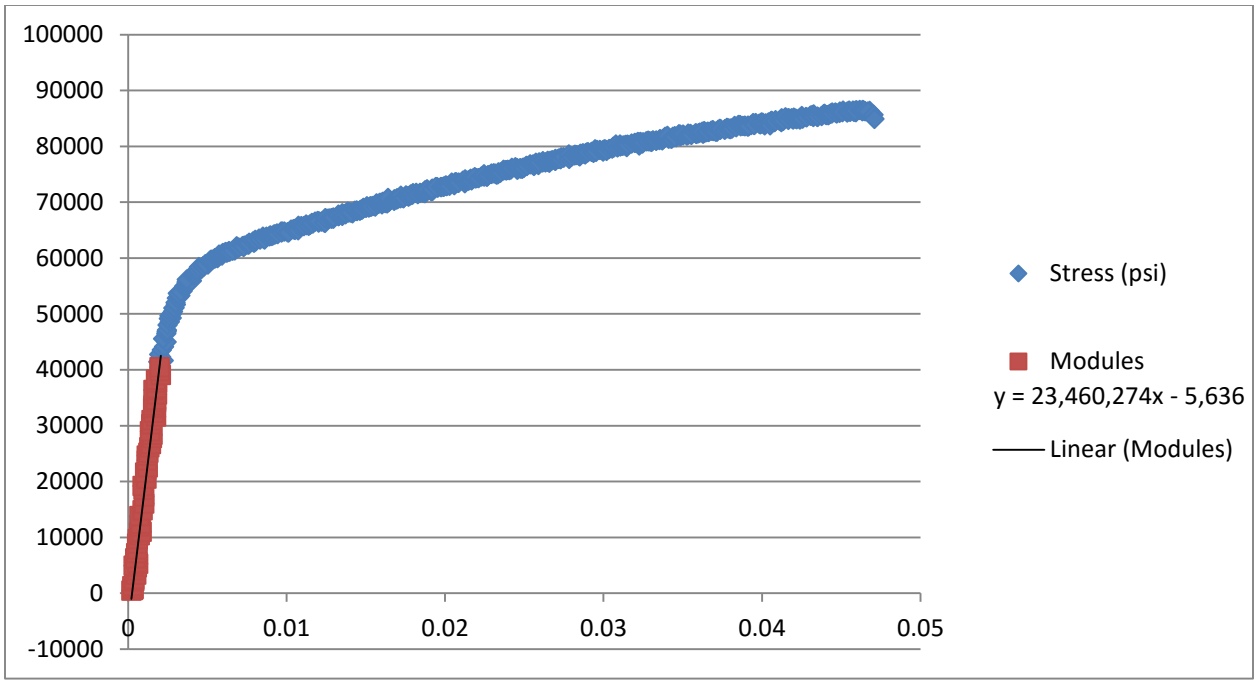
100000
90000
80000
70000
60000
50000
40000
30000
20000
10000
0
-10000
0
0.01
0.02
0.03
0.04
0.05
Stress (psi)
Modules
y = 23,460,274x - 5,636
Linear (Modules)

(a)

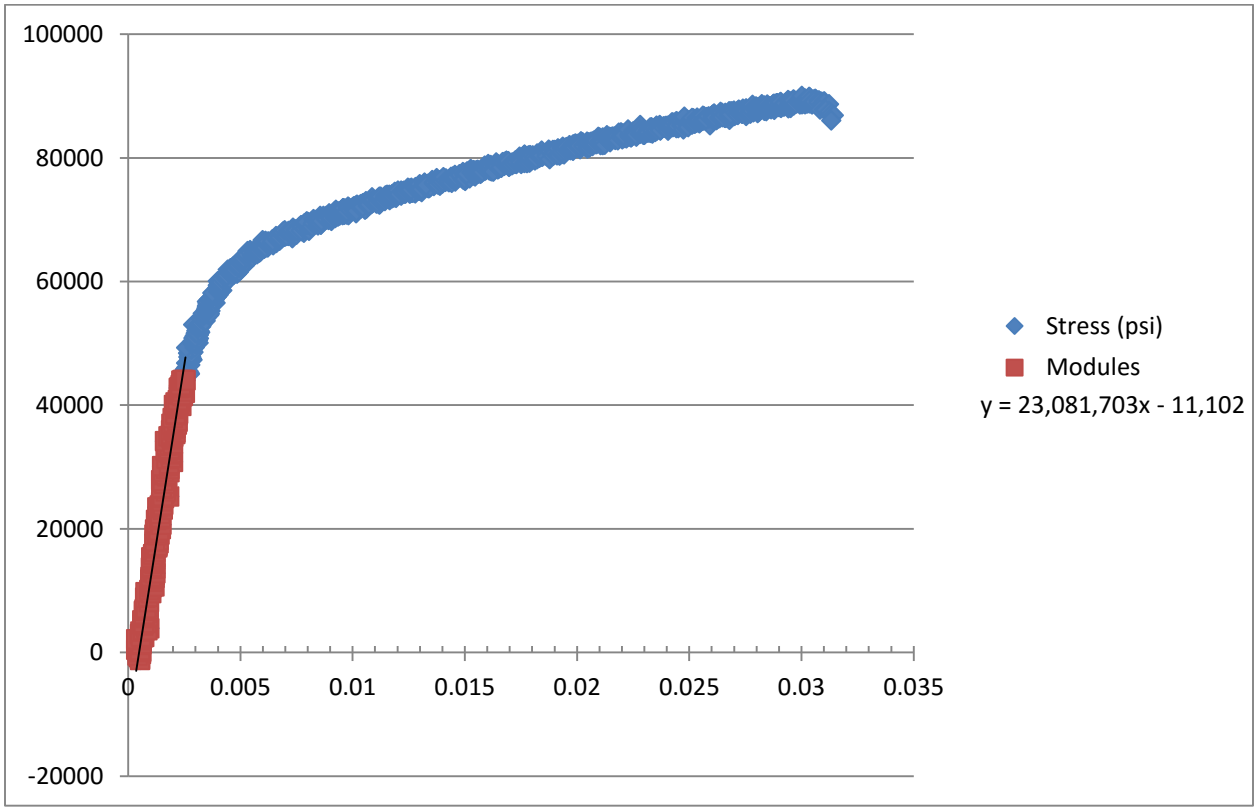
100000
80000
60000
40000
20000
0
-20000
0
0.005
0.01
0.015
0.02
0.025
0.03
0.035
Stress (psi)
Modules
y = 23,081,703x - 11,102

(b)

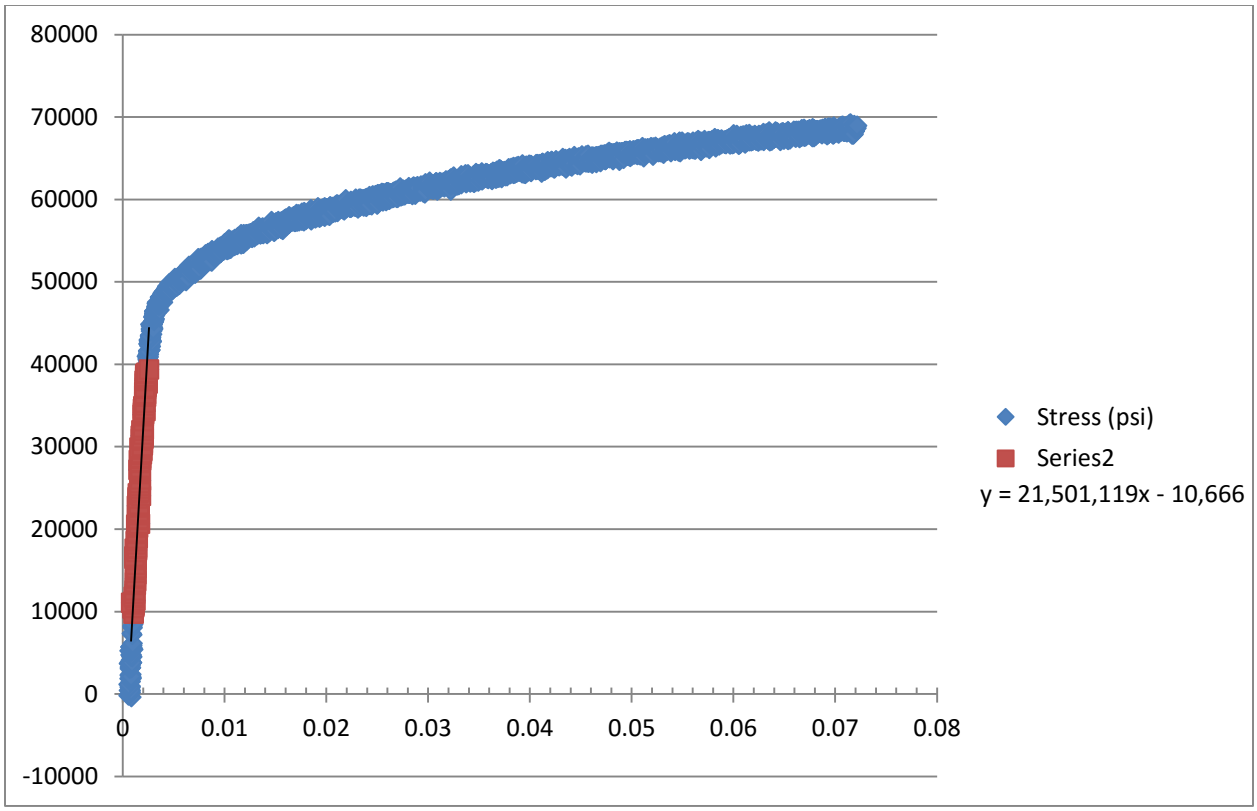

(c)

Figure 7. Stress-strain behavior for DIPs: (a) A04-1; (b) M04-1, and (c) U04-1.

2.3 CHARACTERIZATION OF DIP

Characterization was performed via optical imaging, scanning electron microscopy (SEM) using Hitachi S3400 and S4800 SEM, electron probe microanalysis (EPMA) using JEOL 8200 with wavelength dispersive X-ray analysis, and scanning/transmission electron microscopy (S/TEM). TEM lamella was prepared via the focus ion beam (FIB) *in situ* lift-out technique using a Hitachi NB5000 FIB–SEM and was examined by S/TEM FEI Talos F200X operated at 200 kV and equipped with an extreme field emission gun (X-FEG) electron source and Super-X EDS (energy dispersive spectroscopy) system with 4 Silicon drift detectors (SDD) for chemical analysis.

Manufactures claimed that an oxide film (130-140 µm) is created on the external surface of DIP before a Zn coating is applied. After that, the pipe is covered by the oxidized surface by Zn, and finally by asphalt. In the studied specimen, no Zn was observed between the oxide and the asphalt. On top of it, the oxide layer is not “continuous”.. All these factors may suggest a “weak point and initiation area for failure.”

Figure 8 shows cross-sections of the specimens obtained from 3 different commercial pipes distributers. It is evident that 3-layer structure is present on the surface of each pipe. The asphalt layer (I - outer) is not continuous and is about 50 µm thick for all three pipes. The “mid layer” or outer oxide layer (II) varies in thickness between three manufactures with the thinnest of 42 µm found in U.S. DIP and the thickest being in McWane DIP (65 µm). The thinnest inner layer was found in American DIP (25.2 ± 4.7 µm). The measurement of the total oxide thickness that includes inner (III) and outer (II) oxide layer was also

performed and the summary is shown in Figure 3. The thickest scale was measured on McWane pipe (92.5±17 µm), while the thinnest was measured on American DIP (67±10 µm). Overall the thickness in all three pipes stays between 60-100 µm ranges.

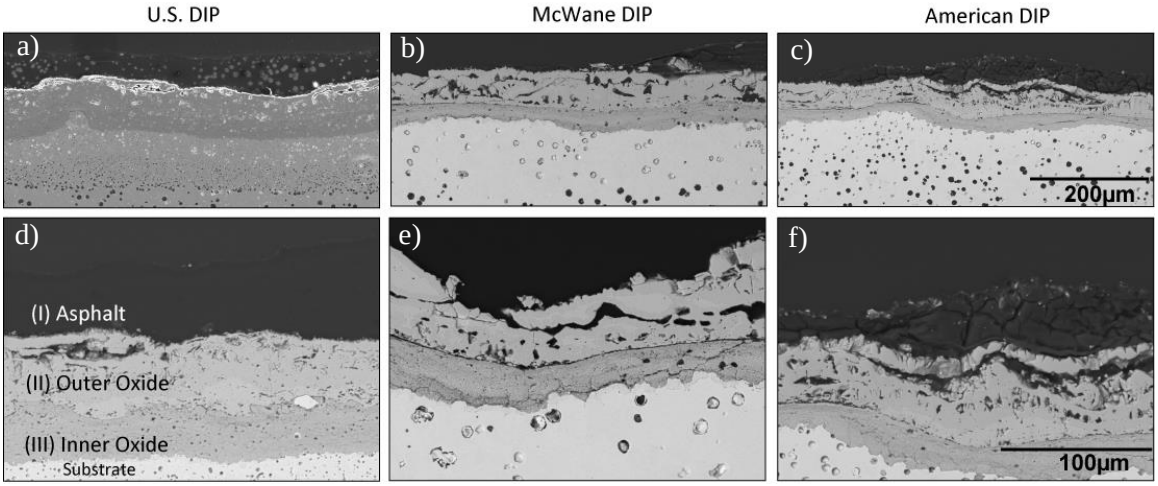

Figure 8. Cross-sections of the DIP pipes in as received state from U.S. (a,d) DIP, (b,e) McWane DIP, and (c,f) AMERICAN DIP.

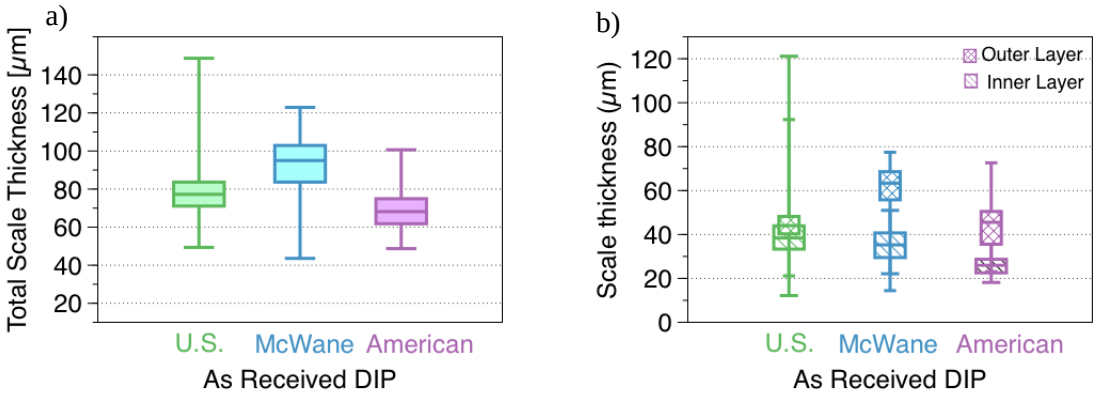

Figure 9. Measurements of (a) the total oxide thickness and of the (b) inner and outer layers.

EDS analysis was performed on all three specimens. The two-layer oxide is mainly Fe-rich with some enrichment in Si in the inner oxide layer. Example of the EDS elemental maps and BSE image showing location of the analysis for US DIP is shown in Figure 10, for McWane DIP in Figure 11, and in Figure 12 for AMERICAN DIP.

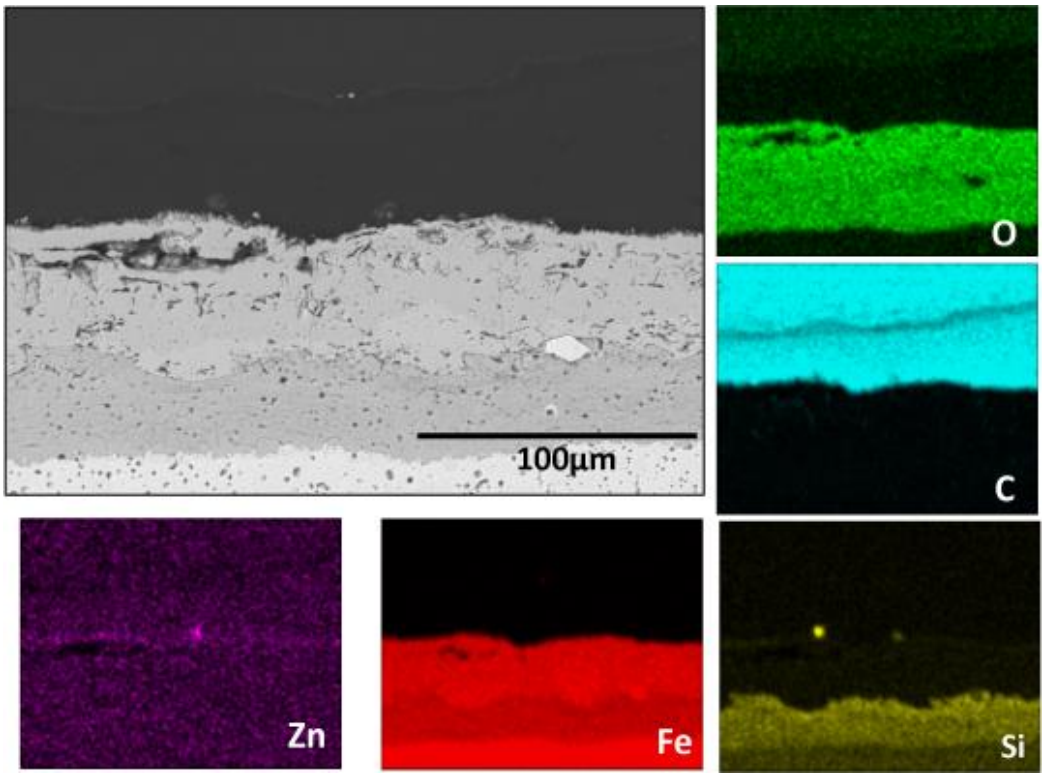

Figure 10. BSE image showing cross-section of layers present on US DIP in as received condition with EDS elemental maps for O, C, Fe, Si, Zn.

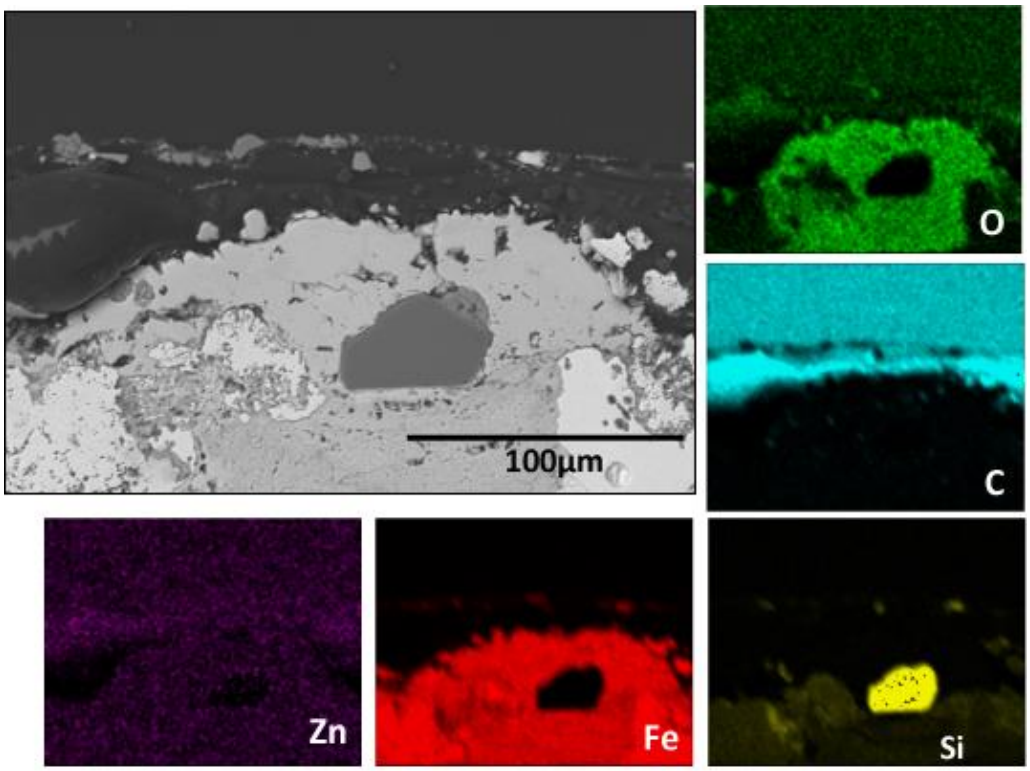

Figure 11. BSE image showing cross section of layers present on McWane DIP in as received condition with EDS elemental maps for O, C, Fe, Si, Zn.

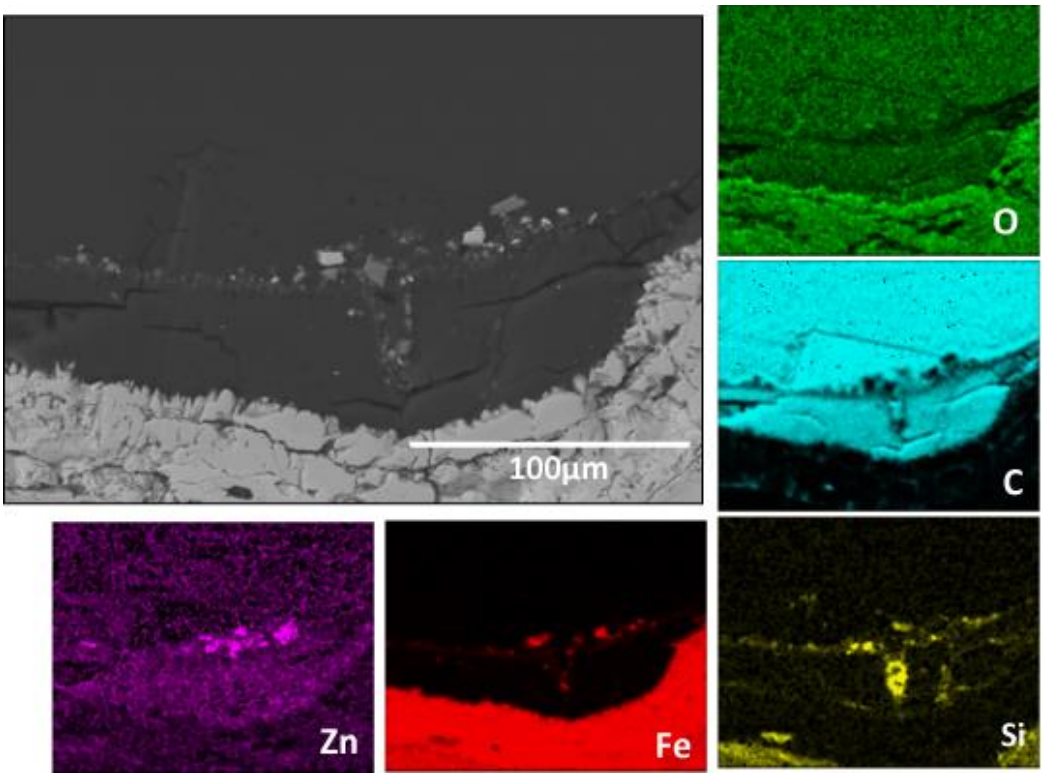

Figure 12. BSE image showing cross-section of layers present on AMERICAN DIP in as-received condition.

EPMA characterization was performed on the American DIP in as-received condition. Figure 13a shows cross-section of the American DIP with an identified location of the EPMA line scan. Figure 13b shows the EPMA results of the composition (at.%) versus distance from the surface generated through the asphalt (I), oxide layer (including outer oxide (II) and inner oxide (III) layers) and substrate. Clearly within the asphalt there is Zn oxide detected (about µm thick) (Fig. 13c). The oxide is mainly Fe oxide with the inner layer being enriched additionally in Si.

Detail examination of the oxide interface between inner and outer layer was carried out as well as analysis of the interface between inner oxide and substrate. Figure 14 shows an example of the BF-STEM and HAADF-STEM showing cross-section of the outer-inner oxide interface outlined by red dash line with arrow pointing to SEM-BSE image of approximate location. Both oxide layers are constructed of equiaxed grains with smaller grain size in the inner oxide layer.

EDS elementals maps were generated from the location shown via BF-and HAADF-STEM in Figure 15. Clearly the oxide is composed of Fe and inner layer is enriched in Si and C, confirming EDS results generated on SEM from the bulk specimen. Additionally, the interface between two oxides is quite smooth.

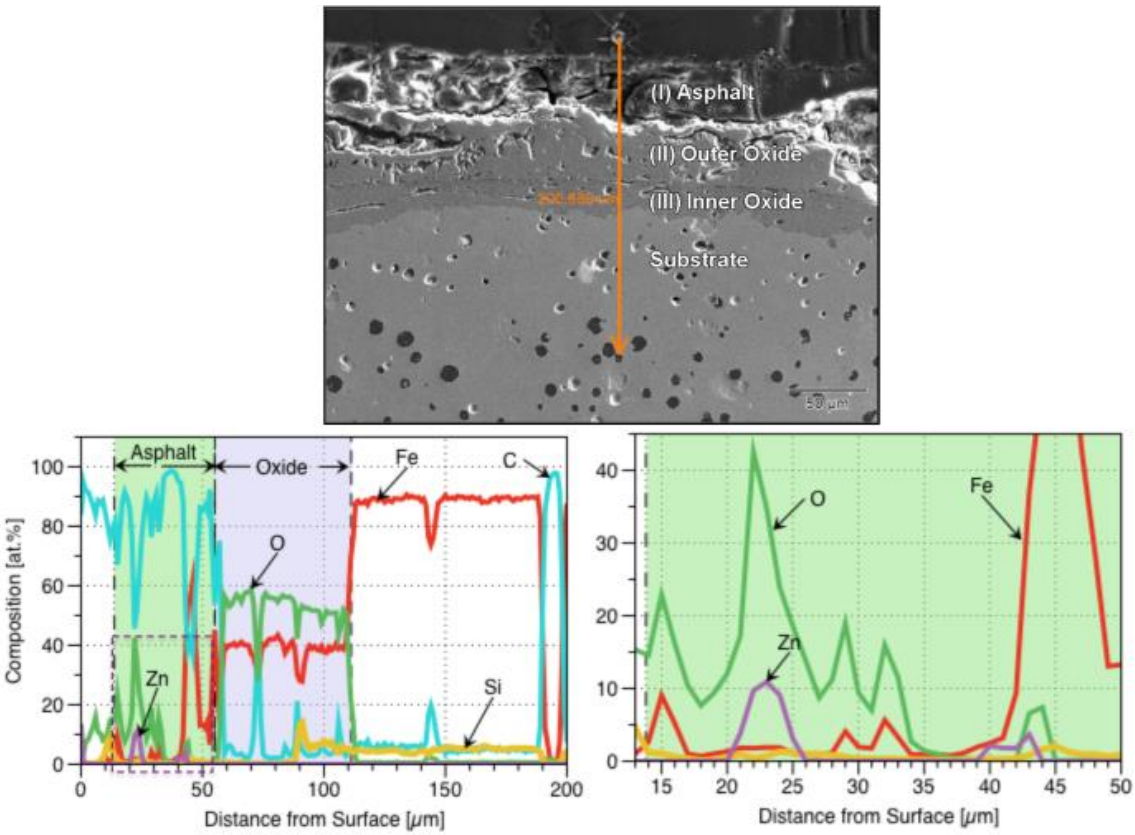

(b) (c)

Figure 13. BSE image showing cross-section of layers present on American DIP in as-received condition with marked EPMA line and (b) corresponding EPMA line scan composition results versus distance with (c) zoom in area showing presence of Zn.

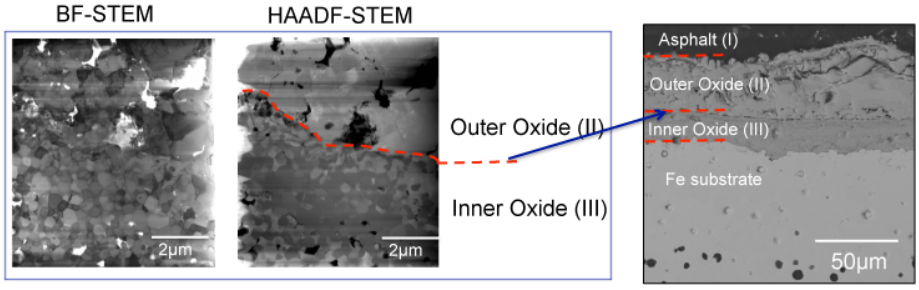

Figure 14. BF-STEM and HAADF-STEM showing cross-section of the outer-inner oxide interface with arrow pointing to SEM-BSE image of approximate location.

EDS elemental maps were also generated from the inner oxide and substrate interface (outline by red dash line). The location from were the maps were generated is shown in Figure 16 via HAADF-STEM. Clearly the inner oxide is composed of Fe and Si. From the metal/oxide interface into the metal carburization (*C map*) is visible, which is outlined by oxidation of Si (*Si and O maps*).

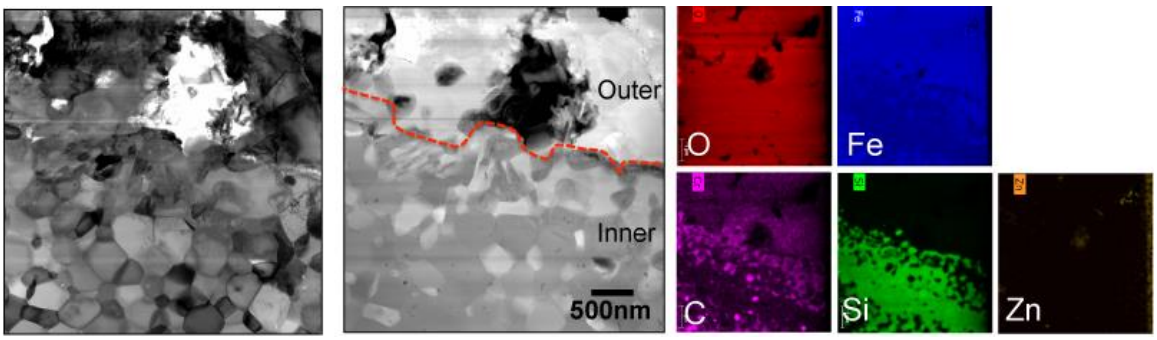

Figure 15. BF-STEM and HAADF-STEM showing cross-section of the outer-inner oxide interface (outline by red dash line) with EDS elemental maps.

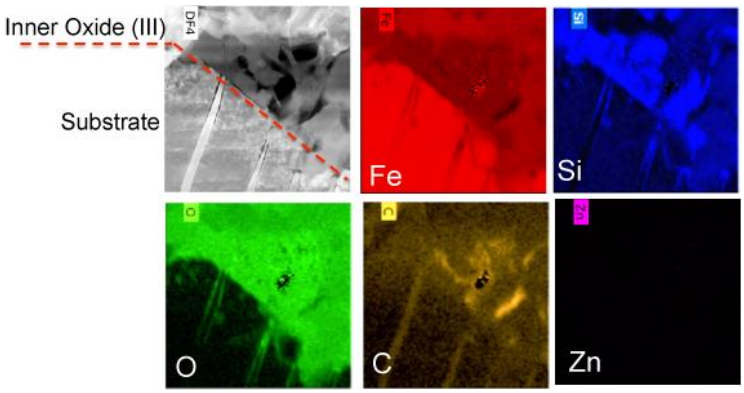

Figure 16. HAADF-STEM showing cross-section of the inner oxide and substrate interface (outline by red dash line) with EDS elemental maps.

Additionally the surface of the asphalt was examined using TEM as shown in Figure 17. Small Zn oxides were found on the surface of the asphalt dispersed randomly in discontinuous manner. The interface between asphalt and outer oxide layer did not show any segregation of Zn (Figure 18).

Further, examination of the specimens revealed that in some locations there is also internal oxidation present and an example of the cross-section with a deep internal oxidation is shown in Figure 19 obtained from the ductile iron after is shown in Figure 19. The deep cracks mixed with internal. Further, EDS analysis of the oxidized crack indicated presence of Fe-rich oxide (center of the crack) Si,Fe-rich oxide mainly in the contact with substrate (Fig. 20). Additionally, segregation of carbon was detected (*C map*) at the interface between either matrix/Si-rich oxide or Si-rich oxide and Fe-rich oxide. This clearly cannot be identified based on these lower magnification maps.

Thus, higher magnification image of the crack is shown in Figure 21 with EDS elemental maps, where it is clearly revealed that the C is not at the substrate/Si,Fe-rich oxide interface but incorporated at the Si,Fe-rich/Fe-rich interface. Surprisingly, EDS maps showed presence of the second phase within the substrate.

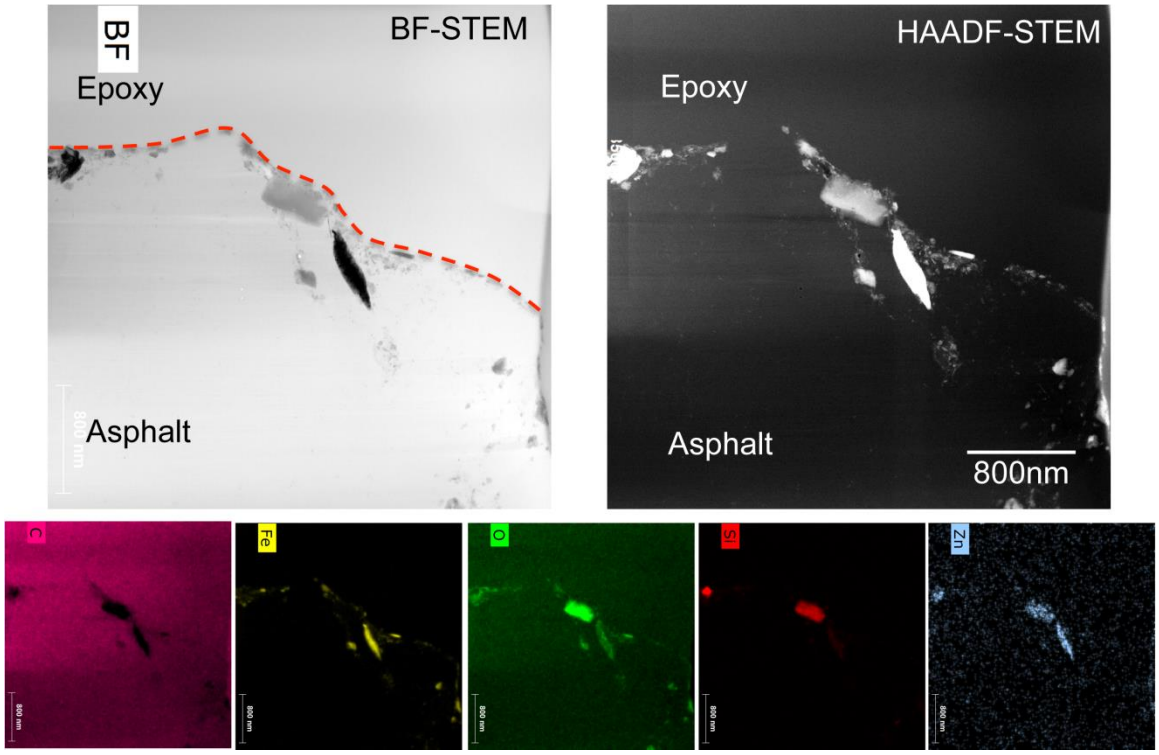

Figure 17. BF-STEM and HAADF STEM images showing cross section of the asphalt with the top surface. EDS elemental maps for that location.

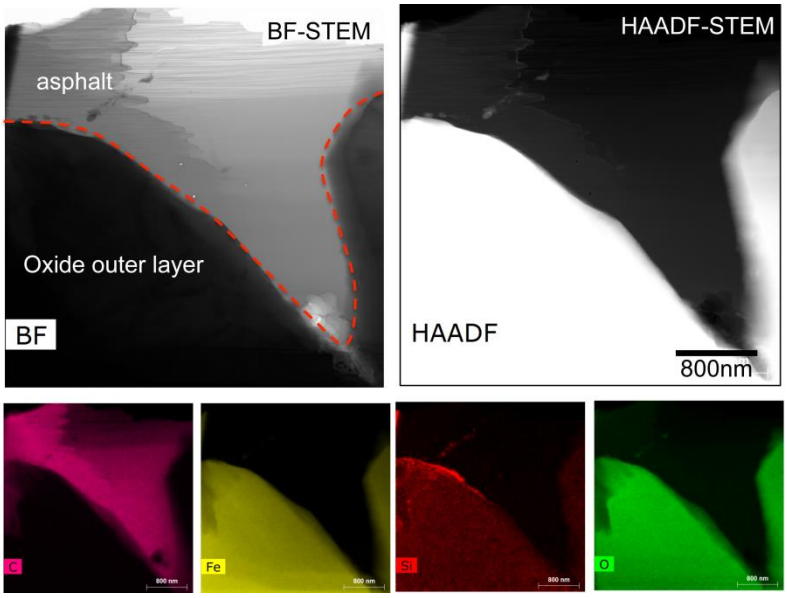

Figure 18. Example of asphalt/oxide interface with EDS maps.

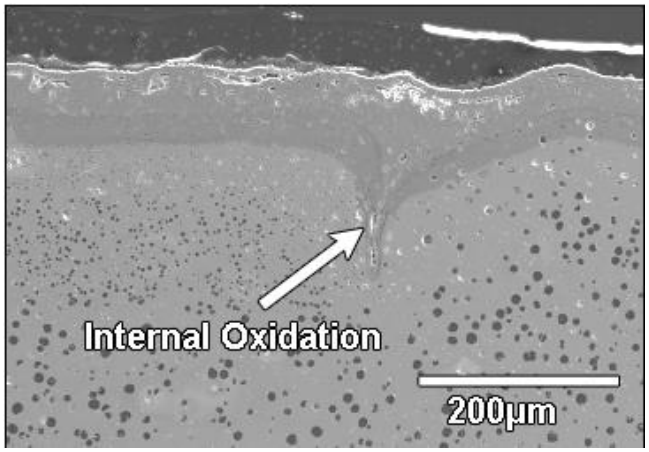

Figure 19. Secondary electron SEM image of the cross-section of DIP after applying grit blasting to the surface.

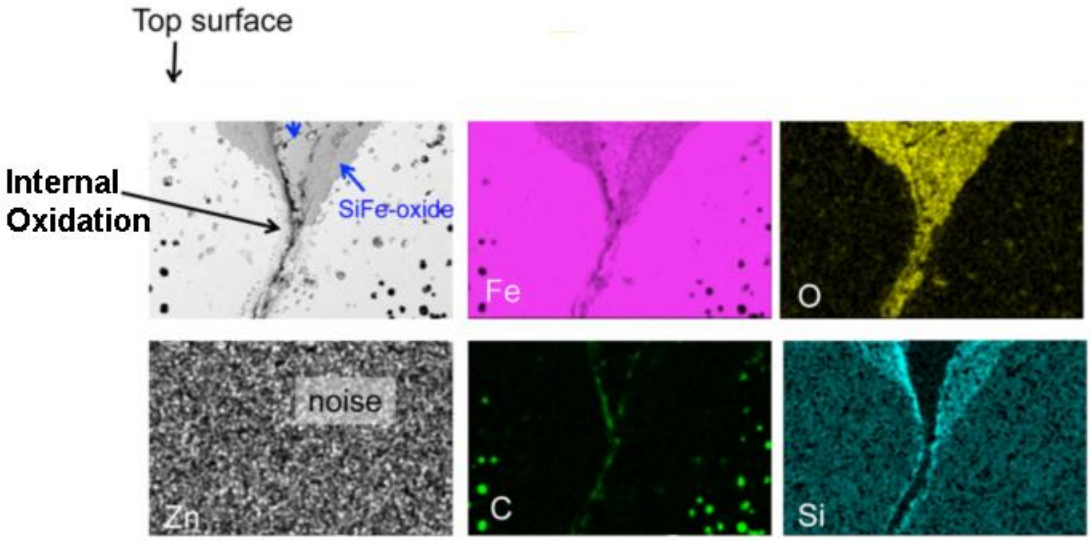

Figure 20. BSE image with corresponding EDS elemental maps.

Oxidation and Time Determination

The aim of the oxidation testing was to determine the thickness of the grown oxide to match the oxide thickness present on the commercial material in as received conditions. Oxidation was performed for 0.5, 1, and 2 hours at 930 °C in air. Also, one test was performed at lower temperature (900 °C) for 8 hours. All the testing was carried out on the specimen prepared from the American DIP. Figure 22 shows lower and higher magnification images of the oxide cross-section. Two layer structure is visible similar to the oxide formed on the commercial pipe.

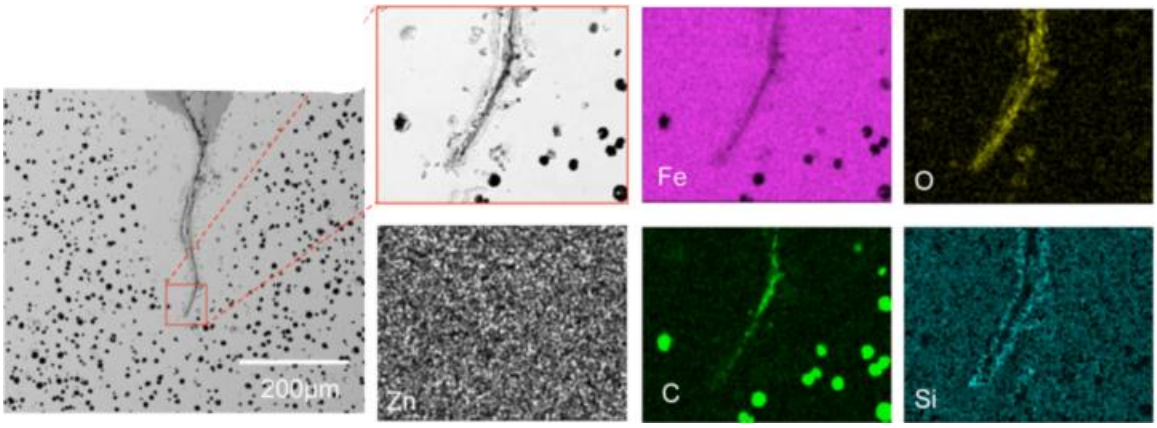

Figure 21. BSE image with corresponding EDS elemental maps generated at higher magnification than maps in Fig. 11.

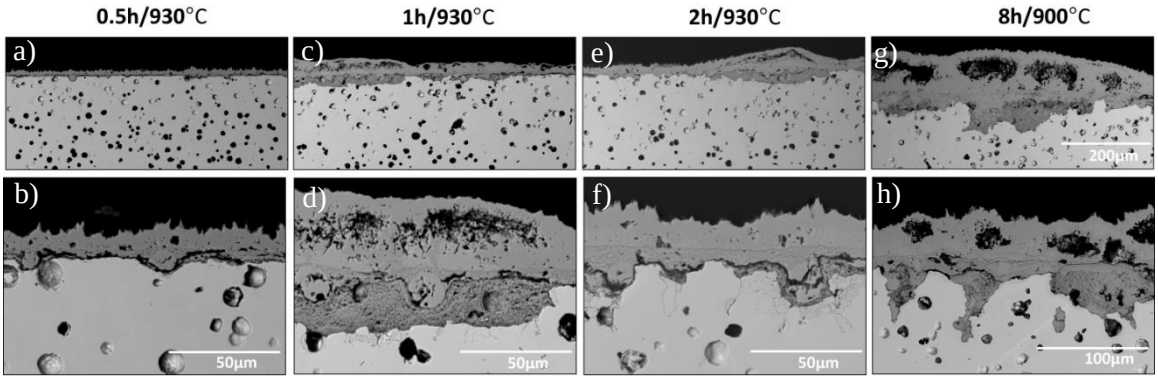

Figure 22. BSE images of the oxide cross-section formed on American DIP after oxidation in air at 930°C after (a,b) 0.5h, (c,d) 1h, (e,f) 2h, and (g,h) after 8h exposure at 900 °C.

The measurement of the total oxide thickness that includes inner and outer oxide layer as well as measurements of individual layers (e.g. inner and outer) were also performed and the summary is shown in Figure 23. As expected, the thickness of the scale grew with time. Also, with time the data were more scattered. The longest exposure time (8 hours) at the lowest temperature (900 °C) resulted in the thickest surface oxide (130 µm). The scale thickness is too thick when compared with the oxide present on commercial product and it is not a desired condition to mimic oxide formed on commercial pipe, which is in the range of 60-90 µm (Fig. 9).

However, oxidation at higher temperature (930 °C) but shorter times was not sufficient to reproduce the thickness of the scale as it was measured on commercial product. All the oxide thicknesses fall below 40 µm, which is too thin and the results suggests that oxidation for 4 hours at 930 °C would be the most suitable at this temperature or oxidation at higher temperature.

As follow, oxidation at higher temperature (950 °C) was performed. Example of the oxide cross-section formed at 950 °C after 1, 2 and 4 hours on American DIP is shown in Figure 23. However, oxidation for 2 h at 950 °C produced a slightly thinner oxidethan the commercial product. These results suggest that oxidation at 950 °C for 2.5-3 hours should produce oxide with the desire thickness.

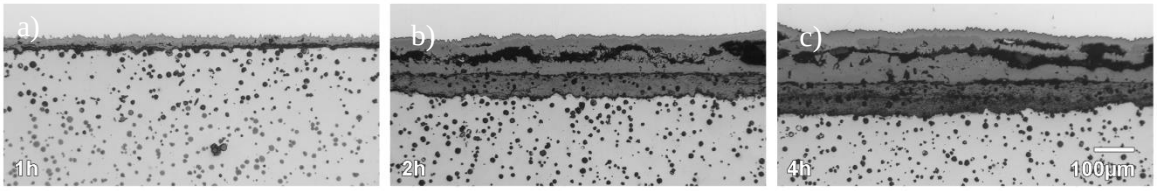

Figure 23. Optical images of the oxide cross-section formed on American DIP after oxidation in air at 950°C after 1h (a), 2h (b), and 4h (c).

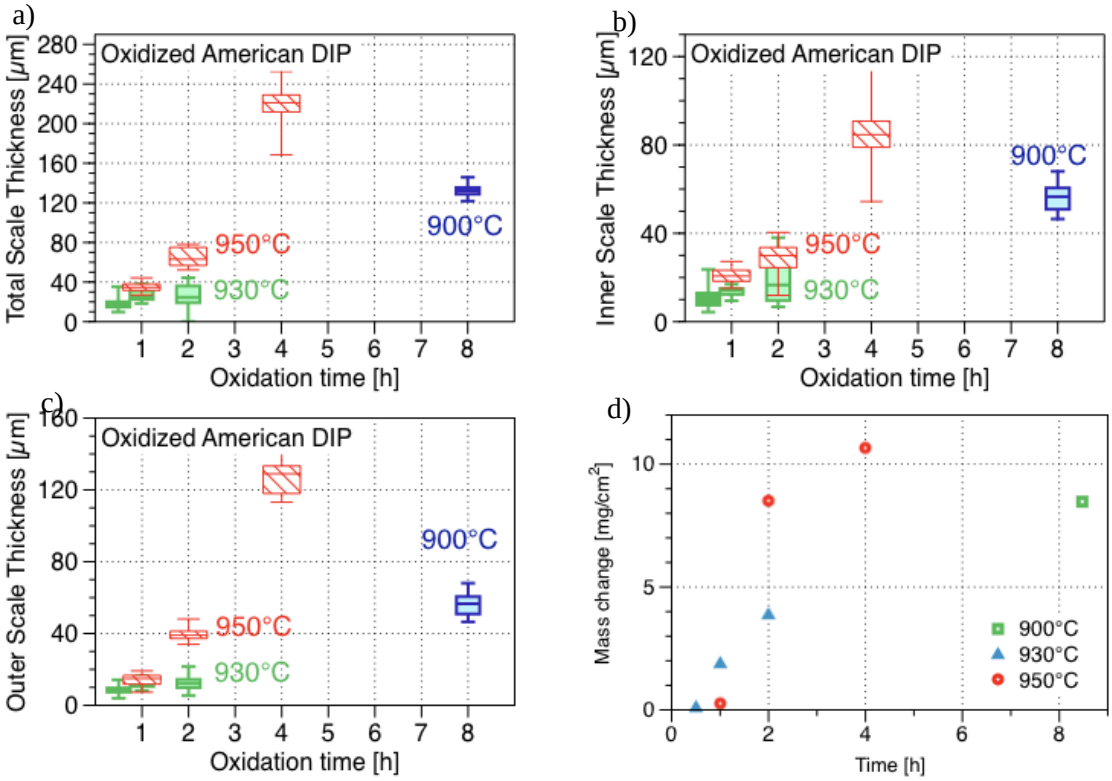

Figure 24. Measurements of the oxide formed on American DIP after oxidation at 900 °C, 930 °C, and 950 °C. (a) Total scale thickness and (b) Inner and c) outer scale thickness. (d) mass change measurements after oxidation at these three temperatures.

Summary

Ductile iron pipes for this study were received from three different distributers. Various characterization techniques were used. The following can be summarized:

- Oxide was a two layer structure composed mainly of Fe.
- Inner oxide layer was enriched in Si.
- Oxidation for 4 hours at 930 °C is recommended to match commercial product or oxidation at 950 °C for 2.5-3 hours. These conditions should produce oxide thickness comparable with oxide formation on the commercial product.

3. CONSOLIDATE AVAILABLE CORROSION DATA (Task 2)

3.1 CORROSION IN SOILS

3.1.1 Soil corrosivity classification

For design and corrosion risk assessment purposes, it is desirable to estimate the corrosivity of soils. One of the simplest classifications is based on a single parameter, soil resistivity. The generally adopted corrosion severity ratings are shown in Table 5.

Table 5 Classification (Corrosivity Rating) Based on Soil Resistivity

Soil resistivity (ohm cm)	Classification
<1000	Extremely corrosive
1000-3000	Highly corrosive
3000-5000	Corrosive
5000-10000	Moderately corrosive
10000-20000	Mildly corrosive
>20,000	Essentially non-corrosive

Sandy soils are high up on the resistivity scale and therefore considered the least corrosive. Clay soils, especially those contaminated with saline water are on the opposite end of the spectrum. The soil resistivity parameter is very widely used in practice, and is generally considered to be the dominant variable in the absence of microbial activity.

4. EXPLORE ACCELERATED LABORATORY TESTING (Task 4)

In the laboratory, the classical cabinet tests do not represent the reality of the behavior in service. For example, the salt spray test is not representative of the aggressive conditions of corrosion in soil, but rather it characterizes the porosity of a coating.The use of coupons (1½ by 1½ in) does not properly account for the presence of residual stresses existing in real DIP. A simple aqueous NaCl solution does not consider the pH buffered by soil bicarbonates and biocorrosion factors.

In addition, the field studies conducted by NBS from 1911-1952 concerning the corrosiveness of some of the soils are practically important in that they furnished the means by which the results of the laboratory experiments could be tested and the limitations and usefulness of newly proposed field tests (for example, on ORNL campus) evaluated.

Soil is an aggregate of minerals, organic matter, water, and gasses (mostly air). The proportions of the basic constituents vary greatly in different soil types and even in the same location (Figure 25).

4.1 ELECTROCHEMICAL TESTS

Electrochemical tests are performed using a cylindrical coupons cut of DIP (Figure 26) in various synthetic solutions (Table 6-9).

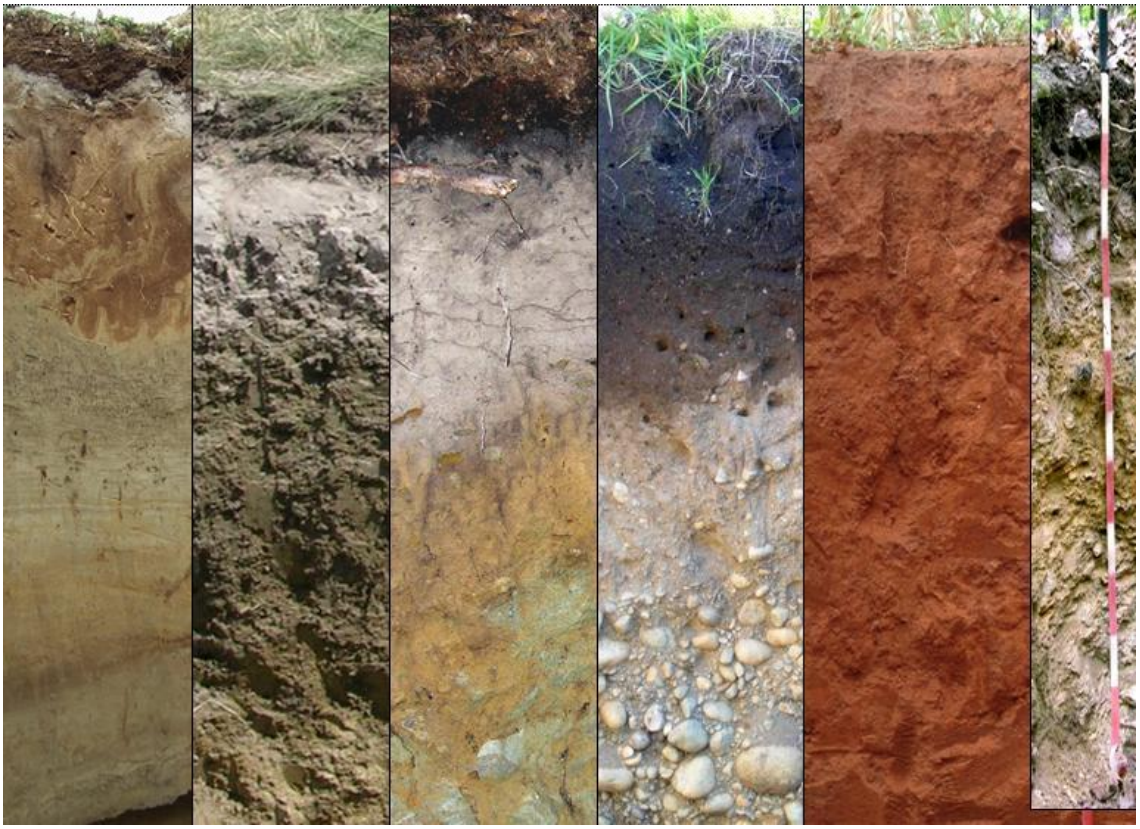

Figure 25. Different soil types.

4.2 EVALUATION OF NBS CORROSION DATA

From 1910-1952 the National Bureau of Standards (now NIST) provided corrosion data from 95 soils and 128 sites. Jointly with the Geographic Information Science & Technology Group we are analyzing this data using quantitative and computational methods to better understand soil corrosion (Figures 27-33).

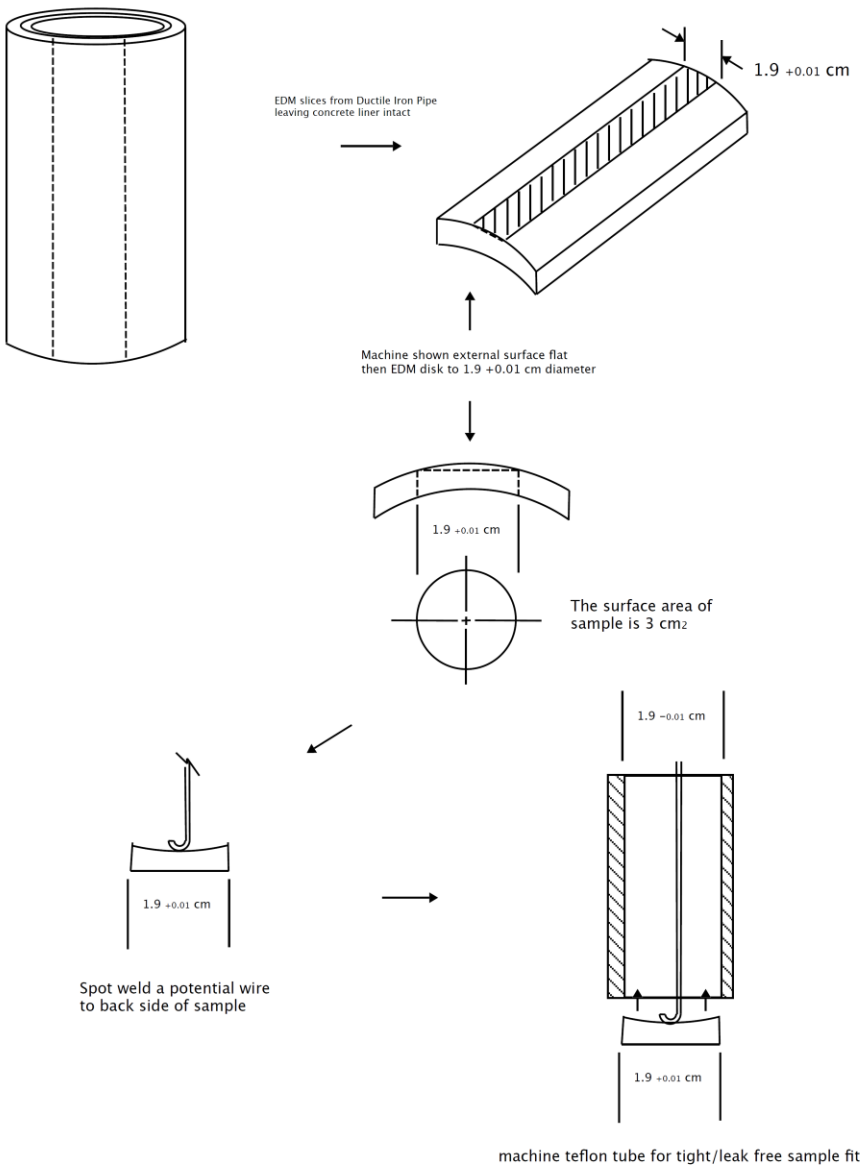

Figure 26. The procedure of sample fabrication for electrochemical tests.

Table 6. Synthetic solutions used to study microbiologically-influenced corrosion (MIC).

Composition (g/l)	#1[(A),3]	#2[(A),4]	#3[(B),5]	#4[6]	#5[7]
$NaHCO_3$	16.8	0.437		4.2	
Na_2CO_3		0.657			
$NaHCO_3/Na_2CO_3$					19[(C)]
Na_2SO_4	14.2	0.071			14.2
NaCl	5.8	0.035	35.06		5.84
$NaClO_4$		12.24			
$NaH_2PO_4 + Na_2HPO_4$			13.1[(C)]		
H_2S					0.034
$Na_2S \cdot 9H_2O$				0.24	
pH	8.9 ± 0.5	8.9 ± 0.5	7.2		9.5

(A) Preconditioning solution of 1 M $NaHCO_3/Na_2CO_3$ was used to pre-form a siderite film.
(B) 0.6, 3, and 15 mM H_2S was added as saturated, pre-analyzed solution after purging 200 ml of the base solution with gold spot nitrogen for four hours.
(C) Assuming equal amount of both substances.

Table 7. Synthetic solutions used to study stress corrosion cracking.

Composition (mg/l)	#1 NS1	#2 NS2	#3 NS3	#4 NS4	#5 NOVATW	#6 C1	#7 C2	#8 C3	#9 C4
$MgSO_4 \cdot 7H_2O$	106	254	89	131		27.4	27.4	27.4	27.4
$CaCl_2 \cdot 2H_2O$	159	73	8	181					
$CaCl_2$						25.5	25.5	25.5	25.5
KCl	149	142	37	122	14.9	3.5	3.5	3.5	3.5
$NaHCO_3$	504	1031	559	483	436.9	19.5	19.5	19.5	19.5
$CaCO_3$					230.2	6.1	60.6	242.2	484.5
$MgCO_3$					354				
$CaSO_4 \cdot 2H_2O$					34.5				
pH (purged with 5% $CO_2 + N_2$)				8.4	7.1	5.9	6.3	6.9	7.2

[3] B. Sherar, P. Keech, D. Shoesmith, Effect of Sulfide on Carbon Steel Corrosion in Anaerobic Near-Neutral pH Saline Solutions, 2013, *Corrosion*, Vol.69, No. 1.
[4] B. Sherar, P. Keech, D. Shoesmith, Effect of Sulfide on Carbon Steel Corrosion in Anaerobic Near-Neutral pH Saline Solutions, 2013, *Corrosion*, Vol.69, No. 1.
[5] R.C. Newman, K. Rumash, B.J. Webster, The Effect of Pre-Corrosion on the Corrosion Rate of Steel in Neutral Solutions Containing Sulphide: Relevance to Microbially Influenced Corrosion, Corrosion Science, Vol.33, No.12, pp.1877-1884, 1992.
[6] B.W. Sherar, I.M. Power, P.G. Keech, S.Mitlin, G. Southam, D.W. Shoesmith, Characterizing the effect of carbon steel exposure in sulfide containing solutions in mictrobially induced corrosion, Corrosion Science 53 (2011), 955-960.
[7] B.W. Sherar, I.M. Power, P.G. Keech, S.Mitlin, G. Southam, D.W. Shoesmith, Characterizing the effect of carbon steel exposure in sulfide containing solutions in mictrobially induced corrosion, Corrosion Science 53 (2011), 955-960.

Table 8. Synthetic solutions used to study soil corrosion behavior (with concentration mg/l).

Composition (mg/l)	#1	#2	#3*	#4	#5	#6	#7	#8	#9
KCl	0.42								
$NaHSO_4 \cdot H_2O$					447.5	8.95			
$NaHCO_3$		420	0.0292	437					
$CaCl_2$	0.18		0.0238						
$MgSO_4$	0.05		0.0455						
K_2SO_4									
$CaSO_4$	0.21								
Na_2CO_3				657					
$Na_2SO_4 \cdot 10H_2O$		1611.1							
Na_2SO_4			0.0312	71			9.216	9.216	9.216
NaCl		146.1	0.0921	35					
$NaClO_4$				12240					
$MgCl_2 \cdot 6H_2O$					26.04	26.04	26.04	26.04	26.04
Na_2S	0.22								
$NaNO_3$	0.11								
NaOH								4	400
KNO_3	0.17		0.0413						
$FeSO_4$	0.17								
pH	7.0± 0.5	8.2± 0.5	8.1		3.5	4.8	7	9.6	12.3

* wt.%

Table 9. Synthetic solutions used to study soil corrosion behavior (with concentration g/l).

Composition (g/l)	#1	#2	#3
$NaHCO_3$	16.8	16.8	0.16
$MgSO_4$			29.04
K_2SO_4			1.82
$CaSO_4$			2
Na_2SO_4	14.2	14.2	37.48
NaCl	5.8	5.8	22.69
pH	8.9		8.8

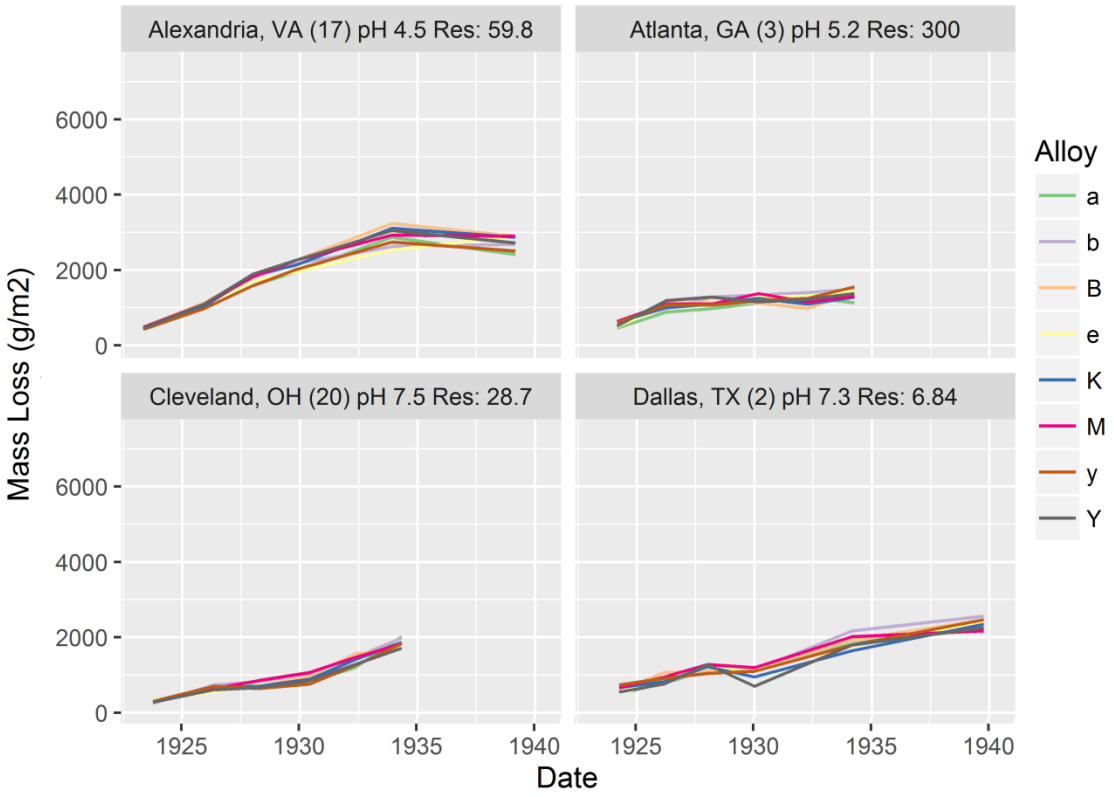
Alexandria, VA (17) pH 4.5 Res: 59.8
Atlanta, GA (3) pH 5.2 Res: 300
Cleveland, OH (20) pH 7.5 Res: 28.7
Dallas, TX (2) pH 7.3 Res: 6.84
Mass Loss (g/m2)
0
2000
4000
6000
1925
1930
1935
1940
Date
Alloy
a
b
B
e
K
M
y
Y

(a)

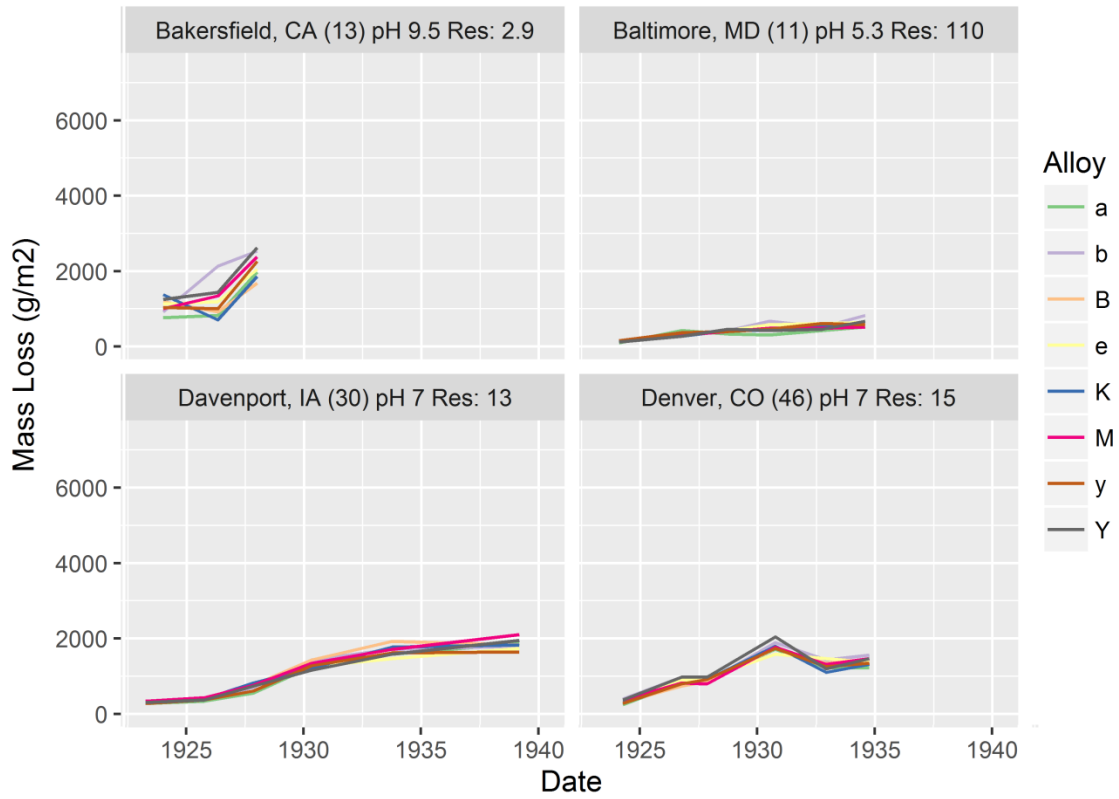
Bakersfield, CA (13) pH 9.5 Res: 2.9
Baltimore, MD (11) pH 5.3 Res: 110
Davenport, IA (30) pH 7 Res: 13
Denver, CO (46) pH 7 Res: 15
Mass Loss (g/m2)
0
2000
4000
6000
1925
1930
1935
1940
Date
Alloy
a
b
B
e
K
M
y
Y

(b)

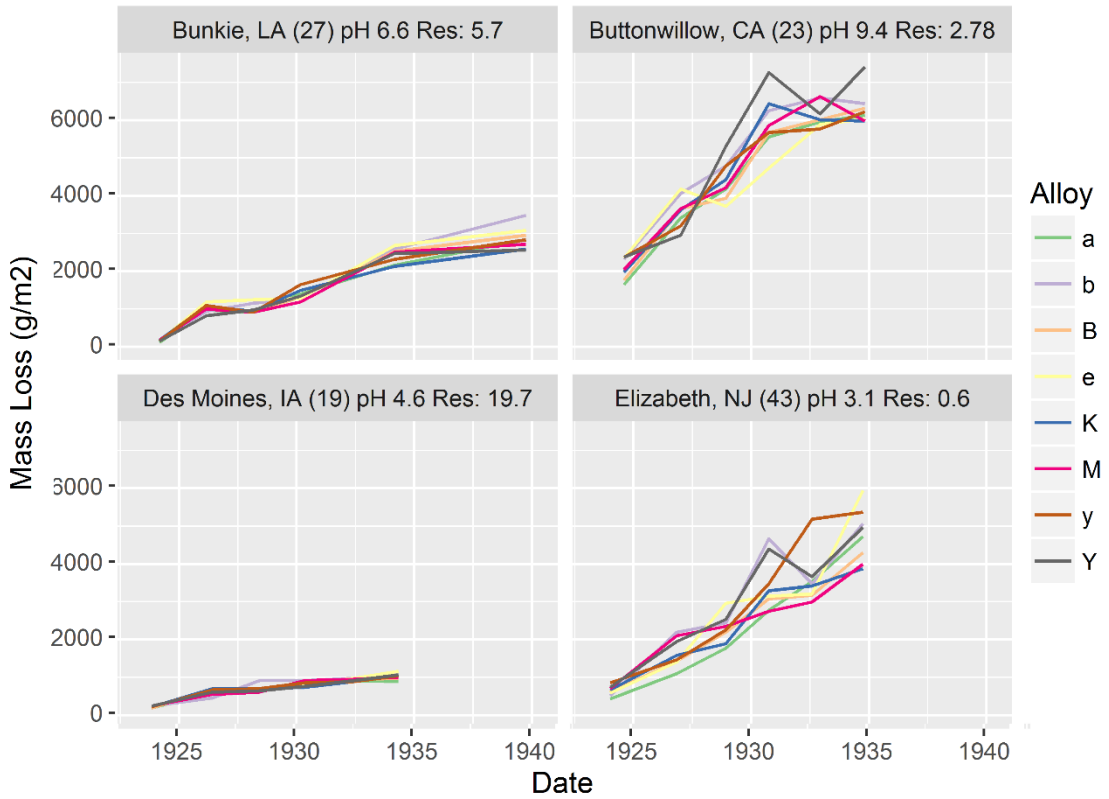
Bunkie, LA (27) pH 6.6 Res: 5.7
Buttonwillow, CA (23) pH 9.4 Res: 2.78
Des Moines, IA (19) pH 4.6 Res: 19.7
Elizabeth, NJ (43) pH 3.1 Res: 0.6
Mass Loss (g/m2)
Date
Alloy
a
b
B
e
K
M
y
Y

(C)

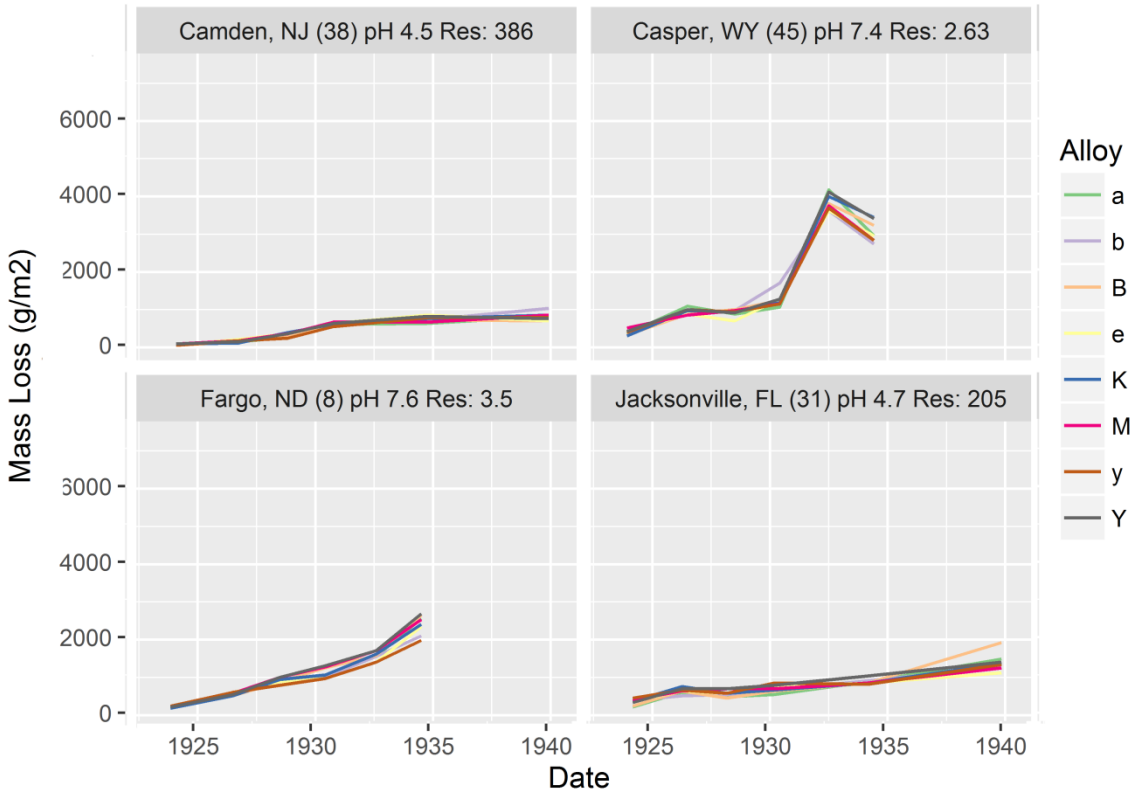
Camden, NJ (38) pH 4.5 Res: 386
Casper, WY (45) pH 7.4 Res: 2.63
Fargo, ND (8) pH 7.6 Res: 3.5
Jacksonville, FL (31) pH 4.7 Res: 205
Mass Loss (g/m2)
Date
Alloy
a
b
B
e
K
M
y
Y

(D)

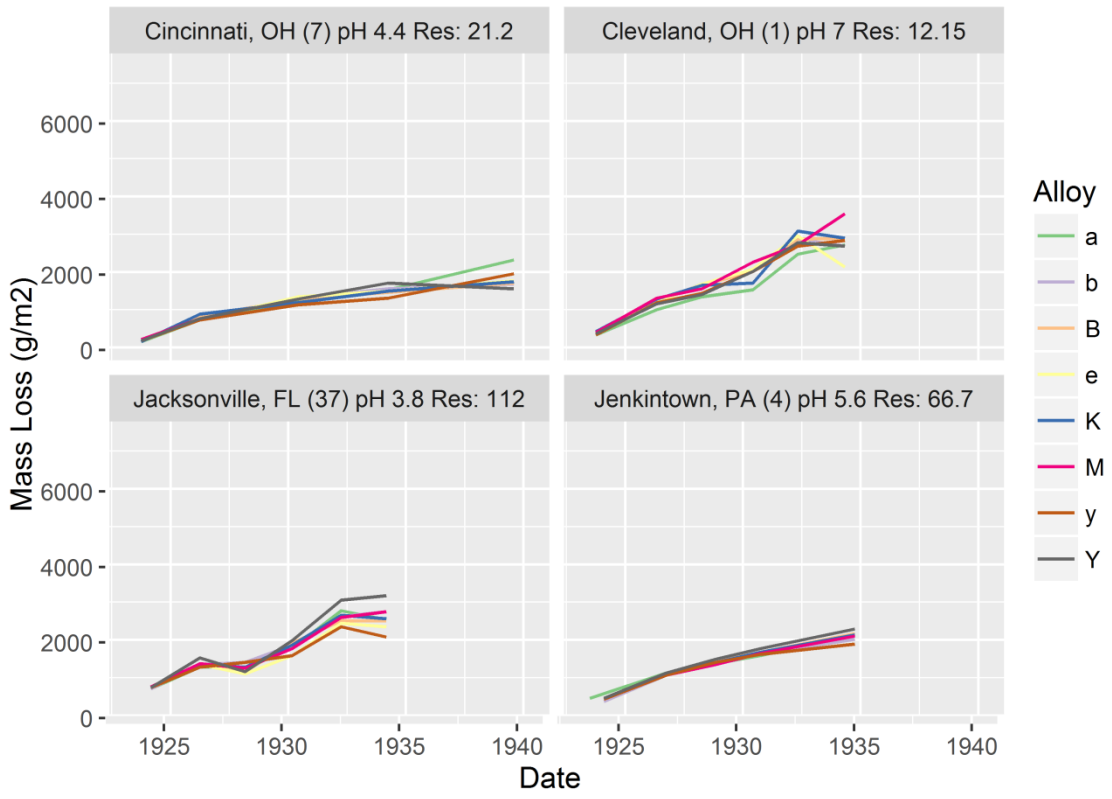
Cincinnati, OH (7) pH 4.4 Res: 21.2
Cleveland, OH (1) pH 7 Res: 12.15
Jacksonville, FL (37) pH 3.8 Res: 112
Jenkintown, PA (4) pH 5.6 Res: 66.7
Mass Loss (g/m2)
0
2000
4000
6000
1925
1930
1935
1940
Date
Alloy
a
b
B
e
K
M
y
Y

(E)

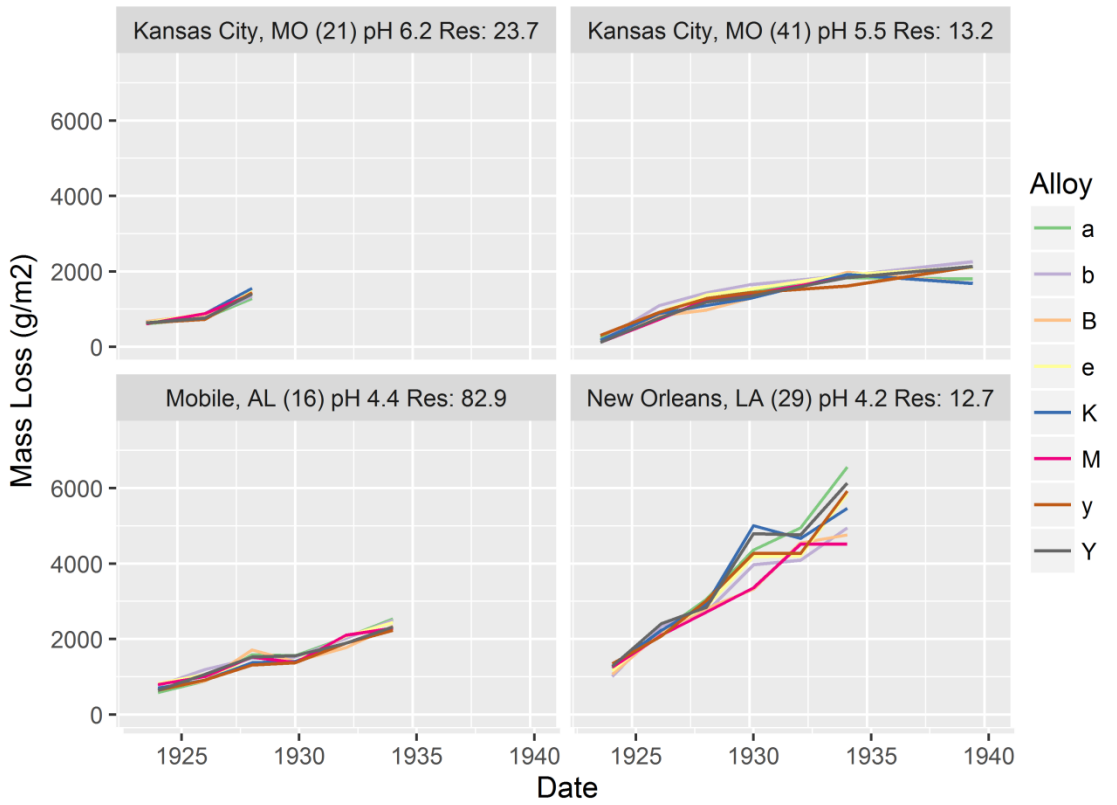
Kansas City, MO (21) pH 6.2 Res: 23.7
Kansas City, MO (41) pH 5.5 Res: 13.2
Mobile, AL (16) pH 4.4 Res: 82.9
New Orleans, LA (29) pH 4.2 Res: 12.7
Mass Loss (g/m2)
0
2000
4000
6000
1925
1930
1935
1940
Date
Alloy
a
b
B
e
K
M
y
Y

(F)

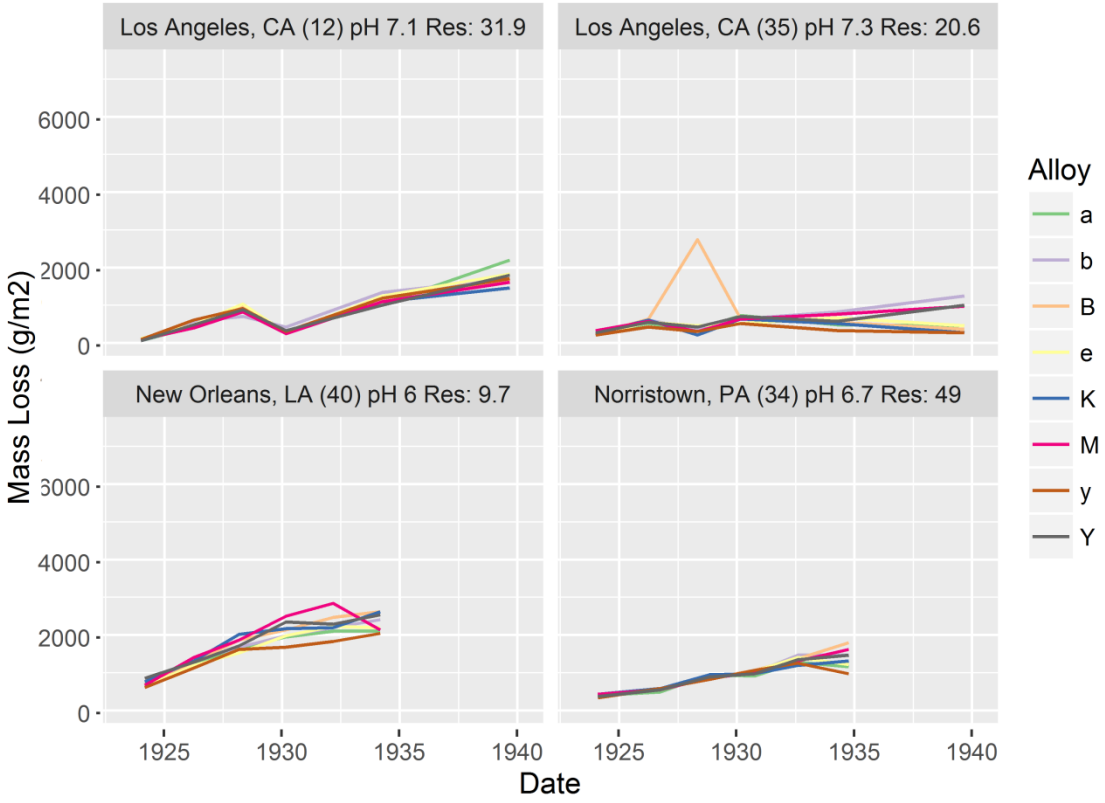
Los Angeles, CA (12) pH 7.1 Res: 31.9
Los Angeles, CA (35) pH 7.3 Res: 20.6
New Orleans, LA (40) pH 6 Res: 9.7
Norristown, PA (34) pH 6.7 Res: 49
Mass Loss (g/m2)
Date
Alloy
a
b
B
e
K
M
y
Y

(G)

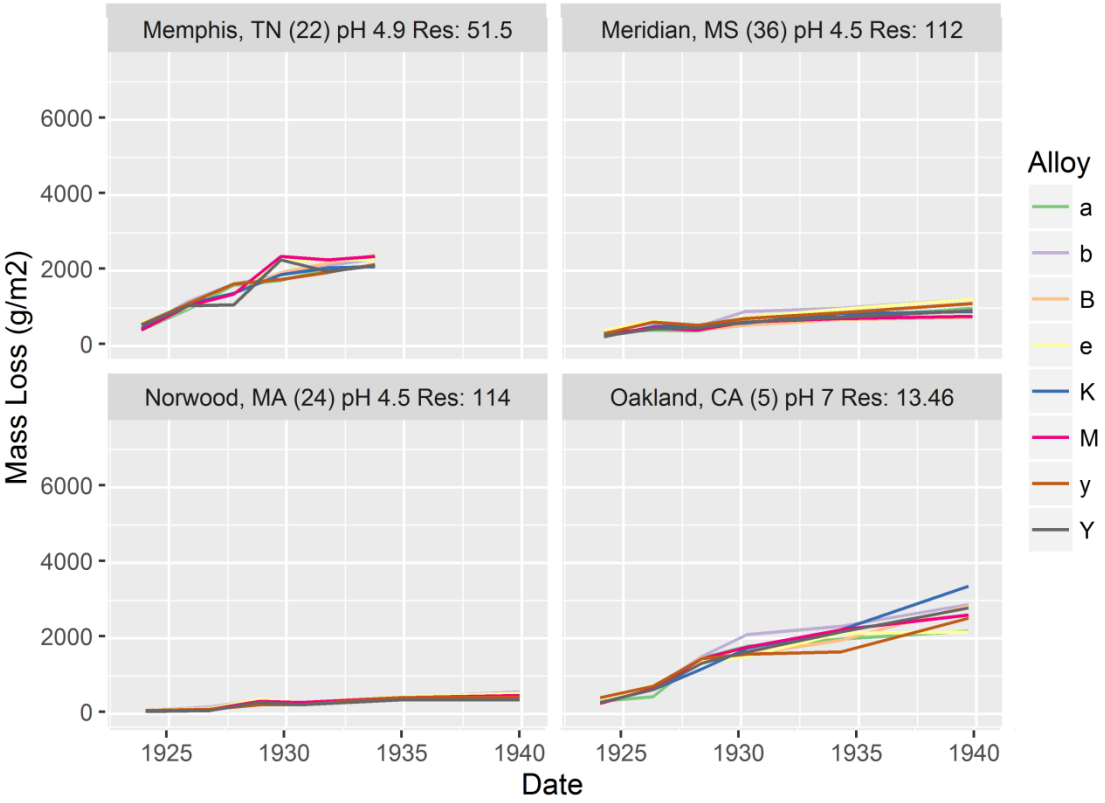
Memphis, TN (22) pH 4.9 Res: 51.5
Meridian, MS (36) pH 4.5 Res: 112
Norwood, MA (24) pH 4.5 Res: 114
Oakland, CA (5) pH 7 Res: 13.46
Mass Loss (g/m2)
Date
Alloy
a
b
B
e
K
M
y
Y

(H)

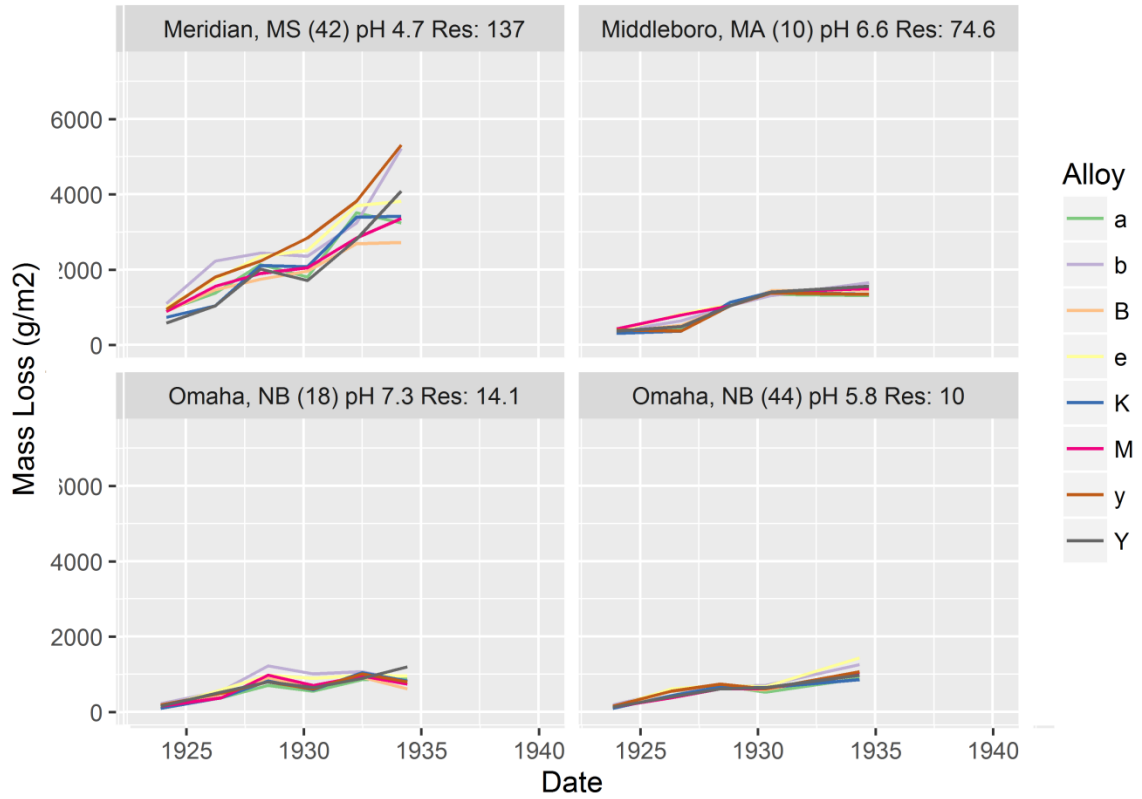
Meridian, MS (42) pH 4.7 Res: 137
Middleboro, MA (10) pH 6.6 Res: 74.6
Omaha, NB (18) pH 7.3 Res: 14.1
Omaha, NB (44) pH 5.8 Res: 10
Mass Loss (g/m2)
Date
Alloy
a
b
B
e
K
M
y
Y

(I)

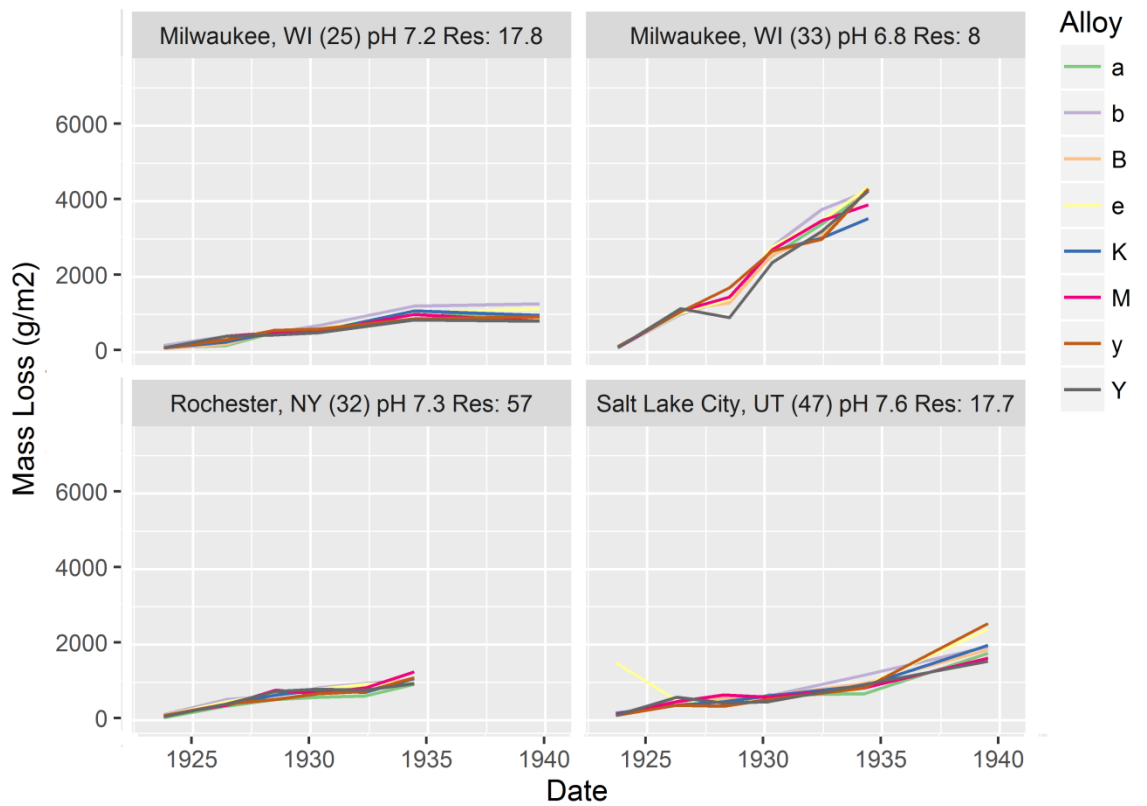
Milwaukee, WI (25) pH 7.2 Res: 17.8
Milwaukee, WI (33) pH 6.8 Res: 8
Rochester, NY (32) pH 7.3 Res: 57
Salt Lake City, UT (47) pH 7.6 Res: 17.7
Mass Loss (g/m2)
Date
Alloy
a
b
B
e
K
M
y
Y

(J)

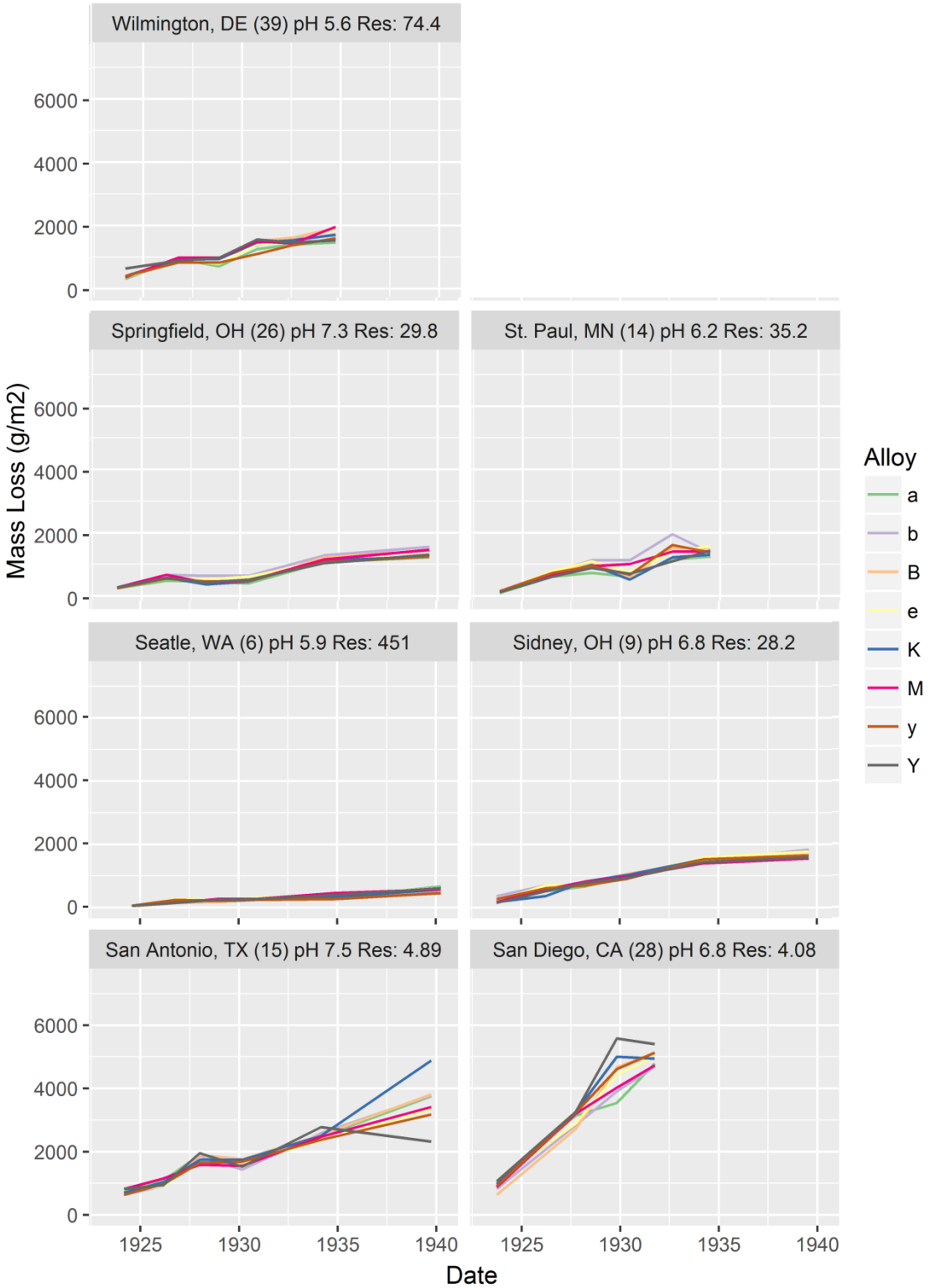

(K)

Figure 27. Graph clusters A, B, C, D, E, F, G, H, I, J, and K represent total mass loss vs time. Each graph title includes location, soil pH, and soil resistivity.

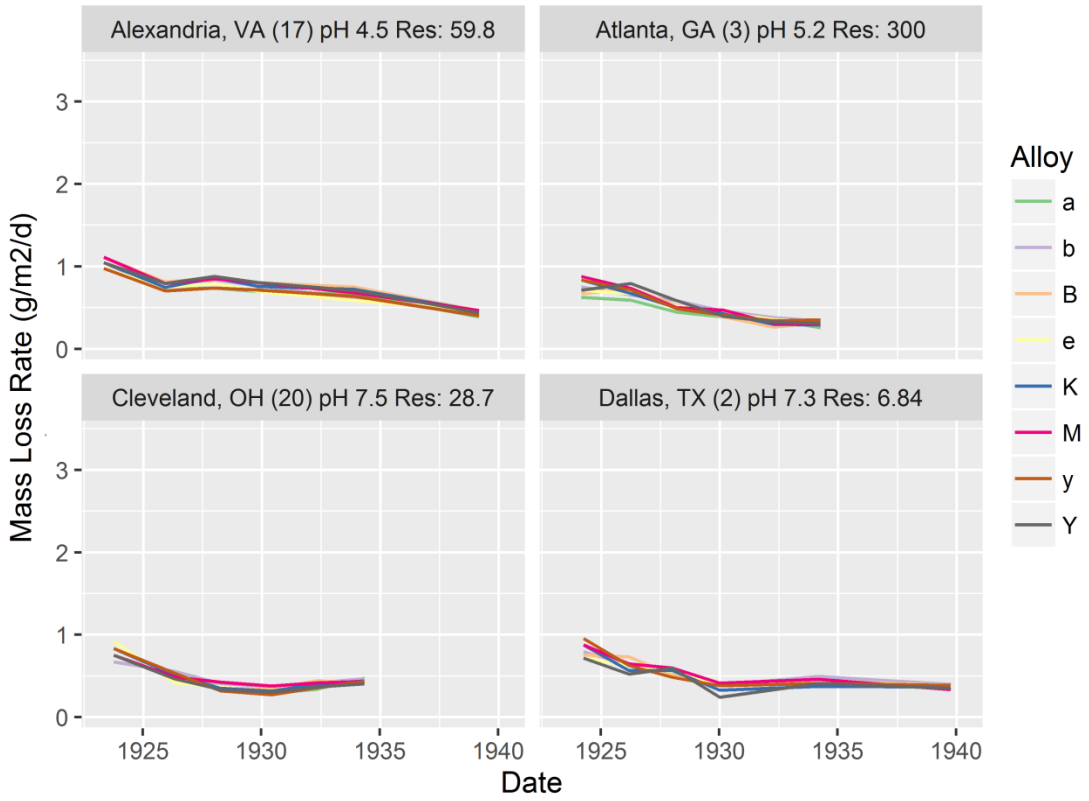
Alexandria, VA (17) pH 4.5 Res: 59.8
Atlanta, GA (3) pH 5.2 Res: 300
Cleveland, OH (20) pH 7.5 Res: 28.7
Dallas, TX (2) pH 7.3 Res: 6.84
Mass Loss Rate (g/m2/d)
Date
Alloy
a
b
B
e
K
M
y
Y

(A)

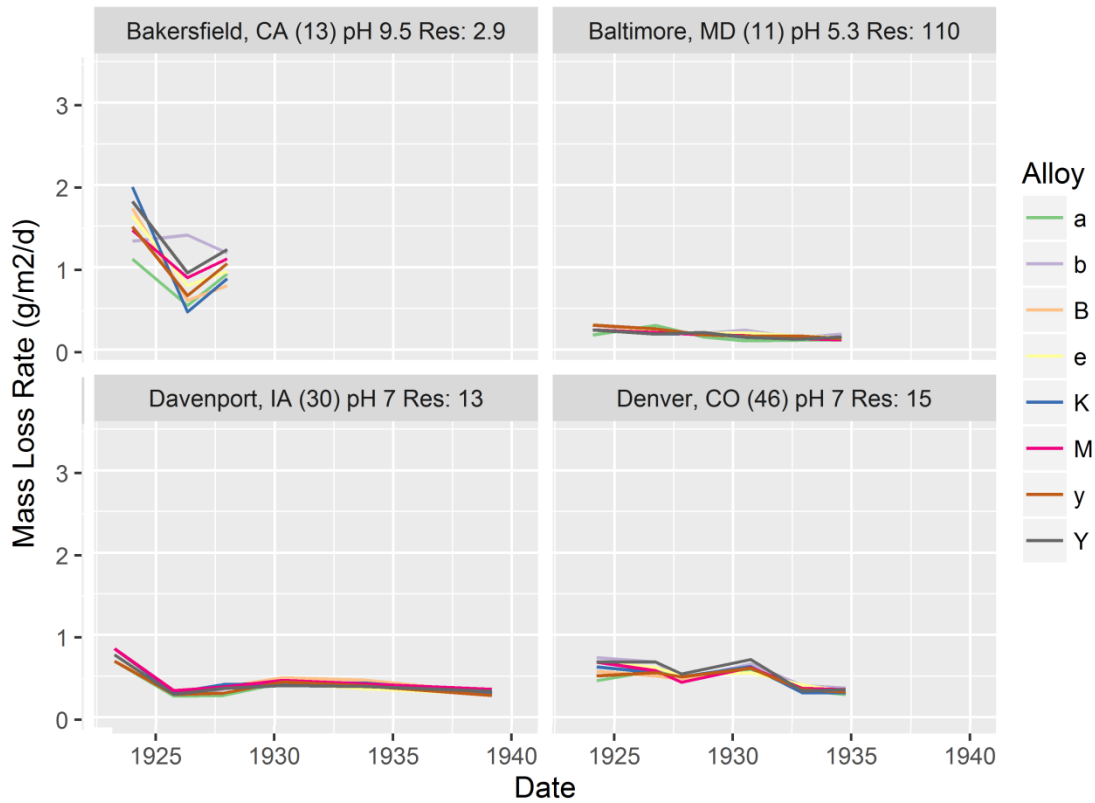
Bakersfield, CA (13) pH 9.5 Res: 2.9
Baltimore, MD (11) pH 5.3 Res: 110
Davenport, IA (30) pH 7 Res: 13
Denver, CO (46) pH 7 Res: 15
Mass Loss Rate (g/m2/d)
Date
Alloy
a
b
B
e
K
M
y
Y

(B)

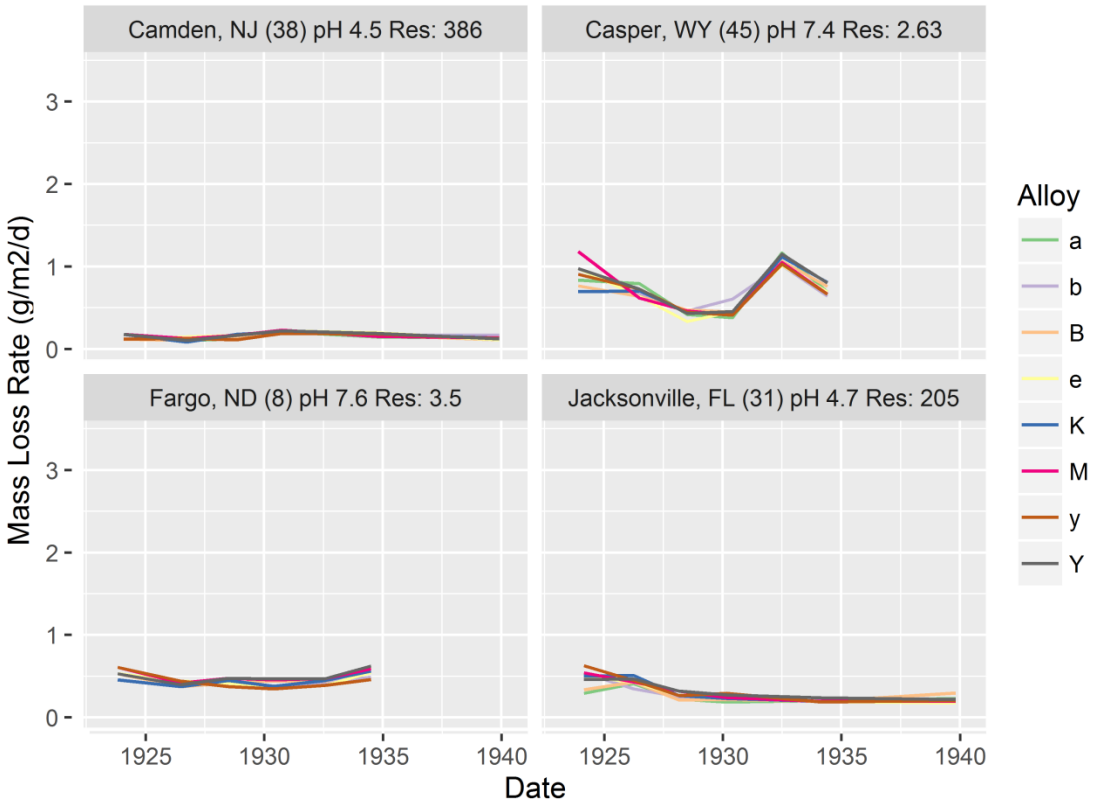
Camden, NJ (38) pH 4.5 Res: 386
Casper, WY (45) pH 7.4 Res: 2.63
Fargo, ND (8) pH 7.6 Res: 3.5
Jacksonville, FL (31) pH 4.7 Res: 205
Mass Loss Rate (g/m2/d)
Date
Alloy
a
b
B
e
K
M
y
Y

(C)

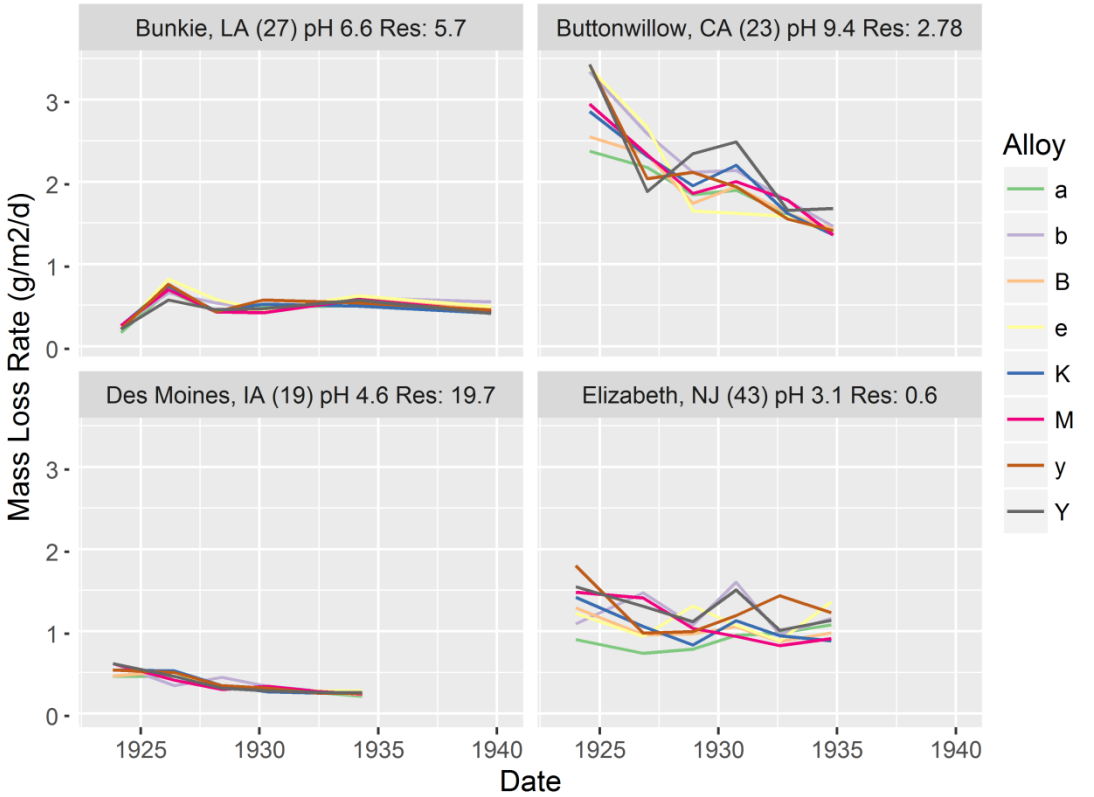
Bunkie, LA (27) pH 6.6 Res: 5.7
Buttonwillow, CA (23) pH 9.4 Res: 2.78
Des Moines, IA (19) pH 4.6 Res: 19.7
Elizabeth, NJ (43) pH 3.1 Res: 0.6
Mass Loss Rate (g/m2/d)
Date
Alloy
a
b
B
e
K
M
y
Y

(D)

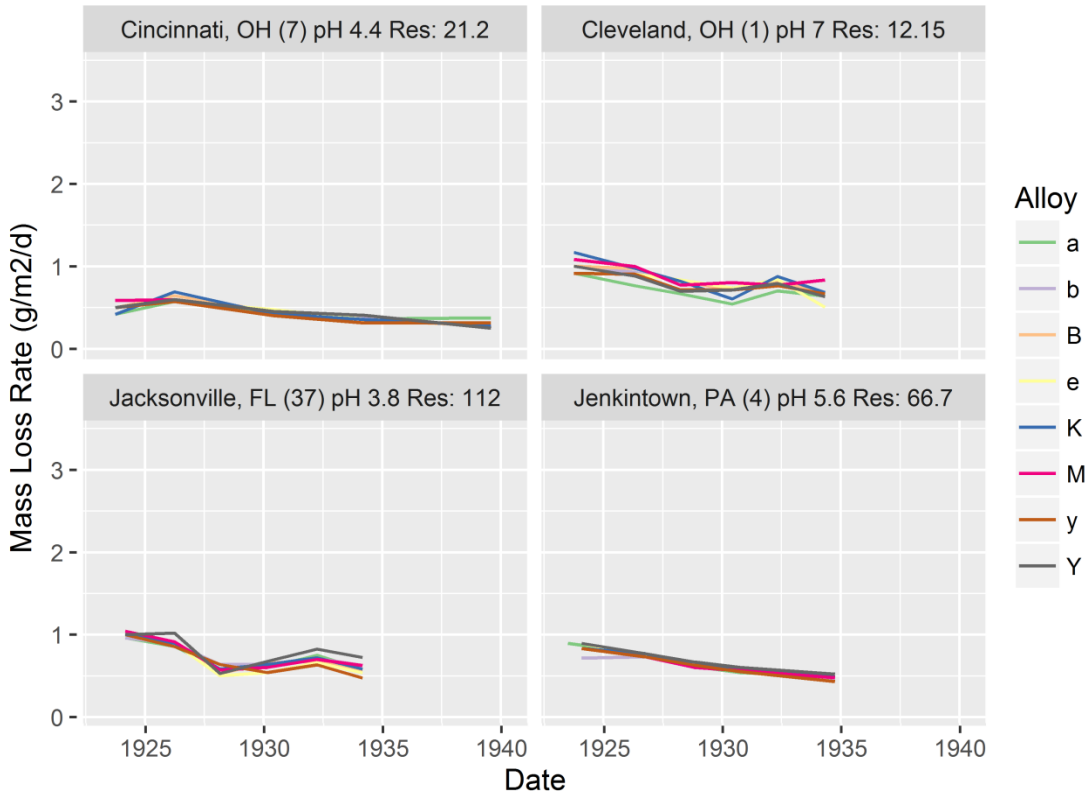
Cincinnati, OH (7) pH 4.4 Res: 21.2
Cleveland, OH (1) pH 7 Res: 12.15
Jacksonville, FL (37) pH 3.8 Res: 112
Jenkintown, PA (4) pH 5.6 Res: 66.7
Mass Loss Rate (g/m2/d)
Date
Alloy
a
b
B
e
K
M
y
Y

(E)

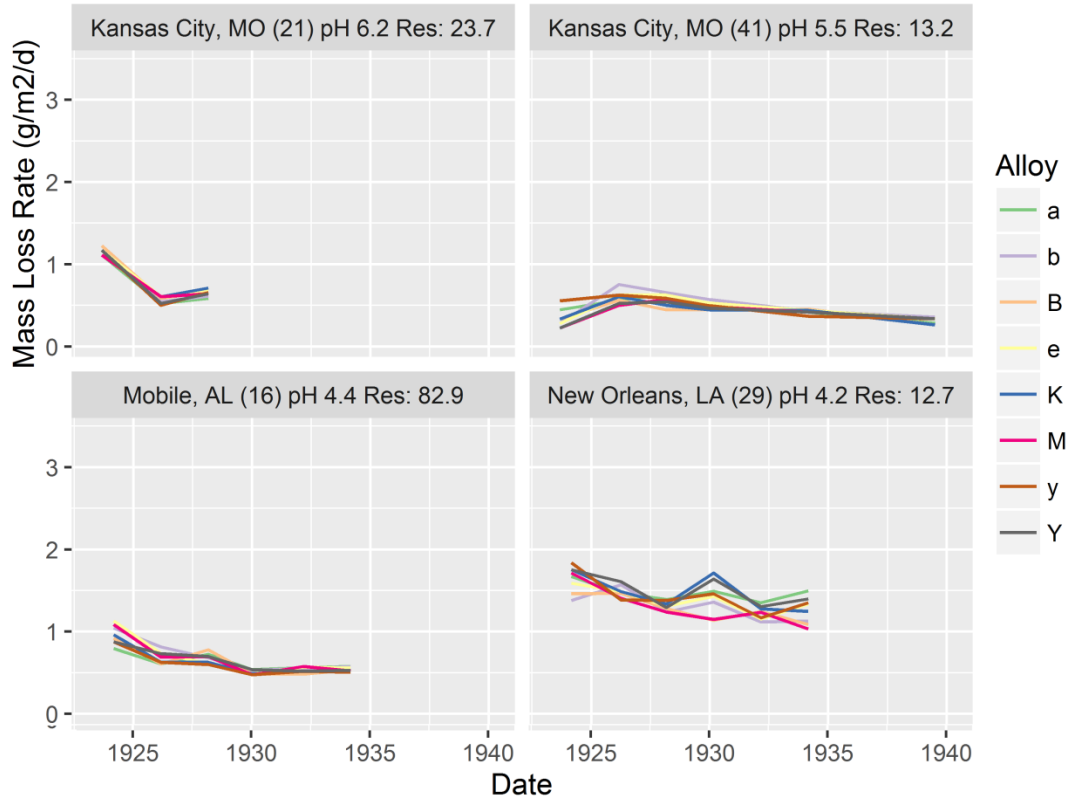
Kansas City, MO (21) pH 6.2 Res: 23.7
Kansas City, MO (41) pH 5.5 Res: 13.2
Mobile, AL (16) pH 4.4 Res: 82.9
New Orleans, LA (29) pH 4.2 Res: 12.7
Mass Loss Rate (g/m2/d)
Date
Alloy
a
b
B
e
K
M
y
Y

(F)

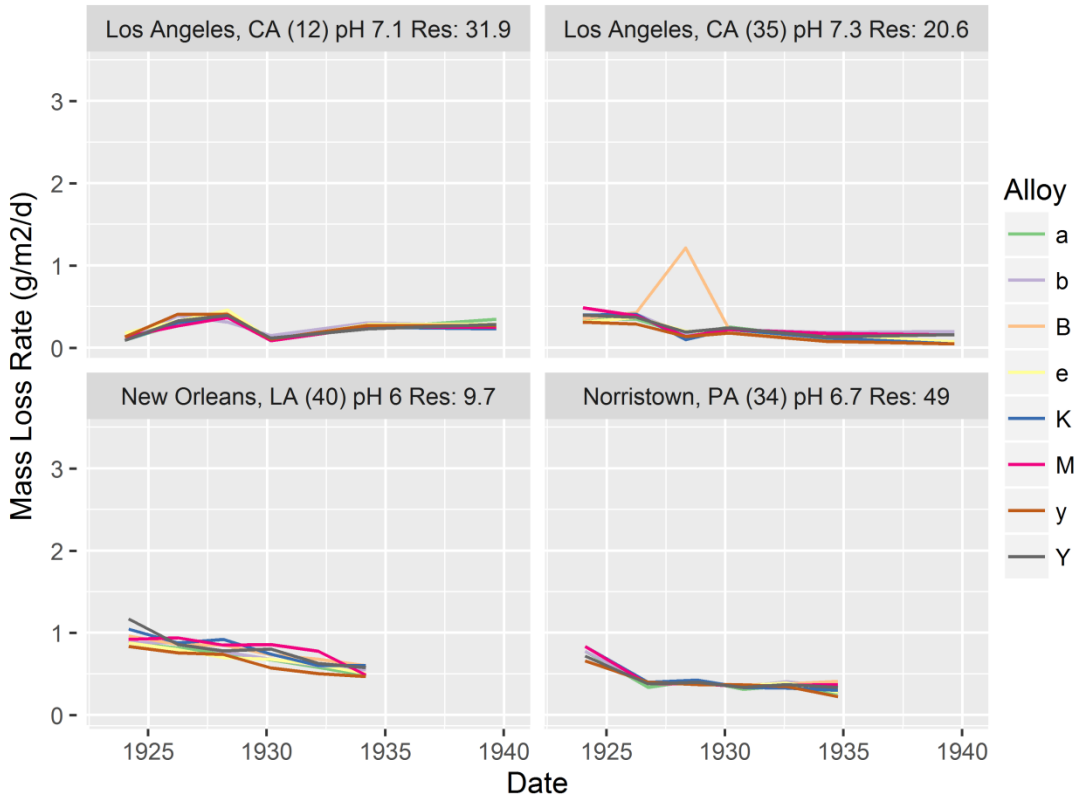
Los Angeles, CA (12) pH 7.1 Res: 31.9
Los Angeles, CA (35) pH 7.3 Res: 20.6
New Orleans, LA (40) pH 6 Res: 9.7
Norristown, PA (34) pH 6.7 Res: 49
Mass Loss Rate (g/m2/d)
Date
Alloy
a
b
B
e
K
M
y
Y

(G)

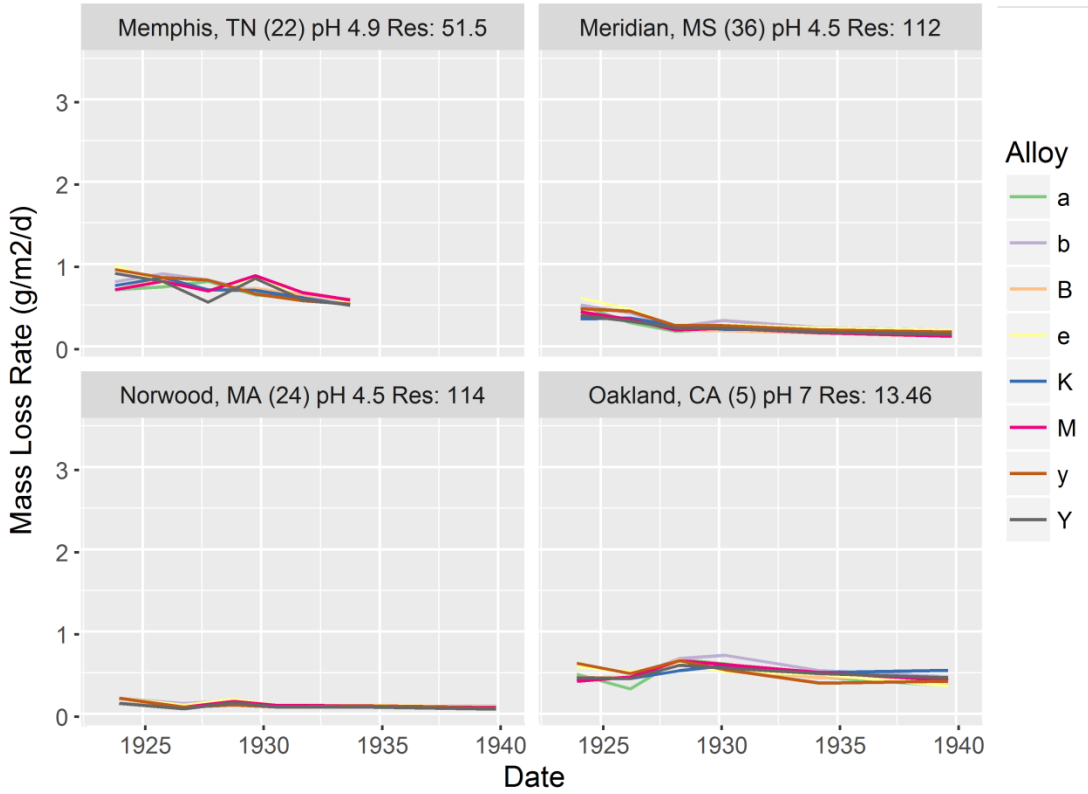
Memphis, TN (22) pH 4.9 Res: 51.5
Meridian, MS (36) pH 4.5 Res: 112
Norwood, MA (24) pH 4.5 Res: 114
Oakland, CA (5) pH 7 Res: 13.46
Mass Loss Rate (g/m2/d)
Date
Alloy
a
b
B
e
K
M
y
Y

(H)

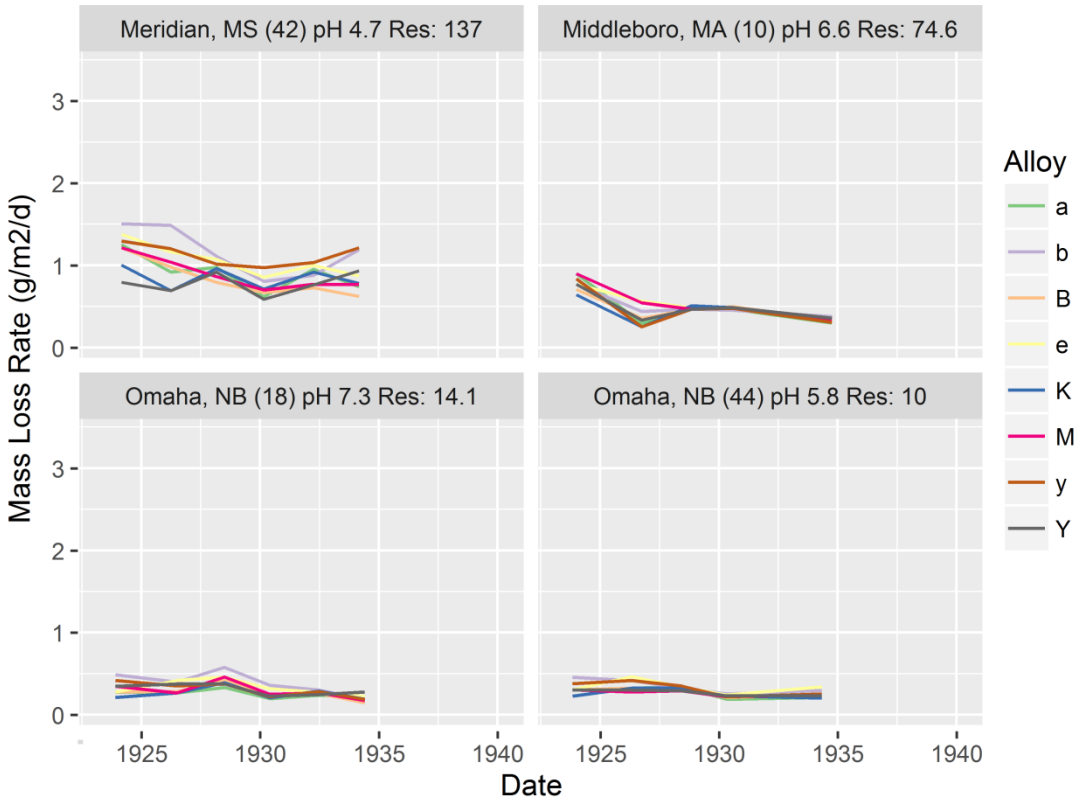
Meridian, MS (42) pH 4.7 Res: 137
Middleboro, MA (10) pH 6.6 Res: 74.6
Omaha, NB (18) pH 7.3 Res: 14.1
Omaha, NB (44) pH 5.8 Res: 10
Mass Loss Rate (g/m2/d)
Date
Alloy
a
b
B
e
K
M
y
Y

(I)

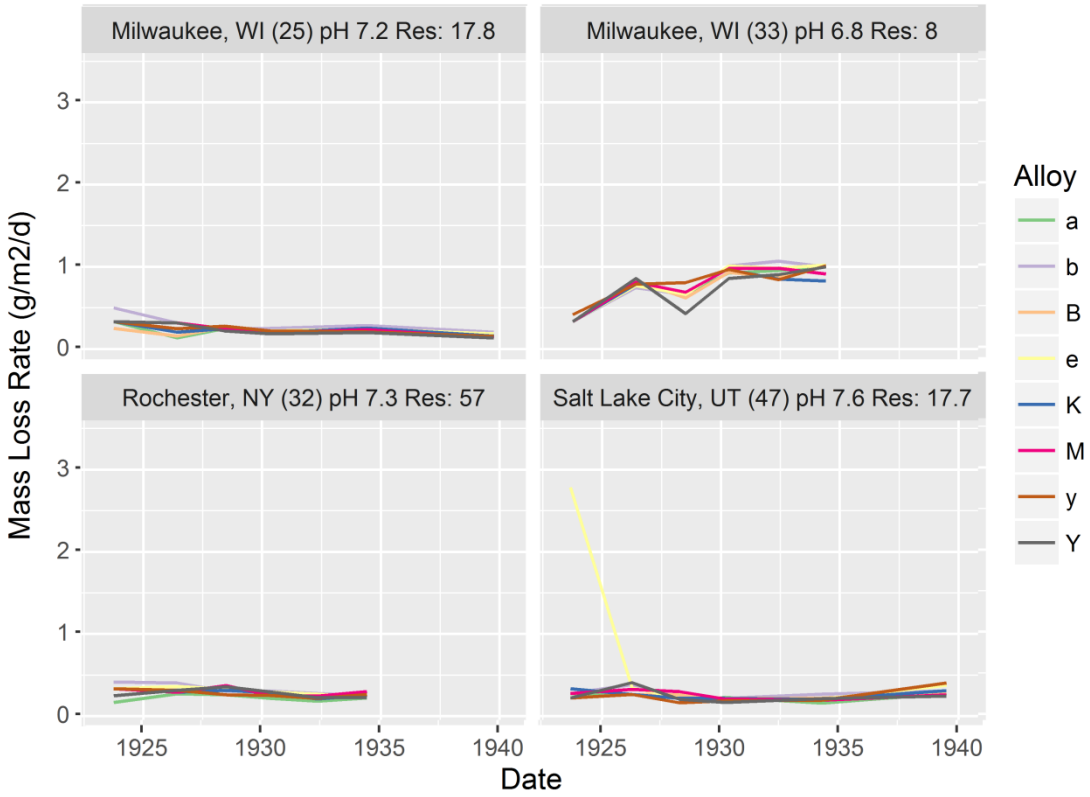
Milwaukee, WI (25) pH 7.2 Res: 17.8
Milwaukee, WI (33) pH 6.8 Res: 8
Rochester, NY (32) pH 7.3 Res: 57
Salt Lake City, UT (47) pH 7.6 Res: 17.7
Mass Loss Rate (g/m2/d)
Date
Alloy
a
b
B
e
K
M
y
Y

(J)

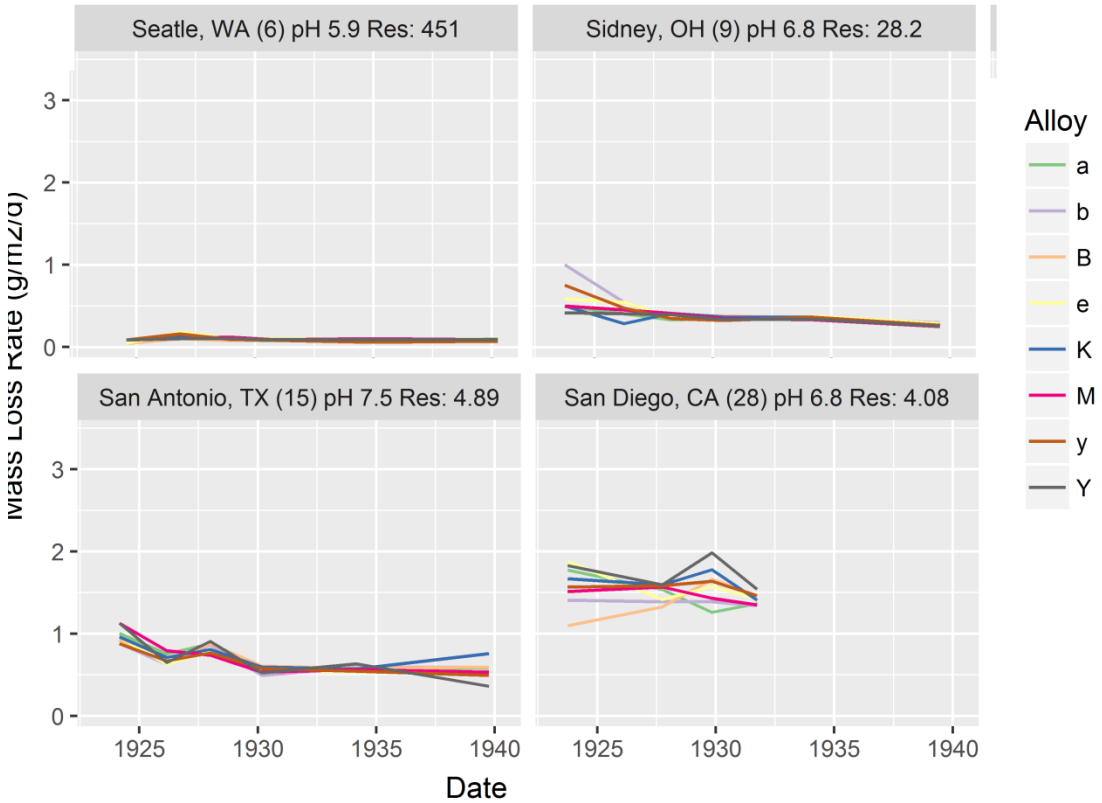

(K)

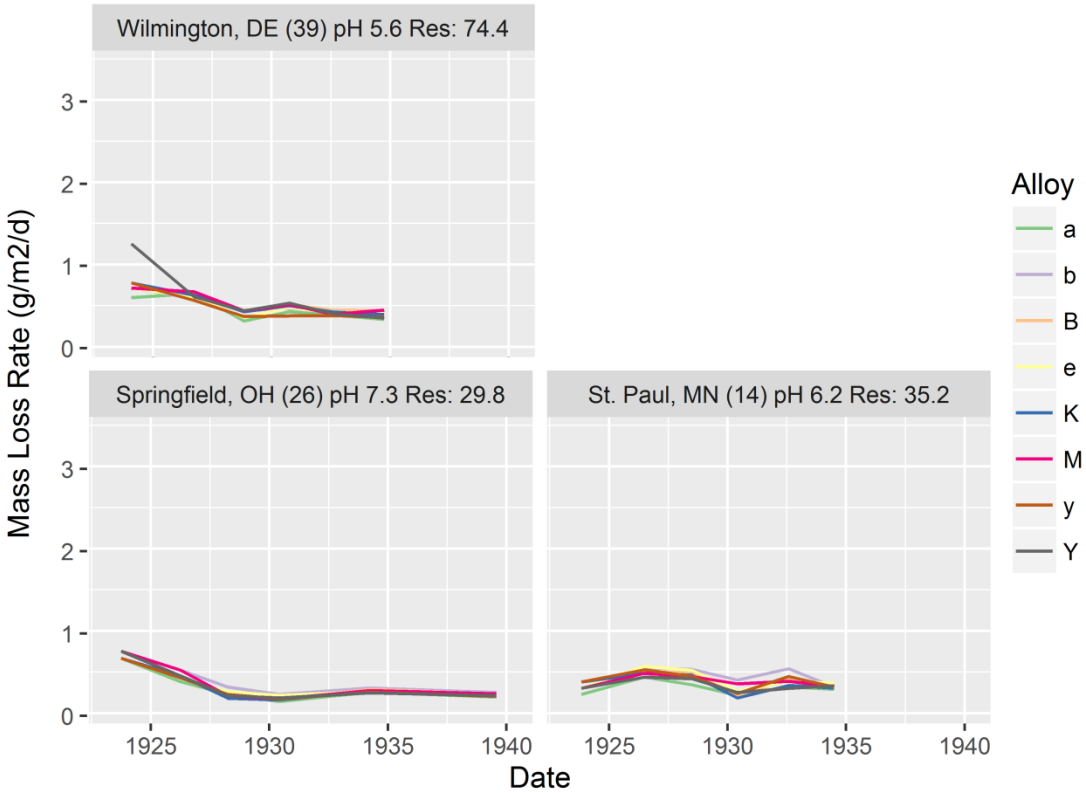

(L)

Figure 28. Graph clusters A, B, C, D, E, F, G, H, I, J, K, and L represent mass loss vs time. Each figure title contains the location, soil pH, and soil resistivity.

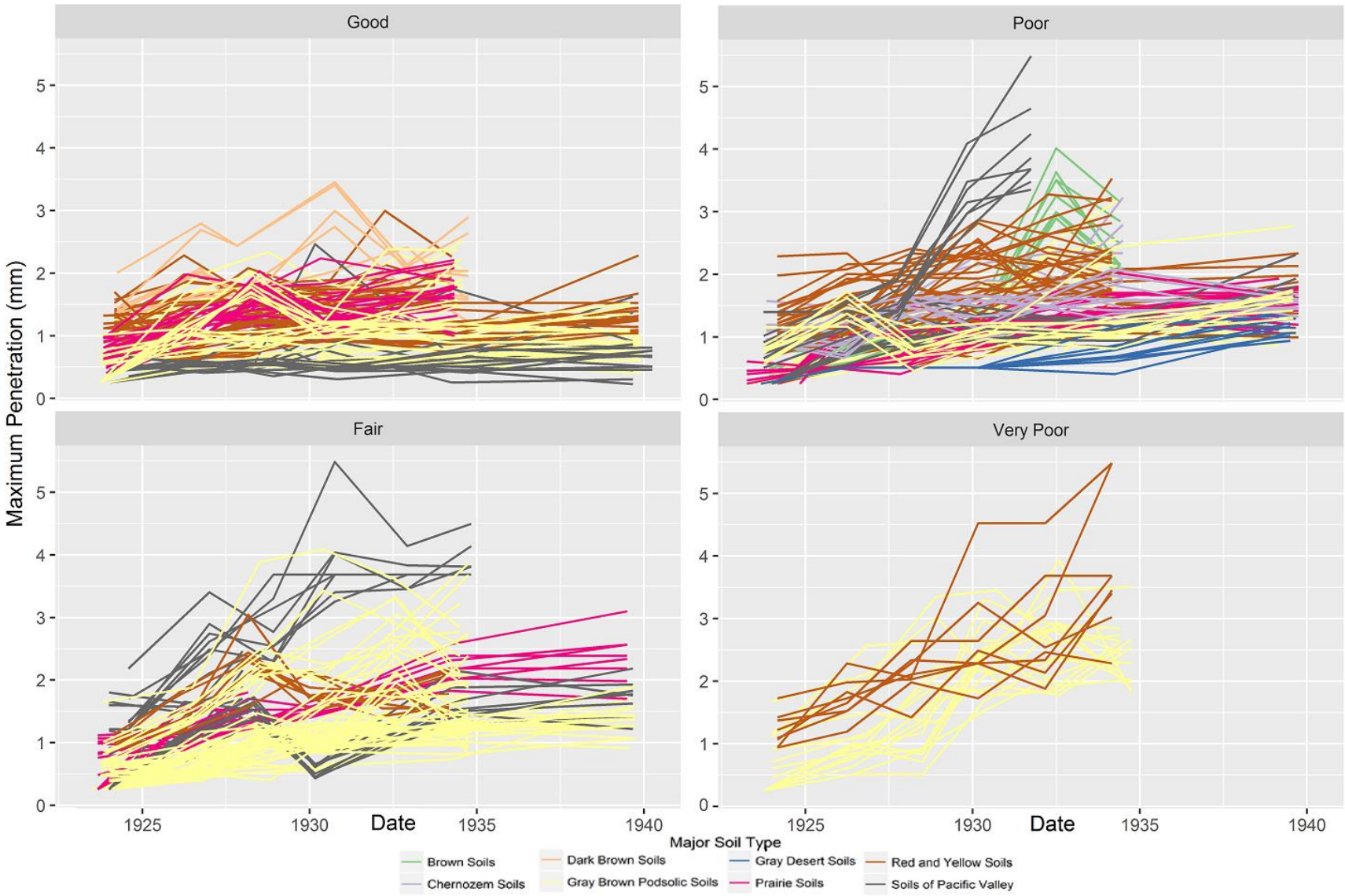

Figure 29. Maximum penetration by drainage for 8 soil types.

44

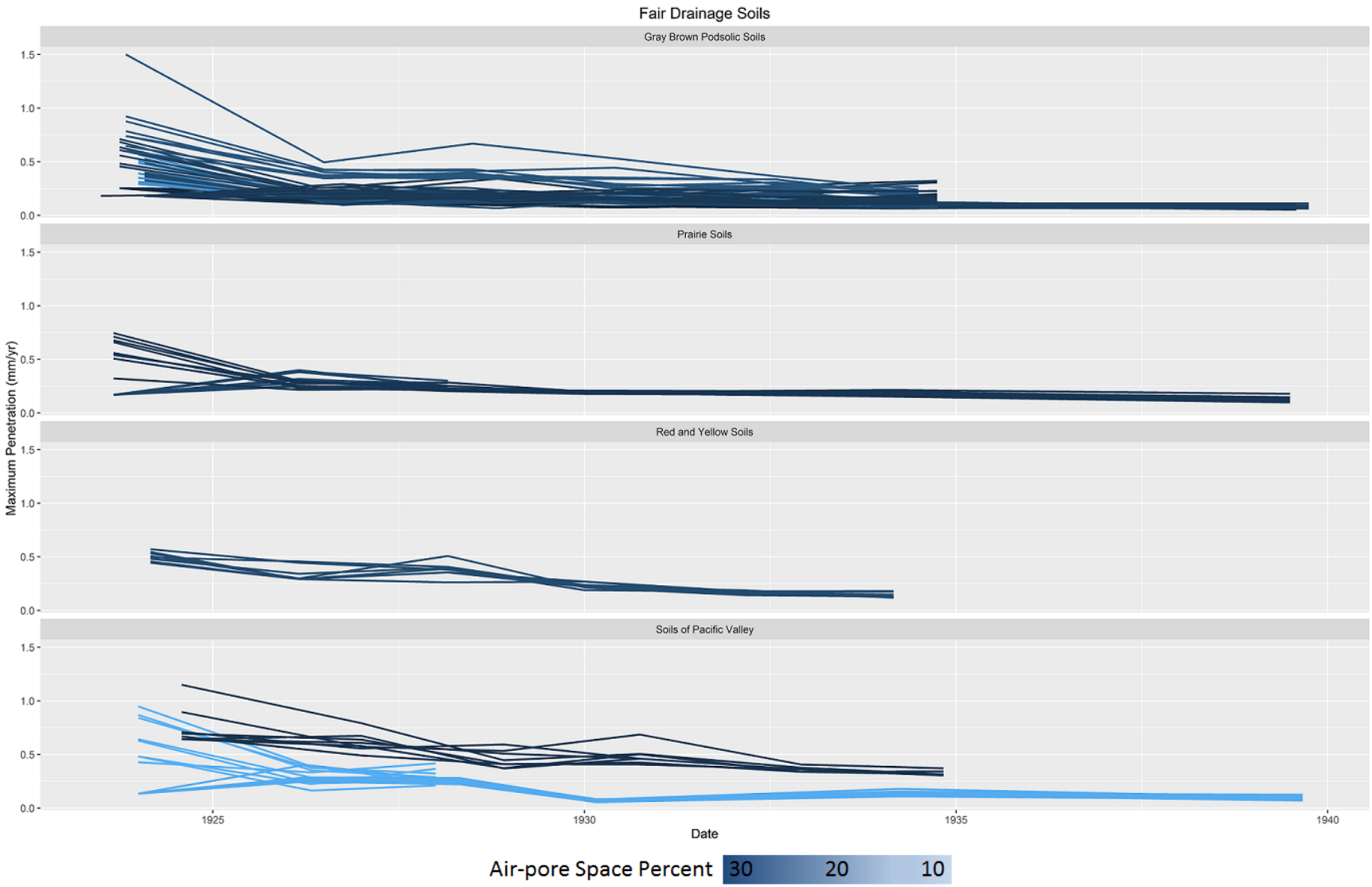

Figure 30. Maximum penetration depth in mm per year defined by air-porosity.

45

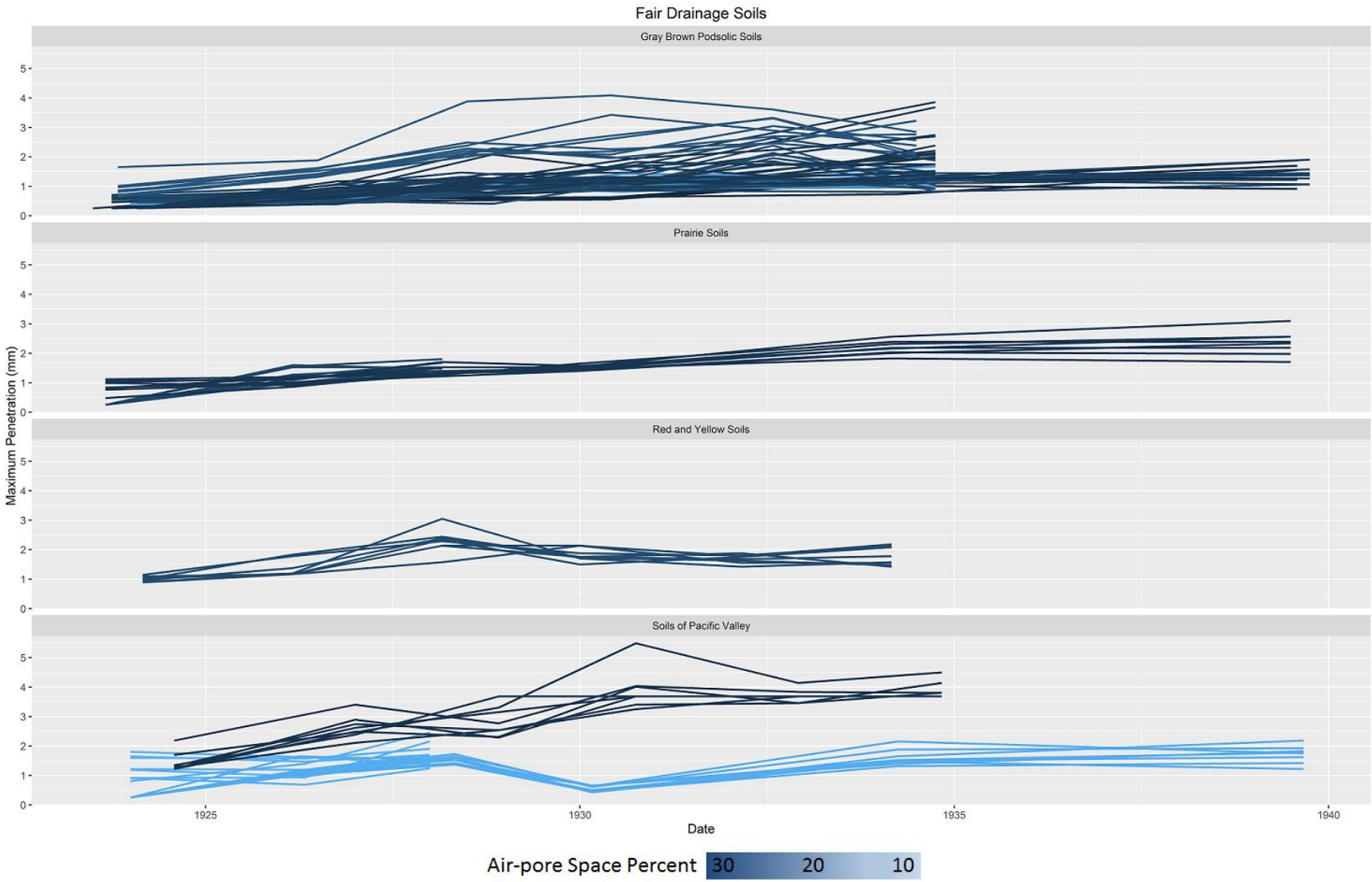

Figure 31. Maximum penetration depth by air-porosity.

46

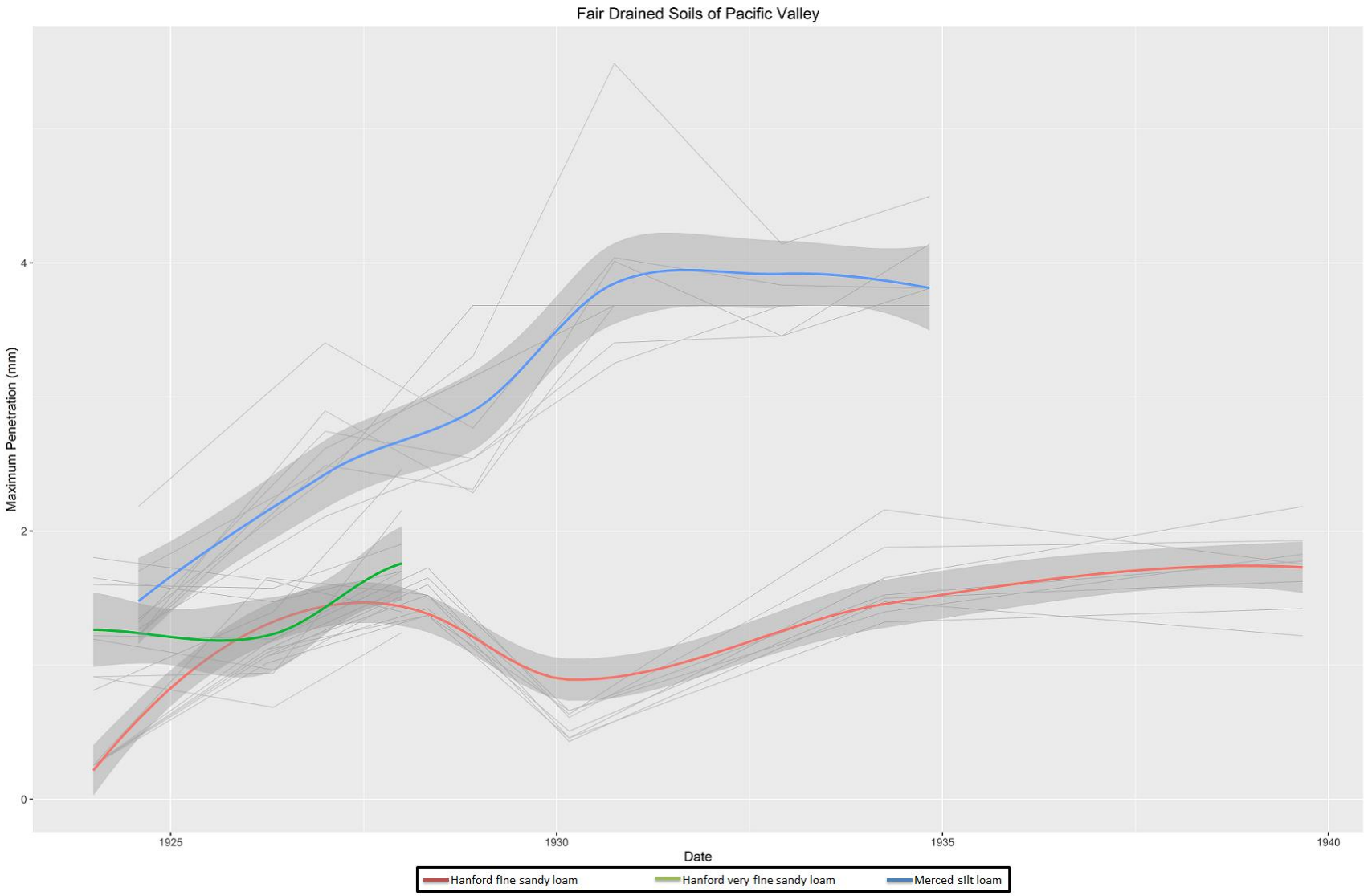

Figure 32. Maximum penetration fair pacific soils by type.

47

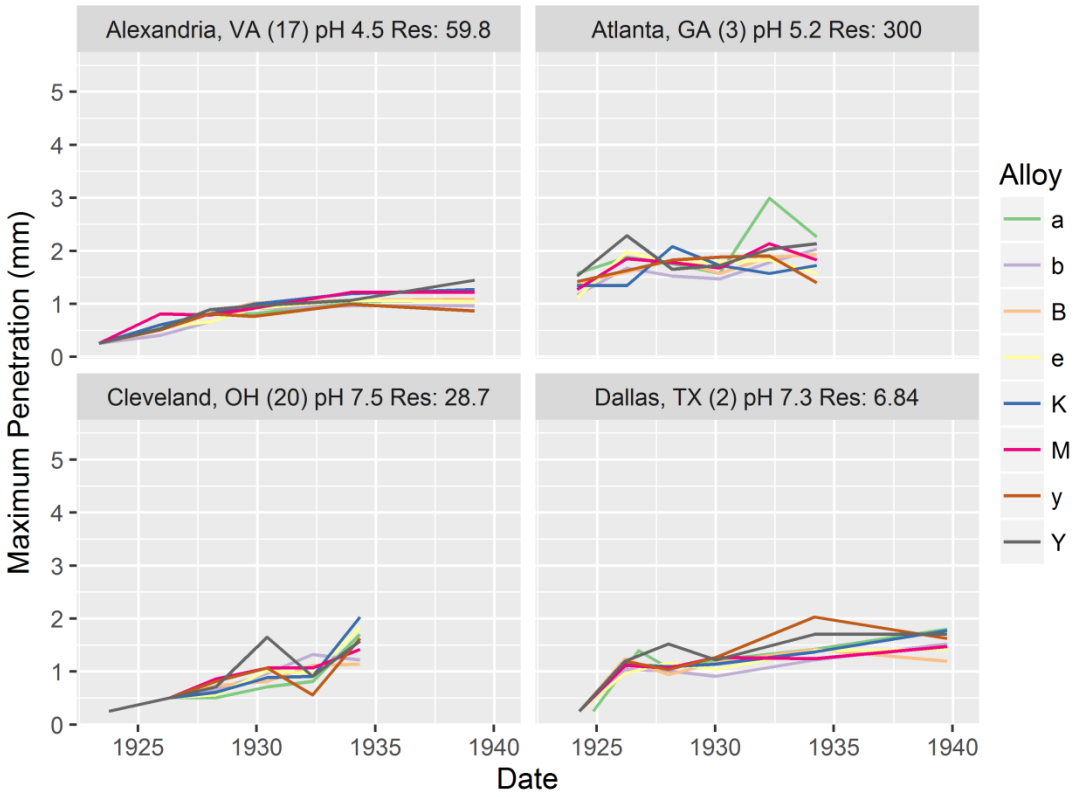
Alexandria, VA (17) pH 4.5 Res: 59.8
Atlanta, GA (3) pH 5.2 Res: 300
Cleveland, OH (20) pH 7.5 Res: 28.7
Dallas, TX (2) pH 7.3 Res: 6.84
Maximum Penetration (mm)
Date
Alloy
a
b
B
e
K
M
y
Y

(A)

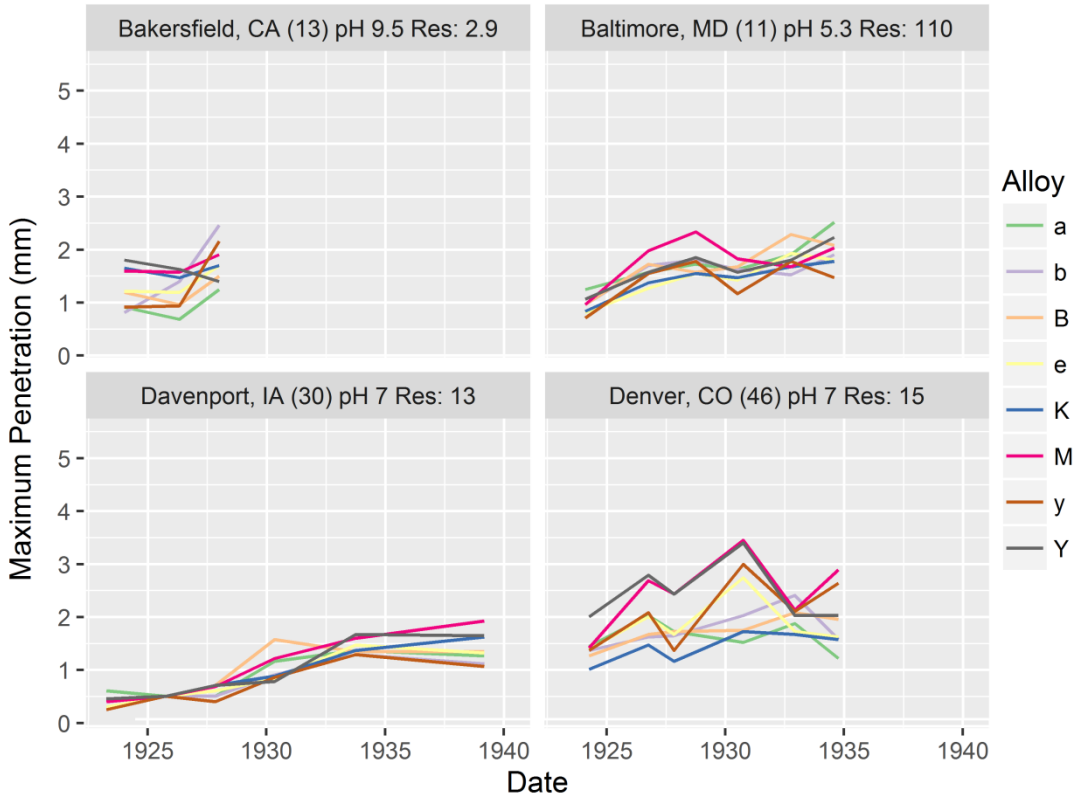
Bakersfield, CA (13) pH 9.5 Res: 2.9
Baltimore, MD (11) pH 5.3 Res: 110
Davenport, IA (30) pH 7 Res: 13
Denver, CO (46) pH 7 Res: 15
Maximum Penetration (mm)
Date
Alloy
a
b
B
e
K
M
y
Y

(B)

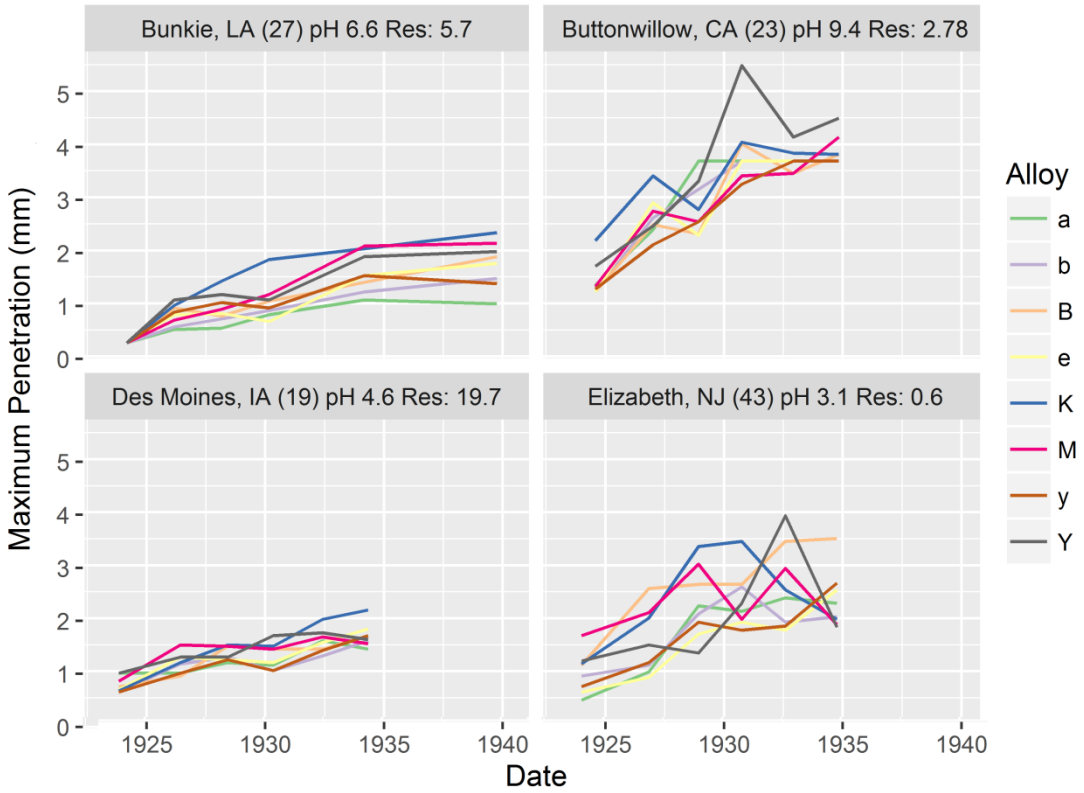
Bunkie, LA (27) pH 6.6 Res: 5.7
Buttonwillow, CA (23) pH 9.4 Res: 2.78
Des Moines, IA (19) pH 4.6 Res: 19.7
Elizabeth, NJ (43) pH 3.1 Res: 0.6
Maximum Penetration (mm)
Date
Alloy
a
b
B
e
K
M
y
Y

(C)

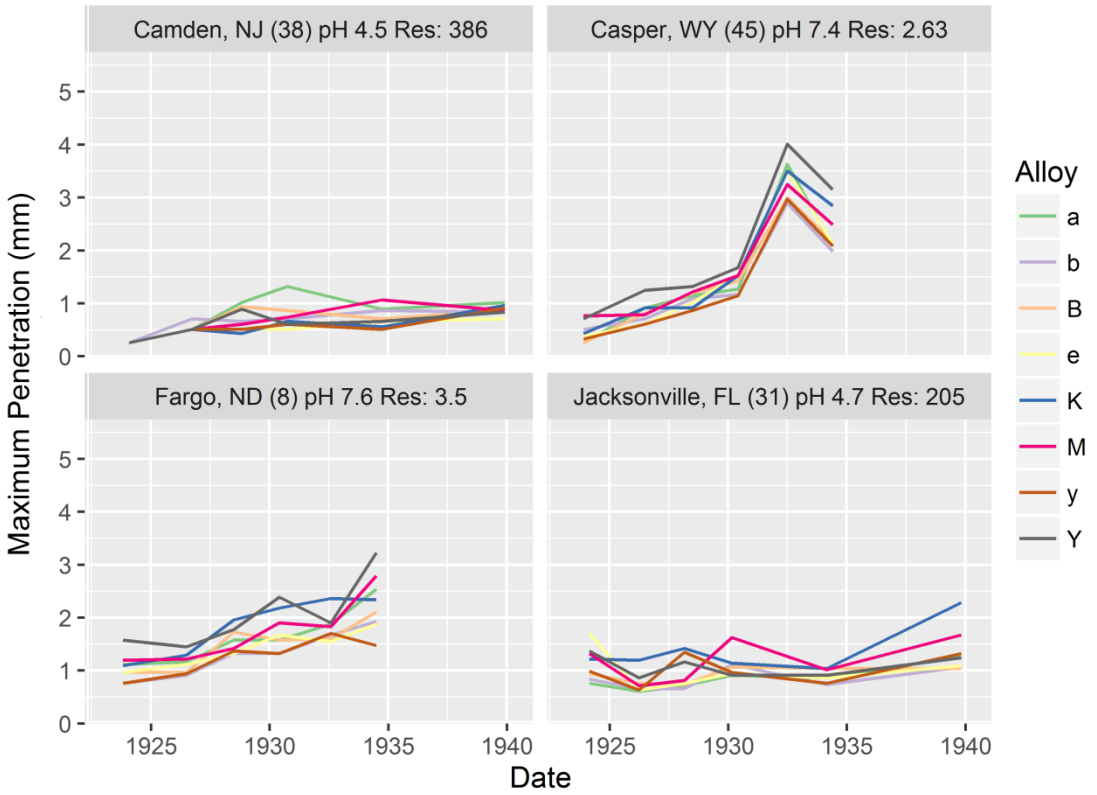
Camden, NJ (38) pH 4.5 Res: 386
Casper, WY (45) pH 7.4 Res: 2.63
Fargo, ND (8) pH 7.6 Res: 3.5
Jacksonville, FL (31) pH 4.7 Res: 205
Maximum Penetration (mm)
Date
Alloy
a
b
B
e
K
M
y
Y

(D)

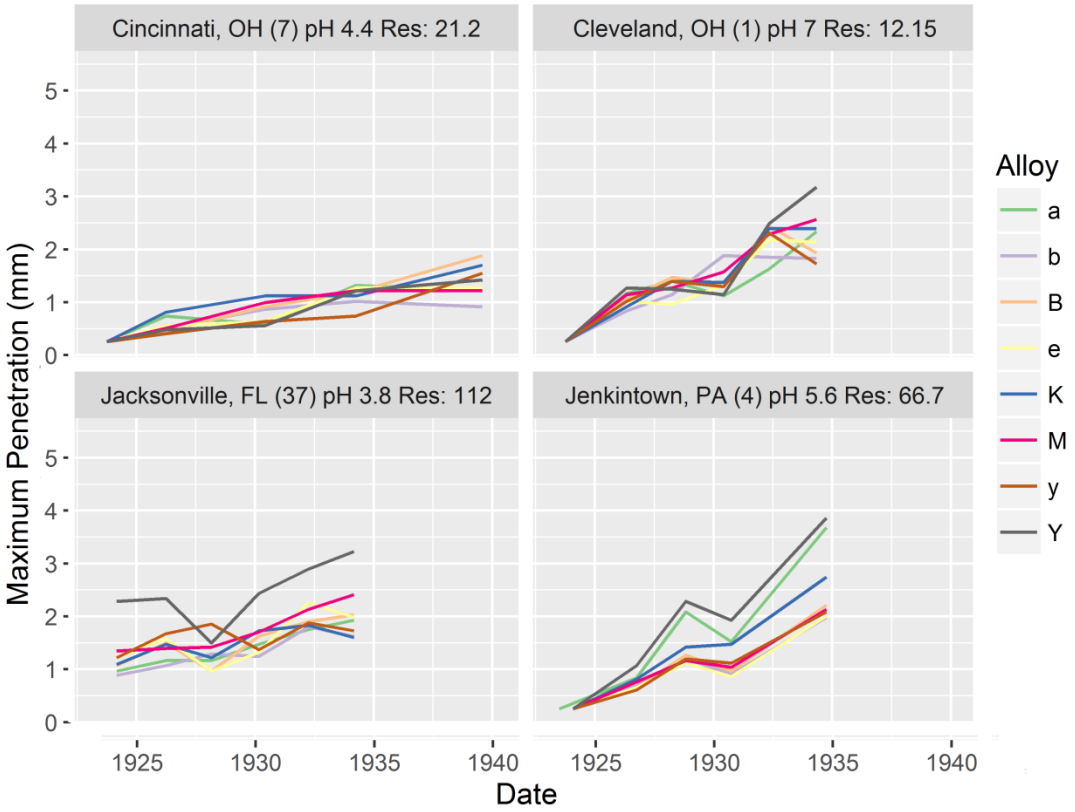
Cincinnati, OH (7) pH 4.4 Res: 21.2
Cleveland, OH (1) pH 7 Res: 12.15
Jacksonville, FL (37) pH 3.8 Res: 112
Jenkintown, PA (4) pH 5.6 Res: 66.7
Maximum Penetration (mm)
Date
Alloy
a
b
B
e
K
M
y
Y

(E)

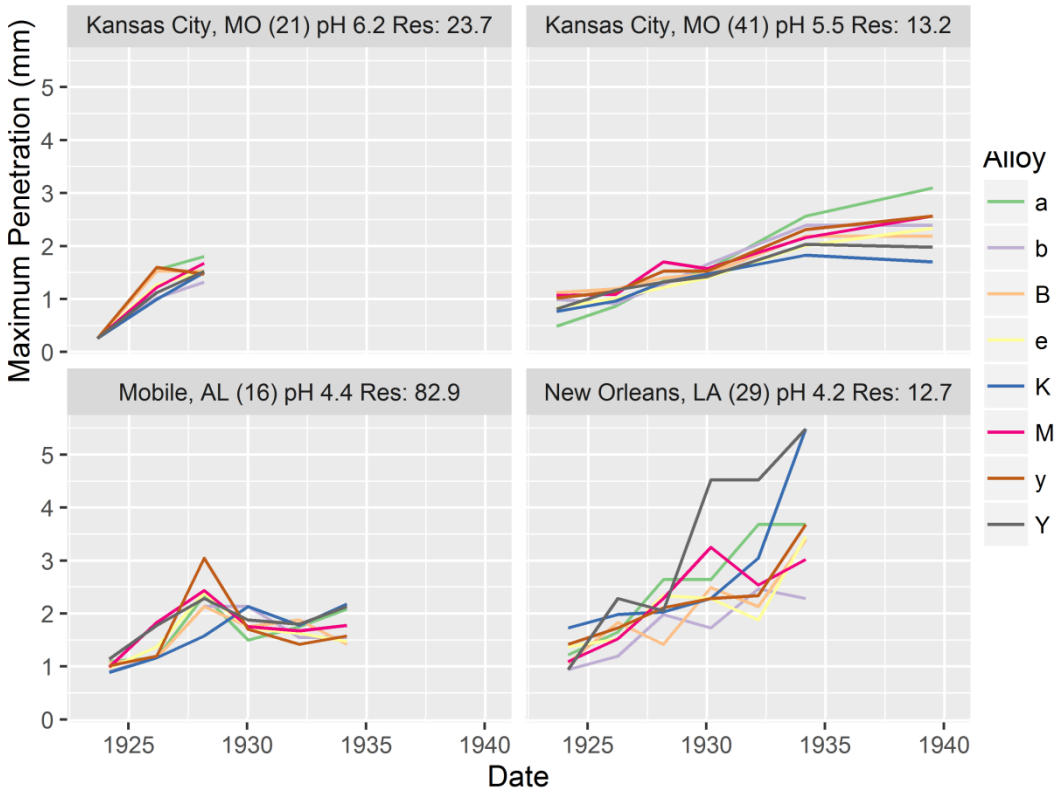
Kansas City, MO (21) pH 6.2 Res: 23.7
Kansas City, MO (41) pH 5.5 Res: 13.2
Mobile, AL (16) pH 4.4 Res: 82.9
New Orleans, LA (29) pH 4.2 Res: 12.7
Maximum Penetration (mm)
Date
Alloy
a
b
B
e
K
M
y
Y

(F)

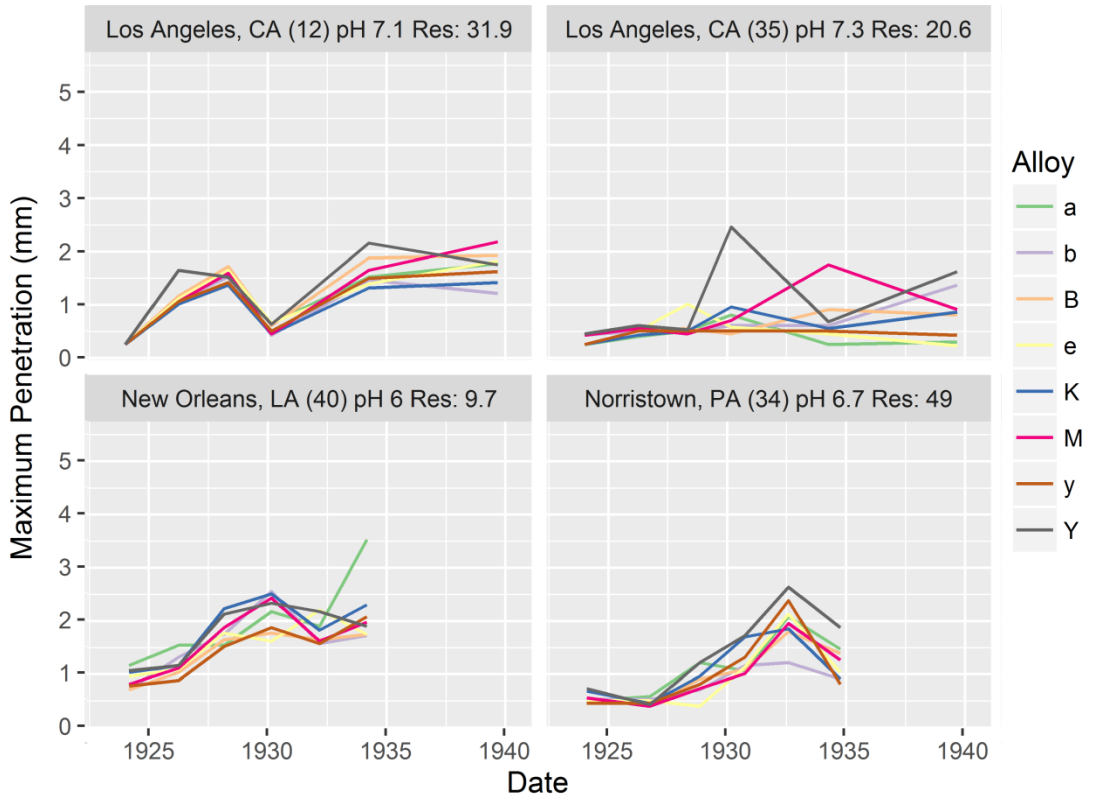
Los Angeles, CA (12) pH 7.1 Res: 31.9
Los Angeles, CA (35) pH 7.3 Res: 20.6
New Orleans, LA (40) pH 6 Res: 9.7
Norristown, PA (34) pH 6.7 Res: 49
Maximum Penetration (mm)
Date
Alloy
a
b
B
e
K
M
y
Y

(G)

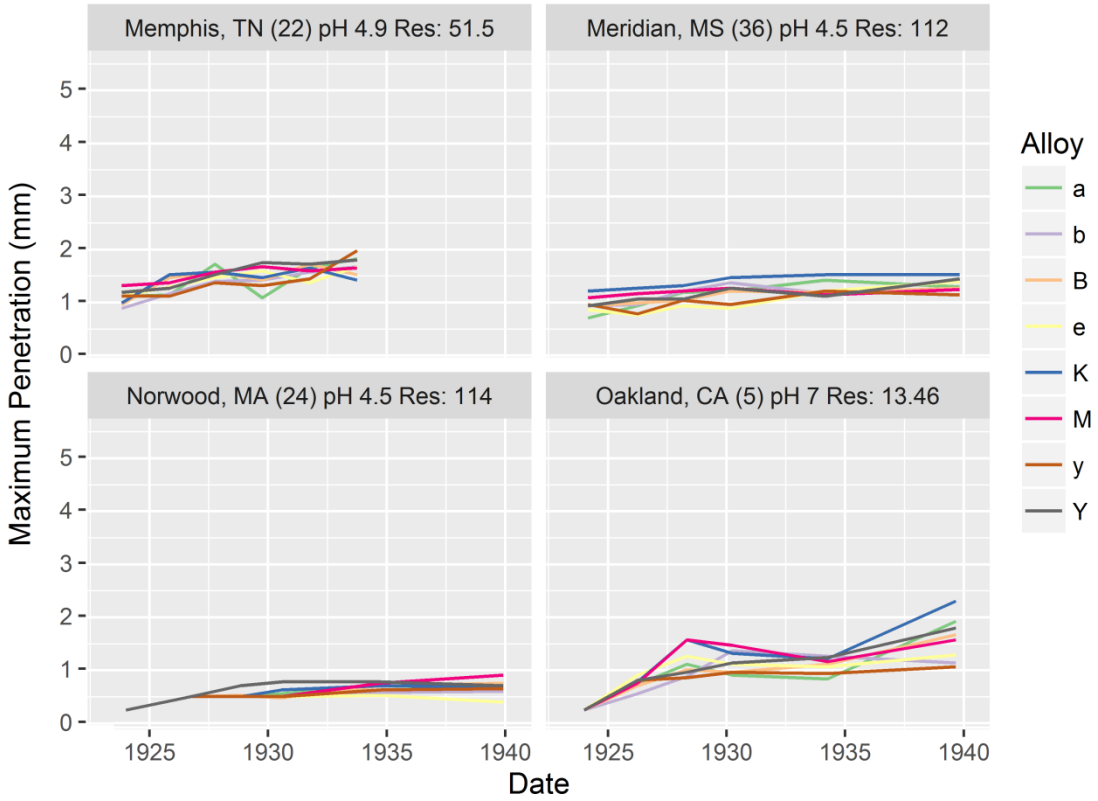
Memphis, TN (22) pH 4.9 Res: 51.5
Meridian, MS (36) pH 4.5 Res: 112
Norwood, MA (24) pH 4.5 Res: 114
Oakland, CA (5) pH 7 Res: 13.46
Maximum Penetration (mm)
Date
Alloy
a
b
B
e
K
M
y
Y

(H)

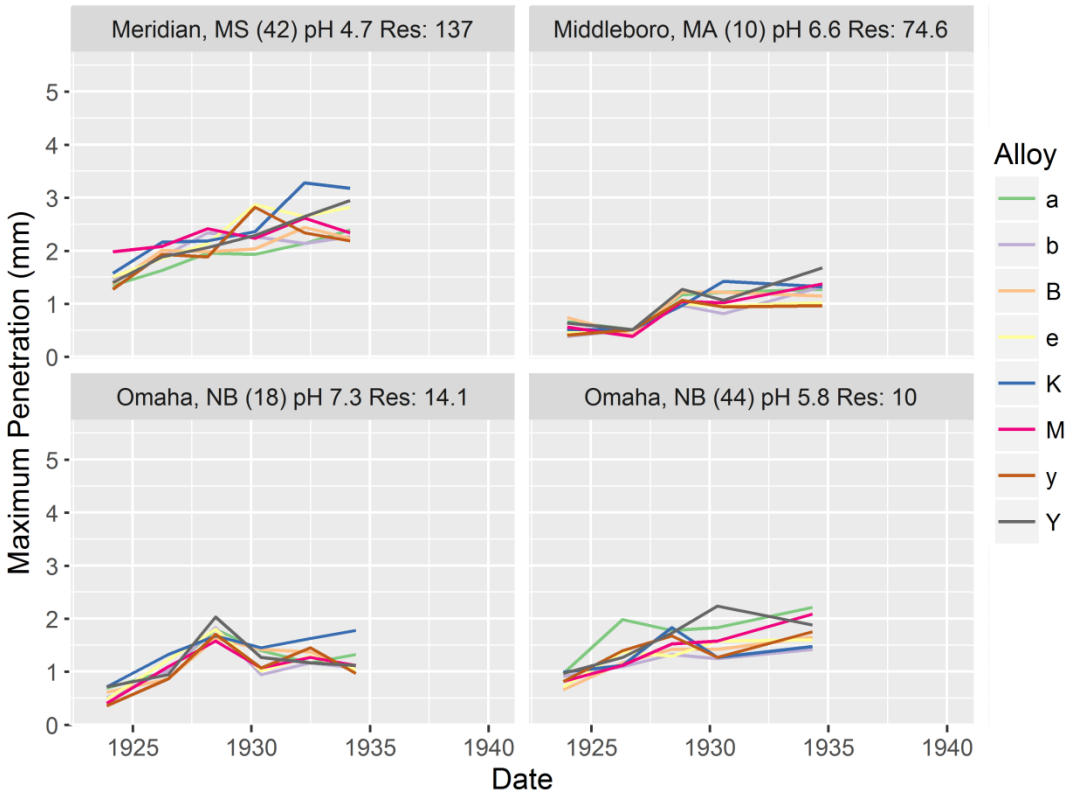
Meridian, MS (42) pH 4.7 Res: 137
Middleboro, MA (10) pH 6.6 Res: 74.6
Omaha, NB (18) pH 7.3 Res: 14.1
Omaha, NB (44) pH 5.8 Res: 10
Maximum Penetration (mm)
Date
Alloy
a
b
B
e
K
M
y
Y

(I)

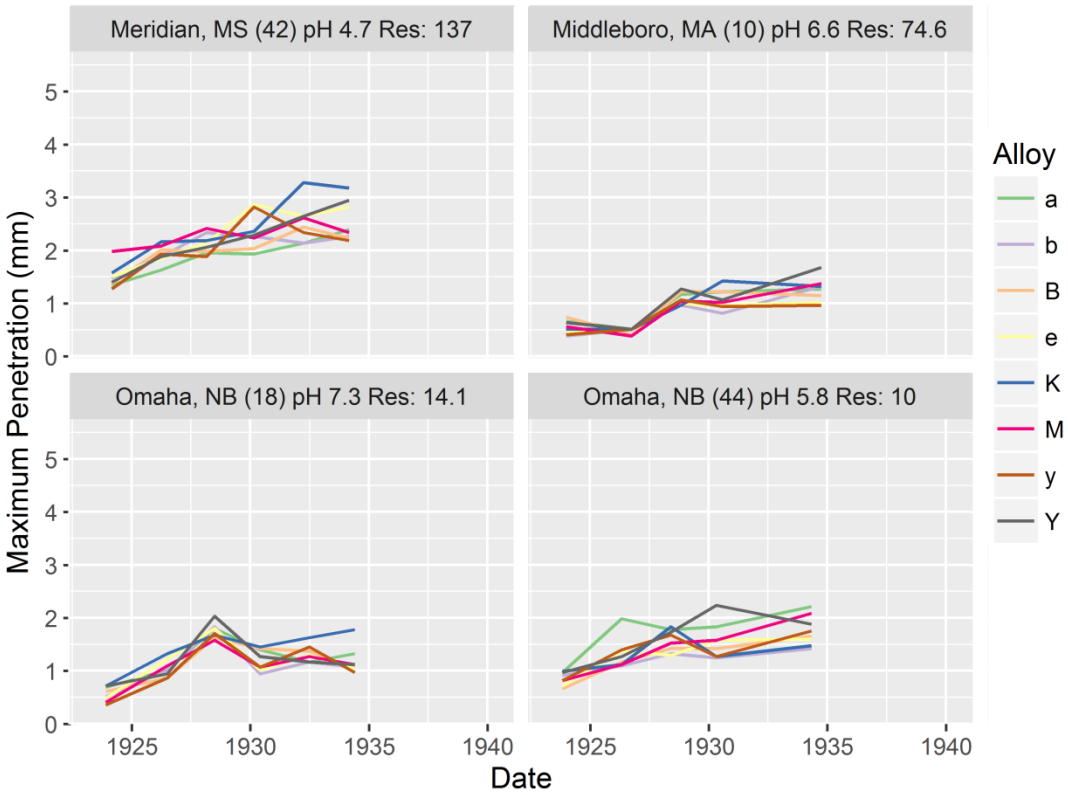
Meridian, MS (42) pH 4.7 Res: 137
Middleboro, MA (10) pH 6.6 Res: 74.6
Omaha, NB (18) pH 7.3 Res: 14.1
Omaha, NB (44) pH 5.8 Res: 10
Maximum Penetration (mm)
Date
Alloy
a
b
B
e
K
M
y
Y

(J)

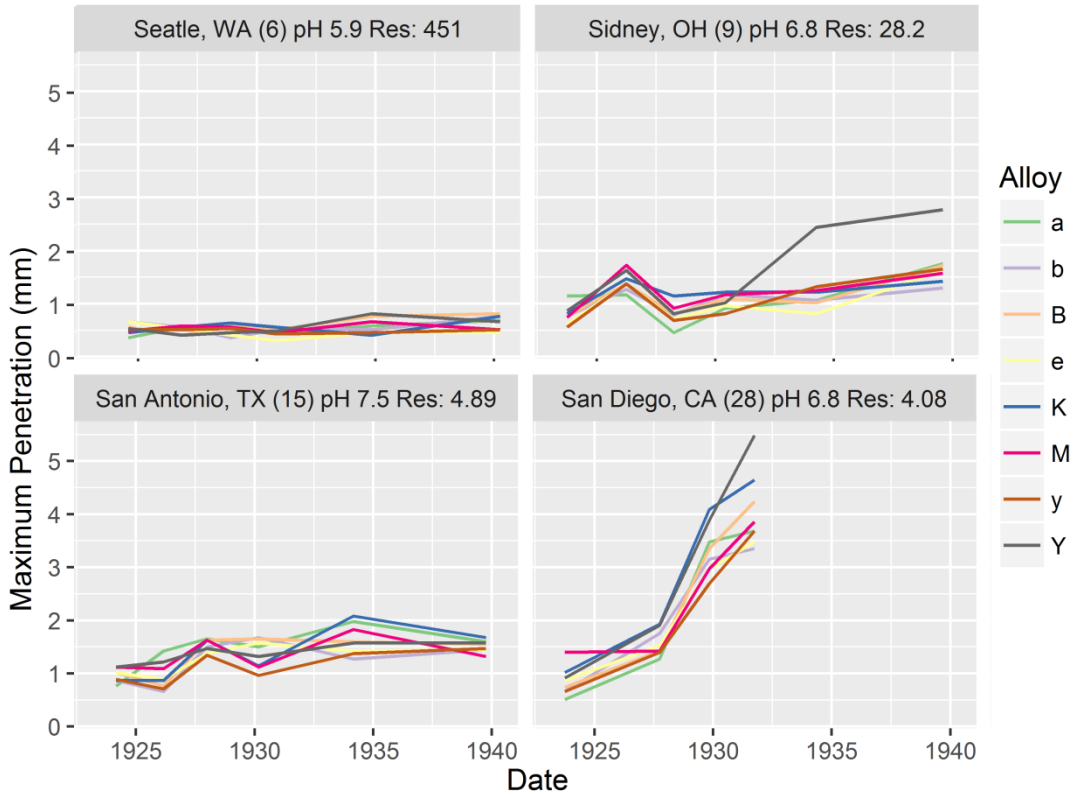

(K)

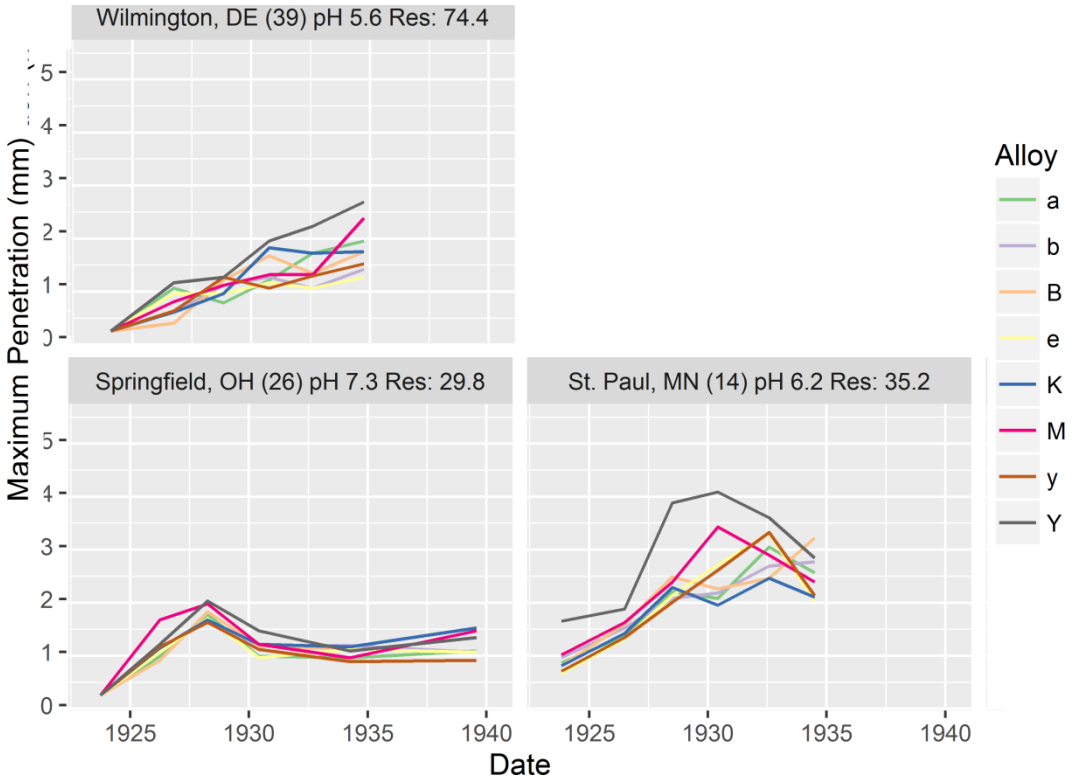

(L)

Figure 33. Graph clusters A, B, C, D, E, F, G, H, I, J, K, and L represent maximum depth penetration over time. Each title features the original location, pH, and electrical resistivity of the soil.